Evolutionarily stable gene clusters shed light on the common grounds of pathogenicity in the *Acinetobacter calcoaceticus-baumannii* complex

Bardya Djahanschiri[1], Gisela Di Venanzio[2], Jesus S. Distel[2], Jennifer Breisch[3], Marius Alfred Dieckmann[4], Alexander Goesmann[4], Beate Averhoff[3], Stephan Göttig[5], Gottfried Wilharm[6], Mario F. Feldman[2] and Ingo Ebersberger[1,7,8*]

1 Applied Bioinformatics Group, Inst. of Cell Biology and Neuroscience, Goethe University Frankfurt, Frankfurt am Main, Germany

2 Department of Molecular Microbiology, Washington University School of Medicine, St Louis, MO 63110, USA

3 Inst. of Molecular Biosciences, Goethe University Frankfurt, Frankfurt am Main, Germany

4 Bioinformatics and Systems Biology, Justus Liebig University Gießen, Gießen, Germany

5 Institute for Medical Microbiology and Infection Control, University Hospital, Goethe University, Frankfurt, Germany.

6 Robert Koch Institute, Project group P2, Wernigerode, Germany

7 Senckenberg Biodiversity and Climate Research Centre (S-BIKF), Frankfurt am Main, Germany

8 LOEWE Center for Translational Biodiversity Genomics (TBG), Frankfurt am Main, Germany

*Correspondence to: ebersberger@bio.uni-frankfurt.de

Abstract

Nosocomial pathogens of the *Acinetobacter calcoaceticus-baumannii* (ACB) complex are a cautionary example for the world-wide spread of multi- and pan-drug resistant bacteria. Aiding the urgent demand for novel therapeutic targets, comparative genomics studies between pathogens and their apathogenic relatives shed light on the genetic basis of human-pathogen interaction. Yet, existing studies are limited in taxonomic scope, sensing of the phylogenetic signal, and resolution by largely analyzing genes isolated from their functional contexts. Here, we explored more than 3,000 *Acinetobacter* genomes in a phylogenomic framework integrating orthology-based phylogenetic profiling and micro-synteny conservation analyses. This allowed to delineate gene clusters in the type strain *A. baumannii ATCC 19606* whose evolutionary conservation indicates a functional integration of the subsumed genes. These evolutionarily stable gene clusters (ESGCs) reveal metabolic pathways, transcriptional regulators residing next to their targets but also tie together sub-clusters with distinct functions to form higher-order functional modules. We shortlisted 150 ESGCs that either co-emerged with, or are found preferentially in, the pathogenic ACB clade. They unveil, at an unprecedented resolution, the genetic makeup that coincides with the manifestation of the pathogenic phenotype in the last common ancestor of the ACB clade. Key innovations are the remodeling of the regulatory-effector cascade connecting LuxR/LuxI quorum sensing via an intermediate messenger to biofilm formation, the extension of micronutrient scavenging systems, and the increase of metabolic flexibility by exploiting carbon sources that are provided by the human host. Specifically, we could show that only members of the ACB clade use kynurenine as a sole carbon and energy source, a substance produced by humans to fine-tune the antimicrobial innate immune response. In summary, this study provides a rich and unbiased set of novel testable hypotheses on how pathogenic

Acinetobacter interact with and ultimately infect their human host. They disclose promising routes for future therapeutic strategies.

Keywords

gene cluster, kynurenine, carbohydrate metabolism, phylogenomics, biofilm, quorum sensing, synteny, virulence, innate immune response

Author Summary

The spread of multi- and pan-drug resistant bacterial pathogens is a world-wide threat to human health. Understanding the genetics of host colonization and infection is essential for devising novel ways of treatment. *Acinetobacter baumannii*, a nosocomial pathogen ranked top by the World Health Organization in the list of bacteria for which novel therapeutic approaches are needed, is a prime example. Here, we have carved out the genetic make-up that distinguishes *A. baumannii* and its pathogenic next relatives comprising the *A. baumannii–calcoaceticus* complex from other and mostly apathogenic *Acinetobacter* species. We found a rich spectrum of pathways and regulatory modules that reveals how the pathogens have modified biofilm formation, iron scavenging, and their carbohydrate metabolism to adapt to their human host. Among these, the capability to metabolize kynurenine is particularly intriguing. Humans produce this substance to contain bacterial invaders and to fine-tune the innate immune response. But *A. baumannii* and its allies have turned the table. They feed on kynurenine, and thus most likely also dysregulate human immune response. In summary, our study substantially deepens the understanding of how a highly critical pathogen interacts with its host, which substantially eases the identification of novel targets for innovative therapeutic strategies.

71

72 ## Introduction

73 *Acinetobacter* is a physiologically and biochemically diverse genus of Gram-negative
74 coccobacilli. Most of its species are considered benign, but the genus harbors with the
75 *Acinetobacter calcoaceticus-baumannii* (ACB) complex a group of closely related human
76 opportunistic pathogens [1, 2] that account for the vast majority of severe hospital-acquired
77 *Acinetobacter* spp. infections [3-7]. *Acinetobacter baumannii*, a notorious nosocomial
78 pathogen, is the most renowned member of the ACB complex and signs responsible for up to
79 5% of the total bacterial infections in hospitals worldwide [8]. By now, antibiotic resistance
80 determinants against virtually all available antibiotics drugs are present in *A. baumannii* [9],
81 and multi- or even pan-drug resistant strains are isolated from 44% of all patients with an *A.*
82 *baumannii* induced infection [10]. At the same time, both the frequency and severity of
83 infections have increased. Recent case studies report mortality rates of up to 70% [11-13] as
84 well as growing numbers of (clonal) epidemic outbreaks [14]. Moreover, community-acquired
85 infections by members of the ACB complex begin to rise [6, 15]. In recent years, significant
86 advancements in the molecular characterization of drug resistance mechanisms have led to
87 more informed drug administration schemes for hospitalized patients [6]. Still, the ease with
88 which *A. baumannii* acquires resistance to novel antibiotics [10] makes it likely that resistant
89 strains and their resistance determinants are going to spread at a faster pace than novel
90 antimicrobials become available [16]. As a consequence, *A. baumannii* ranks top in the WHO
91 charts of pathogens for which drug development is most urgent [17].

92 A systemic understanding of how *A. baumannii* interacts with and infects their human host
93 can lead to novel paths for antimicrobial treatments [18-20]. Three main approaches have
94 been used to elucidate the molecular basis of *Acinetobacter* virulence. Candidate approaches

95 (i) have scanned for virulence factors previously characterized in other bacterial pathogens [4,
96 7, 21-25]. To extend the scope beyond pre-compiled virulence factor catalogs, genome-wide
97 approaches (ii) have assessed, for example, the effect of gene knockouts on the infection
98 process (e.g. [12, 26]), or have identified the transcriptional changes under conditions the
99 bacterium typically encounters in the human host (e. g. [23, 27]). These studies are, in theory,
100 the most comprehensive way to identify virulence-related traits. However, experiments are
101 usually performed only on a small set of model strains (e.g. [28]). Moreover, the limited set of
102 tested conditions cannot reflect the diversity of infection sites in the human body.
103 Consequently, results are hard to generalize. Lastly, factors that contribute only indirectly to
104 virulence are hard to pinpoint. For example, we have only begun to understand how
105 adaptations in the carbohydrate metabolism contribute to the virulence of *A. baumannii* [29].
106 Comparative genomics studies (iii) provided complementary evidence with the potential to
107 overcome limitations imposed by the experimental procedures. They aim at identifying
108 evolutionary changes that correlate with the emergence of pathogenic species [30]. To date,
109 the genus *Acinetobacter* encompasses 72 (validly) named and mostly nonpathogenic species
110 [31], which have been isolated from a broad range of habitats such as floral nectar, tree bark,
111 seawater, but also animals [32]. This diversity provides an almost perfect setup to identify
112 changes in the gene repertoires that are associated with the evolutionary emergence of the
113 pathogenic potential, which eventually manifested in the ACB complex. Thus far, comparative
114 genomics studies have begun to shed light on the general evolution of the genus [9] and the
115 clonal epidemiology [33] of *A. baumannii*. They indicated that a major driver of *A. baumannii*'s
116 success as a pathogen is its remarkably flexible genome [9]. High mutation rates [34] paired
117 with the ability to acquire new, or alter the structure or expression of existing genes [11-13]
118 promote a rapid adaptation to novel and adverse environmental conditions. Moreover, its

119 high genomic plasticity [34-36] facilitates the acquisition of antimicrobial resistance
120 determinants complementing the intrinsic *A. baumannii* resistance [37]. However, against the
121 intuition, most of the known virulence determinants were found also in the nonpathogenic
122 members of the genus (e.g. [4, 38-40]). Thus, it is still largely unknown which genetic changes
123 correlate with the emergence of the ACB complex as opportunistic human pathogens, and the
124 genetic basis underlying the adaptation of *A. baumannii* to the human host largely remains to
125 be understood [41].
126 Here, we exploit the availability of thousands of *Acinetobacter* spp. genomes in the public
127 databases (NCBI RefSeq; [42]) to shed light on the evolution of the pathogenic ACB complex
128 at a resolution that extends from a genus-wide overview to the level of individual clonal
129 lineages within *A. baumannii.* For the first time, we integrate genus-wide ortholog searches,
130 with analyses of gene order conservation providing a highly-resolved view on the joint
131 evolutionary fate of neighboring genes using the type strain ATCC 19606 as a reference. This
132 revealed 150 evolutionarily stable gene clusters ($ESGC_{ACB}$) that are prevalent in the ACB
133 complex and rare or absent in the other members of the genus. The functional annotations
134 of these ESGCs provide insights into the genetic and functional specifics of a clade
135 comprising mostly pathogens, and thus direct the focus to key processes likely relevant for
136 the adaptation of the bacterium to the human host. We find that the ACB complex acquired
137 novel genetic modules for the regulation and formation of biofilms, for the scavenging of
138 micronutrients, and have substantially extended their capabilities to exploit a diverse set of
139 carbon sources. Most notably, we show that members of the ACB complex possess the
140 kynurenine (Kyn) pathway and can grow on kynurenine as a sole carbon and energy source.
141 The implications beyond the tapping of a novel carbon source are compelling. Both
142 metabolites are produced by the human host via tryptophan degradation upon bacterial

143 infection and they contribute to the finetuning of the human innate immune response [43,
144 44]. Thus, the presence of the Kyn pathway allows members of the ACB complex to feed on
145 substances produced by the host to defend against bacterial attack. By that, they potentially
146 interfere with the kynurenine-dependent finetuning of the human innate immune response.

147 Results

148 The ability to infect humans emerged in the course of *Acinetobacter* spp. evolution and is a
149 hallmark of the ACB complex. Here, we exploited the full diversity of *Acinetobacter* genomes
150 available in the public databases that was available at the onset of the study (S1 Table SA1).
151 We use this resource to trace changes in the *Acinetobacter* pan-genome that correlate with
152 the manifestation of pathogenicity in the ACB complex. To make the analyses
153 computationally tractable we devised a two-stage strategy.
154 In the priming stage, we determined the evolutionary relationships within the *Acinetobacter*
155 pan-genome with the orthology inference tool OMA [45]. Because the computational
156 complexity of the OMA ortholog search scales exponentially with the numbers of genes in
157 the pan-genome, we compiled a representative set of strains (Set-R) for this analysis. In
158 brief, we considered all available type, reference and representative genomes, as well as all
159 validly named species for which a genome sequence was available at the study onset. This
160 set was filled to a total number of 232 strains by adding further genomes to maximize the
161 phylogenetic diversity of the taxon set (see Methods, and S2 Suppl. Text: Overview of
162 genome assemblies in Set-R). The corresponding strains together with genome assembly
163 statistics, and, where available, the origins of the isolates are summarized in S3. Members of
164 the ACB complex harbor, on average, 14% more genes than other members of this genus
165 (students t-test - $p<0.001$; S4 Fig. SA3.A). Gene counts were highly correlated with genome
166 lengths (spearman, $\rho=0.98$), and neither the difference in genome length nor the number of

167 encoded genes was significantly correlated with the assembly status (Completeness status
168 "Complete" vs. Others, Kruskal-Wallis, p=0.311) (see SA3 for further information). The Set-R
169 pan-genome comprises 22,350 orthologous groups harboring 783,306 proteins; 16,000
170 proteins remained singletons (see SA4.C for a graphical representation). Rarefaction
171 analyses revealed that the pan-genomes of the entire genus, the ACB complex, and *A.*
172 *baumannii* are open (S2 Suppl. Text: Pan-genome reconstruction). 889 genes represent the
173 core genome of *Acinetobacter* (S5 Table SB1; S2 Suppl. Text: Core-genome reconstruction).
174 Eventually, we tentatively annotated gene function in the Set-R pan-genome by linking the
175 individual genes to COGs [46], to KEGG KOs [47], to entries in the virulence factor databases
176 PATRIC [21] and VFDB [48], and by predicting their subcellular localization. To make this data
177 available to the community, we developed the web application Aci-Dash (https://aci-
178 dash.ingress.rancher.computational.bio/; Fig. 1), the first web-based platform to
179 interactively browse and explore the *Acinetobacter* pan-genome.
180 In the extension stage, we used a targeted ortholog search to complement the orthologous
181 groups from the SET-R analysis with sequences from the remaining 2,820 *Acinetobacter*
182 genomes (Set-F).

183 ### Consistency-based phylogeny of the genus *Acinetobacter*

184 To establish a stable phylogenetic backbone for our analysis, we reconstructed the
185 maximum likelihood evolutionary relationships of the taxa in Set-R and Set-F, respectively,
186 from three non-overlapping partitions of the 889 core genes. The majority-rule consensus
187 phylogenies from the three trees each (Set-R – Fig. 2A, S6 Fig. SC5; Set-F – Fig. 2B, Additional
188 files 7: Fig. SC6 and 8: File SC7) reveal that all named species (at the time of download) as
189 well as the members of the ACB complex are consistently placed into monophyletic clades.
190 Incongruencies between the three partition trees are confined to the branching order within

191 individual species, and here mainly within the densely sampled *A. baumannii* and *A. pittii*.
192 This indicates that genetic recombination, which is most likely the source of the incongruent
193 phylogenetic signal [49], is common enough only within species to interfere with
194 phylogenomic reconstructions based on hundreds of genes [50]. Across the genus, we
195 detected and corrected individual taxonomic assignments that are at odds with the
196 phylogenetic placement of the taxa, and most likely indicate mislabeled strains ([51, 52]).
197 Specifically, we corrected 16 of such instances within the ACB clade, of which ten were
198 wrongly classified as *A. baumannii* according to NCBI RefSeq. In turn, 60 out of 182 genomes
199 with an unknown taxonomic assignment were placed within the ACB clade (see S8 Table SC1
200 for species and clade assignments including the corrections). Interestingly, a comparison of
201 the average pair-wise nucleotide identity (ANI) across all genomes within Set-R revealed that
202 at least two genomes placed into the ACB clade cannot be associated with any known
203 species (ANI <95%, c. f. S9 Fig. SC3). This indicates that the full species diversity of the ACB
204 complex is not yet fully charted.
205 To ease the integration of the phylogenetic information into the following sections, we used
206 one species each to name the individual clades in the *Acinetobacter* phylogeny (Figure 2A).

207 Lifestyle and host switches during *Acinetobacter* evolution

208 The two earliest branching clades, named after *A. qingfengensis* (QI) and *A. brisouii* (BR),
209 respectively, solely comprise environmental species. *A. apis*, which was isolated from bees
210 [53], appears as an exception. However, *Acinetobacter* species are sporadically observed in
211 the bee gut, though they are not considered part of the gut microbiome [54]. Instead, they
212 likely represent environmental bacteria that were taken up by the bee with the food [55].
213 Thus, the capability to colonize animals evolved later and most likely in the ancestral species
214 prior to the split of the *A. lwoffii* (LW) clade (Fig. 2B). Usually, members of the LW clade are

215 nonpathogenic. Repeated cases of human infection have only been reported for individual
216 strains that mainly group with *A. lwoffii* and *A. radioresistens*, which manifested in vascular
217 catheter-induced bloodstream infections with a low mortality rate [56]. Thus, human
218 infection is likely an exception rather than the rule for this clade. Species descending from
219 the most recent common ancestor *A. baumannii* shares with the *A. baylyi* clade (BA, in
220 particular *A. ursingii*) and with the *A. haemolyticus* clade (HA), respectively, are found
221 increasingly often associated with human pathogenicity, suggesting a progressive adaptation
222 to humans as a host [57]. Members of the monophyletic ACB complex (ACB clade), which
223 subsumes the *A. pittii clade* (PI), the *A. nosocomialis* clade (NO), and the *A. baumannii* clade
224 (B), are all potentially pathogenic, although *A. calcoaceticus* has, thus far, very rarely been
225 seen in the context of human infection. It can be speculated that the few reported cases
226 were due to a miss-classified strain from a different species (see subsection "Consistency-
227 based phylogeny of the genus Acinetobacter" above). Thus, *A. calcoaceticus* at least
228 substantially reduced its pathogenic potential if not lost it completely [25].

229 ## Functional innovation in the Set-R pan-genome

230 We next scanned the Set-R pan-genome for gains of function on the lineage towards
231 contemporary *A. baumannii*. We tentatively stratified the pan-genome by assigning each
232 orthologous group to the inner node in the *Acinetobacter* phylogeny that represents the last
233 common ancestor (LCA) of the two most distantly related taxa in that group (Fig. 3A). For
234 each node, we then determined the set of significantly enriched gene functions using the
235 gene ontology (GO) terms from the sub-ontology Biological Process. Because genes with a
236 sparse phylogenetic distribution cannot drive the shared phenotype of a clade, we confined
237 the GO term enrichment analysis to only the subset of orthologous groups, where orthologs
238 were detected in at least half of the subsumed taxa of a node (Fig. 3B; Table 1; S10 Tables

239 SD1). This revealed several processes with potential relevance for pathogenicity, e.g. cell
240 adhesion, siderophore biosynthesis, and response to oxidative stress. However, reproducing
241 previous observations [4, 38-40], the corresponding genes were assigned to nodes in the
242 phylogeny that predate the emergence of the ACB clade. Only three significantly enriched
243 GO terms were assigned to the node representing the LCA of the ACB clade, and no term
244 was significantly enriched in the genes private to *A. baumannii*.
245

246 Table 1 Selection of overrepresented GO terms in the assigned gene sets of the inner nodes.[1]

Node	GO	Biological Process	p_cor[2]	RT[3]	RB[4]	d[5]	SC[6]	SA[7]	%B[8]	%ACB[9]	%nACB[10]
ACB+BR (n=230)	GO:0018189	pyrroloquinoline quinone biosynthesis	$<10^{-7}$	8.6	5.0	9	192	5	97.8	98.7	17.0
	GO:0006855	drug tm transport	$<10^{-7}$	2.4	9.5	5	53	1	96.4	96.8	23.4
	GO:0015810/3	aspartate/L-glutamate tm transport	$<10^{-7}$	4.3	2.5	10	96	2	96.4	97.8	24.8
	GO:0071705	nitrogen compound transport	$<10^{-7}$	2.8	9.1	4	62	1	100	100	27.7
	GO:0019439	aromatic compound catabolism	$5.2*10^{-3}$	2.2	14.0	4	49	2	92.7	95.7	28.4
	GO:0006631	fatty acid metabolism	$<10^{-7}$	3.3	6.5	7	73	1	89.1	91.4	36.2
	GO:0019619	3,4-dihydroxybenzoate catabolism	$<10^{-7}$	3.2	10.6	8	72	1	90.9	92.5	39.0
	GO:0007155	cell adhesion	$<10^{-7}$	4.6	10.6	2	103	1	98.2	98.9	40.4
	GO:0010124	phenylacetate catabolism	$<10^{-7}$	10.4	8.5	8	233	4	89.6	90.6	45.7
ACB+LW (n=223)	GO:0031388	organic acid phosphorylation	$<10^{-7}$	2.9	2.4	6	54	1	98.2	98.9	14.9
	GO:0009437	carnitine metabolism	$3.1*10^{-3}$	0.2	0.1	6	3	1	94.5	88.2	22.0
	GO:0071705	nitrogen compound transport	$<10^{-7}$	4.4	10.5	4	83	2	99.1	94.6	23.4
	GO:0036104	Kdo2-lipid A biosynthesis	$<10^{-7}$	2.4	3.8	8	45	1	94.5	91.4	29.8
	GO:0009435	NAD biosynthesis	$<10^{-7}$	3.4	15.7	11	65	1	89.1	91.4	30.5
	GO:0009116	nucleoside metabolism	$<10^{-7}$	3.5	13.0	6	67	1	96.4	95.7	31.2
	GO:0055085	tm transport	$<10^{-7}$	24.2	149.4	4	459	7	90.2	89.1	38.7
	GO:0019557/6	histidine catabolism to glutamate and formate/formamide	$<10^{-7}$	9.9	6.1	10	188	3	95.8	97.5	41.6
	GO:0006351	transcription, DNA-templated	$<10^{-7}$	86.9	320.1	9	1645	21	95.5	93.7	41.8
	GO:0019290	siderophore biosynthesis	$<10^{-7}$	8.0	4.8	8	170	3	95.8	72.8	41.8
ACB+BA (n=152)	GO:0045150	acetoin catabolism	$<10^{-7}$	33.6	0.8	7	36	1	100	100	14.9
	GO:0019290	siderophore biosynthesis	$<10^{-7}$	29.9	5.6	8	32	1	96.4	97.8	22.0
	GO:0006351	transcription, DNA-templated	$<10^{-7}$	76.5	0.03	9	82	2	84.5	84.9	26.2
ACB+HA (n=143)	GO:0022904	respiratory electron transport chain	$<10^{-7}$	45.9	5.39	5	44	0	90.9	79.6	11.3
	GO:0006351	transcription, DNA-templated	$<10^{-7}$	78.3	314.8	9	75	0	90.9	91.4	27.0
ACB (n=93)	GO:0009372	quorum sensing	$<10^{-7}$	8.8	0.3	3	13	2	86.4	90.3	0.0
	GO:0006351	transcription, DNA-templated	$<10^{-7}$	98.9	318.1	9	146	5	92.0	87.1	0.0
	GO:0006979	response to oxidative stress	$4.7*10^{-5}$	9.5	17.4	3	14	1	89.1	78.5	0.0

247

[1] The full list of enriched terms is provided in Additional file 10 Table SD1.1.
[2] corrected p-value
[3] Ratio of genes with term in test set of that node ($\times 10^{-3}$)
[4] Ratio of genes in background set of that node ($\times 10^{-4}$)
[5] Depth of term in GO tree
[6] Count of subjects with term in study set of that node
[7] Number of ortholog groups associated with proteins in the study set. For this table, redundancy was reduced by selecting the lowest depth GO terms if any two GO terms had non-empty intersections between their sets of protein sequence identifiers or associated ortholog group identifiers.
[8] Mean prevalence of associated ortholog groups in *A. baumannii*
[9] Mean prevalence of associated ortholog groups in the ACB clade
[10] Mean prevalence of associated ortholog groups in *Acinetobacter* spp.

248 ## Evolutionary and functional units in the ATCC 19606 gene set

249 The GO term enrichment analysis revealed only a weak signal for the gain of biological
250 processes that can be directly connected to bacterial virulence in the evolutionarily younger
251 nodes of the *Acinetobacter* phylogeny. However, two factors confound the analysis. Only
252 about two-thirds of all unique sequences in the *Acinetobacter* spp. pan-genome is annotated
253 with a GO term and many of the genes with only unspecific terms. Moreover, the sporadic
254 presence of orthologs to individual genes in taxa outside the ACB clade, e.g. as a result of
255 recombination, confounds the phylogenetic stratification of the pan-genome. To increase
256 both power and resolution, we widened the focus and traced the emergence and evolution
257 of gene clusters in *Acinetobacter* spp. using the type strain *A. baumannii* ATCC 19606 as a
258 reference. For each gene in the type strain, we integrated its node assignment, the
259 abundance of orthologs within *A. baumannii*, within other members of the ACB clade, and
260 within the remaining taxa in SET-R, respectively, and, where applicable, the overrepresented
261 GO terms (Fig. 4). As a recurrent theme, we observed that genes linked to the same
262 overrepresented GO term reside adjacent to genes with highly similar phylogenetic
263 abundance patterns, despite being occasionally assigned to different nodes in the
264 phylogeny. We subsequently connected neighboring genes with significantly similar
265 abundance patterns across the entire genome of *A. baumannii* ATCC 19606 to form
266 candidate clusters. A candidate cluster was then propagated to represent an evolutionarily
267 stable gene cluster (ESGC), which likely forms a functional entity if its gene order was found
268 conserved within the ACB clade (S11 Table SE1.3). Subsequently, we shortlisted 150 $ESGC_{ACB}$
269 that are abundant among members of the ACB clade and, at the same time, rare or even
270 absent outside the clade (SE1.3 and SE1.4; see S2 Suppl. Text: Workflow of ESGC
271 identification and shortlisting). As the last step, we manually validated the automatic

272 $ESGC_{ACB}$ assignment for 44 clusters whose sets of genes were each functionally annotated to
273 a level that allowed us to infer general cluster function (Fig. 5), and for further 10 clusters
274 with an unknown function but that are almost exclusively found in the ACB clade (Fig. 6).
275 These 54 $ESGC_{ACB}$ can be broadly distinguished into four categories: The cluster comprises (i)
276 a known operon or metabolic gene cluster (e.g., $ESGC_{ACB}$-0622, phenylacetate metabolism),
277 (ii) a group of functionally related genes that are linked to genes, whose functional link, e.g.
278 acting as a transcriptional regulator, was unknown thus far (e.g., $ESGC_{ACB}$-0162), (iii) super-
279 clusters connecting two or more clusters with distinct functions to form a higher-order
280 functional unit ($ESGC_{ACB}$-0394, *adeFGH* and *hisQMP*), and (iv) clusters of genes with an
281 unknown function (e.g., $ESGC_{ACB}$-0503 to 0510; Fig. 6). We hypothesize that the adaptation
282 of pathogenic *Acinetobacter* species to their human host is likely mirrored in the various
283 functions that these $ESGC_{ACB}$ convey. In the following sections, we highlight a selection of
284 clusters related to persistence, micronutrient acquisition, and the evolution towards
285 nutritional flexibility (see S2 Suppl. Text: Gene clusters (ESGCs) not discussed in main
286 manuscript).

287 ## The evolutionary emergence of the ACB clade coincides with changes in quorum sensing and
288 biofilm formation

289 Quorum sensing and biofilm formation are key determinants of *A. baumannii* virulence [58-
290 60]. Both functions are represented by $ESGC_{ACB}$-0162 (14 genes) and 0410 (8 genes).
291 $ESGC_{ACB}$-0162 represents the regulatory module of this process. It harbors the Lux-type
292 quorum sensing system (QS_{Lux}), which regulates motility and biofilm formation in *A.*
293 *baumannii,* and additionally, a biosynthetic gene cluster containing a non-ribosomal peptide
294 synthetase here referred to as NRPS cluster. Both genes of QS_{Lux}, *abaI* and *abaR,* are
295 separated by a short gene that was tentatively named *abaM* (Fig 7A; see also S2 Suppl. Text:

296 Characterization of AbaM). This three-gene architecture is conserved in the ACB clade, and it
297 is common in *Burkholderia* spp. [61], where the intervening short gene acts as a negative
298 regulator of the QS_{Lux} system [62]. Recently, initial evidence emerged that AbaM in the *A.*
299 *baumannii* strain AB5075 indeed regulates quorum sensing and biofilm formation [63]. In
300 the light of our results, we propose that AbaM is an understudied modulator of quorum
301 sensing in the entire ACB clade.
302 The NRPS cluster (Figure 7A) produces a three-amino acid lipopeptide, Ac-505 [60], which
303 likely plays a central role in regulating bacterial motility and biofilm formation [64].
304 Disrupting its biogenesis alters the expression of numerous factors involved in biofilm
305 formation and surface adherence [65], in particular the chaperon-usher pili (CUP) and the
306 archaic chaperon-usher pili (CSU). Consequently, host cell adhesion and virulence of *A.*
307 *baumannii* are substantially reduced. Here, we provide first-time evidence that the
308 evolutionary fate of the NRPS cluster is intimately intertwined with that of the QS_{Lux} cluster.
309 We found that the rare strain-specific loss of the QS_{Lux}-cluster determines the loss of the
310 NRPS cluster, which implies that they not only form an evolutionary but also a functional
311 unit. Interestingly, strains lacking $ESGC_{ACB}$-0162 are not randomly distributed. Most
312 prominently, the cluster is missing in almost all (48/55) *A. baumannii* strains representing
313 the international clone type (IC) 8 (Fig. 5). The formation of a higher-order module
314 comprising the QS genes and an NRPS biosynthetic gene cluster is a repeated scheme during
315 bacterial evolution. For example, the methane-oxidizing bacterium *Methylobacter*
316 *tundripaludum* harbors an NRPS biosynthetic gene cluster that was integrated between the
317 *abaI* and *abaR* orthologs. And the production of the corresponding extracellular factor is
318 under control of the QS cluster [66]. NRPS-dependent molecules have been implicated to
319 mediate interspecific communications across kingdoms both in symbiotic and pathogenic

320 communities. In *P. aeruginosa*, the interplay of N-acyl-L-homoserine lactone-dependent
321 quorum-sensing signaling and an NRPS-dependent biosynthesis of bacterial cyclodipeptides
322 (CDPs), which act as auxin signal mimics, modulates the communication to its host plant
323 *Arabidopsis thaliana* [67]. It can be speculated that $ESGC_{ACB}$-0162 may similarly coordinate,
324 the communication between the bacteria and their human host.
325 $ESGC_{ACB}$-0410, harbors the Csu cluster responsible for biofilm formation on abiotic surfaces
326 via archaic chaperon-usher pili [68, 69] (Figure 7B) together with a transcriptional regulator
327 of the TetR/AcrR family (TFTRs) (S12 Fig. SE3.0410). TFTRs represent one-component
328 systems that regulate a broad variety of cellular processes in bacteria, among them many
329 that are related to virulence such as efflux pump expression and biofilm formation [70, 71].
330 Notably, they are often encoded alongside their target operons. To the best of our
331 knowledge, regulation of the Csu cluster via an adjacent TFTR has never been reported.
332 Thus, next to the two-component systems BfmRS [72] and GacSA [73], a third hitherto
333 undescribed one-component system, seems to be involved in regulating the formation of
334 Csu pili.
335 In line with our finding that $ESGC_{ACB}$-0162 and $ESGC_{ACB}$-0410 have similar abundance
336 patterns (cf. Figure 5), the regulation of the Csu cluster appears under the direct control of
337 Ac-505 [26, 65]. Thus, Ac-505 likely acts as a modulator between biofilm formation on
338 abiotic and biotic surfaces. However, contrary to the QS_{Lux} - NRPS supercluster, the Csu
339 cluster was lost multiple times independently in the ACB clade (Figure 5). Given its terminal
340 position in the regulator-effector cascade, this indicates a lineage-specific fine-tuning of
341 biofilm formation. Interestingly, within *A. baumannii*, we find that all 55 IC8 strains in our
342 dataset lack both the QS_{Lux} - NRPS supercluster and the Csu cluster, which points towards
343 substantial changes in the way how IC8 strains regulate biofilm formation.

344 ## KatA – an ACB clade specific catalase

345 The genome of *A. baumannii* ATCC 19606 harbors five putative catalases: *katA*, *katE*, *katE-*
346 *like*, *katG*, and *katX* [23, 74]. Note, that both Sun et al. [74] and Juttukonda et al. [23, 74]
347 refer to a catalase labeled *katE*, which, however, represent different genes (locus tags
348 A1S_1386/A1S_3382 and DJ41_RS22765/DJ41_RS10660 in *A. baumannii* ATCC 17978 and
349 ATCC 19606, respectively). We, therefore, named the latter *katE*-like. *KatA* is the only
350 catalase that is exclusively found in the ACB clade. The corresponding gene resides in a
351 cluster next to a putative MFS transporter and a cytochrome b561 ($ESGC_{ACB}$-0624, Fig. 7C).
352 The KatA cluster is highly conserved in all species of the ACB clade except *A. calcoaeceticus*,
353 where it has been lost (cf. Figs 5 and 7C). Upon host infection, both neutrophils and
354 macrophages recruit radical oxygen species (ROS) for bacterial clearance [75, 76], and thus
355 ROS defense mechanisms are an essential contributor to bacterial virulence. However, an
356 initial investigation in *Ab* ATCC 17978 found no obvious link between KatA and ROS
357 protection [23]. Still, the abundance pattern of $ESGC_{ACB}$-0624 is perfectly in line with the
358 hypothesis that this cluster contributes to virulence in pathogenic members of the ACB
359 clade, and more comprehensive studies are needed to elucidate its precise role during
360 bacterial infection.

361 ## Metabolic adaptation – Micronutrient acquisition is refined in the ACB-clade

362 All members of the genus *Acinetobacter* must supply their demand of essential
363 micronutrients, most importantly iron and zinc. Acquisition systems for these two metals are
364 therefore represented in the genus-wide core genome (Figure 8). However, both iron and
365 zinc are actively sequestered by the host to starve invading pathogens, a strategy referred to
366 as nutritional immunity [77]. This likely results in a strong selective pressure for the

367 pathogenic ACB clade to optimize scavenging systems such that the reduced bioavailability
368 of these metal ions in the host can be counterbalanced.
369 Acquisition systems for iron, whose limited availability at the host-pathogen interface is
370 considered one of the key obstacles for invading and persisting within the human host, are a
371 showcase example. The iron transporter system *feoABC* represents the evolutionary core of
372 iron uptake. It is complemented, in many but not all taxa [28] both inside and outside of the
373 ACB clade, by the baumannoferrin cluster (Figure 8). Two further clusters extend the
374 spectrum of iron uptake systems exclusively in the ACB clade. $ESGC_{ACB}$-0498 represents the
375 2,3-dihydroxybenzoic acid synthesis cluster (*entAB*), which synthesizes a siderophore
376 precursor [78]. $ESGC_{ACB}$-0368 and 0369 together resemble the acinetobactin biosynthesis
377 clusters *bauA-F*, *basA-I* and *barAB*. However, a third cluster, $ESGC_{ACB}$-0485, that very likely
378 represents an ABC-type Fe^{3+}-hydroxamate transport system seems to extend the diversity of
379 iron uptake systems in the ACB clade even further. It encodes a substrate-binding protein, an
380 iron complex ABC transporter (permease), an ATP-binding protein, and an N-
381 Acetyltransferase protein (GNAT family). The AraC-family-like transcriptional regulator,
382 which is located downstream on the opposite strand in $ESGC_{ACB}$-0485, likely controls the
383 expression of this cluster. In line with this operon-like organization, these genes are jointly
384 downregulated under mucin-rich conditions [79]. The complex and seemingly redundant
385 infrastructure for iron uptake in the ACB clade seems at odds with a recent study in *A.*
386 *baumannii* ATCC 17978, which stated that acinetobactin is the only system that is necessary
387 for *A. baumannii* to grow on host iron sources [80]. However, here we show that this
388 conclusion does not generalize to the entire ACB clade. The pathogens *A. nosocomialis* and
389 *A. seifertii*, for example, lost the acinetobactin cluster (cf. Fig. 5). Instead, it is conceivable

390 that the diversity of iron acquisition systems is an adaptation to diverse niches each
391 requiring different strategies of iron scavenging.
392 Given the essentiality of zinc (Zn), it is not surprising to see that also Zn uptake was refined
393 on the lineage towards the ACB clade. The zinc uptake system Znu, including the distal *znuD*
394 gene, which facilitates resistance to human calprotectin-mediated zinc sequestration [23], is
395 evolutionarily old and part of the genus-wide core genome (Figure 8) The histidine utilization
396 (Hut) system (*hutCDUHTIG*, $ESGC_{ACB}$-0215) is prevalent in the ACB clade, though not
397 exclusively. This system ensures the bio-availability of Zn via the histidine catabolism both
398 under high availability and starvation of Zn. However, it requires histidine to be abundant.
399 Interestingly, the most recent acquisition in the Zn metabolism is the putative
400 metallochaperone, ZigA. The corresponding gene resides directly adjacent to $ESGC_{ACB}$-0215,
401 and thus is likely an evolutionary more recent extension of this cluster. *zigA* was found active
402 only under Zn starvation, where it increases the bioavailability of Zn also under histidine
403 depletion [81] and counteracts nutritional starvation.
404 Manganese (Mn^{2+}) is required only in small amounts and is mostly used for coping with
405 reactive oxygen species (ROS), as Mn^{2+}, other than Fe^{2+}, does not promote the Fenton
406 reaction that converts H_2O_2 to highly damaging hydroxyl radicals [82, 83]. Therefore, Mn
407 uptake systems should be prevalent in bacteria frequently exposed to ROS stress,
408 particularly in the pathogenic *Acinetobacter* strains. Thus far, only one Mn acquisition
409 system, *mumRTLUHC* [84], has been identified in *Acinetobacter spp*. This system is
410 represented by $ESGC_{ACB}$-0611 and plays an essential role in protecting *A. baumannii* against
411 calprotectin-mediated Mn depletion by the host and contributes to bacterial fitness in a
412 murine pneumonia model [84]. $ESGC_{ACB}$-0611 is found throughout the genus though less
413 frequently in clades that are more distantly related to the ACB clade (cf. Figures 5 and 8).

414 Within the HA-clade, several species including *A. tjernbergiae*, *A. junii*, *A. beijnerickii,* and *A.*
415 *haemolyticus* lack both the putative manganese transporter gene *mumT* and the gene
416 encoding a putative hydrolase *mumU* (S12 Fig. SE3.0611). Within IC 3, several strains lack the
417 entire cluster. These taxa either found alternatives to Mn^{2+}-dependent processes for coping
418 with oxidative stress, are more vulnerable to ROS, or they scavenge Mn^{2+} via a mechanism
419 that is still hidden in functionally uncharacterized gene clusters.
420 In summary, we see a clear signal that the ACB clade is enriched for genes and gene clusters
421 that functionally complement the genus-wide available and evolutionarily old metal uptake
422 systems. In line with the reinforcement hypothesis, these more recently acquired clusters
423 seem particularly important for metal scavenging during infection, i.e. when the metals are
424 actively sequestered by the host [80, 81].

425 ### Carbohydrate metabolism - Evolution towards nutritional flexibility

426 The ability of individual *Acinetobacter* strains to utilize a broad spectrum of carbon sources is
427 important for their adaptation to different environments, including the human host [40, 85-
428 88]. However, it is largely unknown when the corresponding metabolic pathways were
429 acquired during *Acinetobacter* evolution, how widespread they are, and if and to what
430 extent they are connected to the pathogenicity of the ACB clade. More than 20 of the
431 shortlisted $ESGCs_{ACB}$ represent pathways that shuttle metabolites into the carbohydrate
432 metabolism of the bacterium (Figure 5, in red font, and see Figure 9 for a selection), many of
433 which are prevalent in the human body. The corresponding gene clusters mostly channel
434 these metabolites into catabolic processes (see below). However, the genes involved in the
435 glucose/gluconate metabolism seem to fuel anabolic processes.

436 Glucose / Gluconate metabolism

437 Glucose and gluconate serve as carbon and energy sources for individual species in the
438 genus *Acinetobacter*, e.g., *A. soli, A. apis,* and *A. baylyi.* For *A. baylyi* ADP1 it was shown that
439 the glucose catabolism involves the Entner-Doudoroff pathway [89]. Members of the ACB
440 clade have lost the ability to use glucose as a carbon source [90] (see also S13 Fig. SF6C and
441 S14 Table SF2). It is, thus, surprising that we find the genetic infrastructure to feed both
442 molecules into the bacterial metabolism almost exclusively in the ACB clade.
443 $ESGC_{ACB}$-0112 comprises the gluconate permease (GntP) that shuttles gluconate from the
444 periplasm into the bacterial cell (Figure 9, yellow pathway). The cluster further encodes the
445 kinase GntK, which phosphorylates gluconate into 6-phosphogluconate, and the enzymes
446 Edd and Eda of the Entner-Doudoroff pathway, which link to the pentose phosphate
447 pathway that produces pyruvate. Members of the ACB clade also possess two variants of a
448 glucose dehydrogenase (*gdh*), which catalyze the reaction from D-glucose to D-gluconate in
449 the periplasm [91]. The membrane-bound variant (*gdhA*), forms together with an outer
450 membrane porin a cluster of two genes, $ESGC_{ACB}$-0287 (cf. S15 SE2.0287), which is
451 ubiquitous across *Acinetobacter* spp. We note that the porin is orthologous to OprB in *P.*
452 *aeruginosa*, where it facilitates the diffusion of various sugars - including glucose - into the
453 periplasm. The second, soluble Gdh (*gdhB*) is confined to and nearly ubiquitous in the ACB
454 clade (S16 Fig. SF3, S11 Table SE1.1, HOG3408).
455 The prosthetic group for both Gdh, pyrroloquinoline quinone (PQQ), is a small, redox-active
456 molecule that serves as a cofactor for several bacterial dehydrogenases. $ESGC_{ACB}$-0497
457 comprises six genes that together represent the PQQ biosynthesis pathway: *pqqABCDE* and
458 an additional membrane-bound dipeptidase referred to as *pqqF* in *Klebsiella pneumoniae*
459 [92] (cf. Figure 9, pink). All genes reside contiguously on the same strand suggesting an

460 operonic structure. The complete cluster is present in almost all genomes of the ACB clade,
461 although we had to manually confirm the presence of *pqqA*, because its length (40 amino
462 acids) is below the length cutoff of the ortholog assignment tool. Only 31 out of 2436 strains
463 in the ACB clade have lost the ability to synthesize PQQ, among them the model strain *A.*
464 *baumannii* ATCC 17978. Cluster abundance outside the ACB clade is low (<20%), but it is
465 present in all strains of species with demonstrated ability to assimilate glucose and
466 gluconate (i.e. *A. soli*, *A. baylyi*, and *A. apis*, cf. [90]; SE2.0497).
467 The holoenzymes *GdhA* and/or *GdhB*, in theory, could establish a gapless route for glucose
468 via this gluconate 'shunt' into the cell for further degradation via the Entner-Doudoroff
469 pathway, even in the absence of a dedicated Glucose transporter. Why then does none of
470 the tested strains in the ACB clade grow with glucose as sole carbon and energy source? We
471 hypothesize that they utilize this route for anabolic processes exclusively, e.g. for the
472 production of polysaccharides as it was demonstrated for *P. aeruginosa* [93].

473 ## Carbohydrate Catabolism

474 The ACB clade has substantially increased its repertoire of catabolic pathways for alternative
475 carbon sources compared to taxa outside this clade [94]. For a small number of mostly hand-
476 picked *A. baumannii* strains, previous studies have experimentally confirmed the ability to
477 grow on tricarballylate and putrescine, malonate, butanediol and acetoin, phenylacetate,
478 muconate, glucarate, galactarate (mucate), and 4-hydroxyproline as sole carbon sources [40,
479 85]. Our analyses identified the corresponding gene clusters among the $ESGC_{ACB}$. Hence, the
480 ability to use these resources is prevalent in the ACB clade, whereas non-ACB species have
481 to rely largely on different carbon sources. We will highlight two examples that likely
482 represent an adaptation to humans as a host.

483 D-glucarate (saccharate) is a major organic acid in human serum [95]. $ESGC_{ACB}$-0568
484 comprises all necessary genes for glucarate and galactarate (mucic acid) degradation (Figure
485 9). In *Salmonella enterica* serovar Typhimurium deletion of the D-glucarate/D-galactarate
486 permease ortholog attenuated virulence [96]. Further, galactarate digestion was shown to
487 increase the colonization fitness of intestinal pathogens in antibiotic-treated mice and to
488 promote bacterial survival during stress [97]. Given that $ESGC_{ACB}$-0568 is almost exclusively
489 confined to the ACB clade, it is conceivable that this cluster contributes to colonization and
490 virulence in pathogenic *Acinetobacter* species. It is therefore interesting that within *A.*
491 *baumannii* the cluster is almost absent in IC2 strains (0.08% prevalence in Set-F; *cf.* Figure 5).
492 Carnitine is essential for the oxidative catabolism of fatty acids in humans [98]. $ESGC_{ACB}$-0016
493 comprises six genes necessary for catabolizing carnitine [99]. A LysR-type transcriptional
494 regulator likely controls the activity of this cluster. The remaining five genes represent a
495 putative tartrate dehydrogenase (*ttuC*), a BCCT-family carnitine transporter (Aci01347), a
496 generically annotated alpha/beta hydrolase which possibly catalyses the conversion of D-
497 acylcarnitine into L-carnitine (see Figure 9, green), and the genes encoding the two subunits
498 of the carnitine monooxygenase CntA and CntB. The latter two genes are separated by a
499 gene that is tentatively annotated as an NAD-dependent succinate-semialdehyde
500 dehydrogenase. However, two lines of evidence indicate that the precise function of this
501 gene as well as that of the putative tartrate hydrogenase might both differ. In the literature,
502 the putative succinate-semialdehyde dehydrogenase is speculated to act as malic
503 semialdehyde dehydrogenase [99], an enzyme that converts malate semialdehyde into
504 malate. Further, the putative tartrate dehydrogenase belongs to the KEGG orthologous
505 group KO7246 which is annotated as a D-malate dehydrogenase. The product of the latter
506 enzyme, pyruvate, can be further processed into oxaloacetate, which serves as a substrate

507 for the tricarboxylic acid (TCA) cycle (cf. Figure 9). Assuming that the putative malic
508 semialdehyde dehydrogenase produces D-malate, then, in the presence of an appropriate
509 transporter, this cluster should allow the members of the ACB clade to utilize D-malate as a
510 carbon source. We tested this hypothesis, and confirmed that *Ab* ATCC 19606 indeed grows
511 on D-malate (S13 Fig. SF6B), which corroborates initial growth experiments [100]. We note
512 that the unusual production of the D-malate enantiomer rather than L-malate would have a
513 further interesting implication. It potentially allows the bacterium to accumulate D-malate in
514 conditions when carnitine is abundant, without interfering with the stoichiometry of the
515 remaining substrates of the TCA cycle.
516 Thus far, two *A. baumannii* strains have been shown to use carnitine as sole carbon source
517 [101]. We evaluated exemplarily that the absence of the cluster indeed correlates with
518 *Acinetobacter* inability to grow on carnitine and is not functionally complemented by an
519 alternative degradation pathway. Both, *A. baylyi* ADP1 and the *A. calcoaceticus* type strain
520 (DSM 30006), which both lack the $ESGC_{ACB}$-0016, did not grow on carnitine after 24h.
521 The clusters abundance profile reveals that the ability to metabolize carnitine occurs also
522 outside the ACB clade (31 strains in Set-R; cf. Figure 5). However, 25 of these strains were
523 isolated from infected patients, 2 from hospital sewage water, and only 3 strains were
524 sampled from the environment (cf. S17 Table SF7). The isolation origin of the one strain is
525 unknown. The presence of the carnitine cluster, therefore, correlates surprisingly well with
526 the pathogenic potential of a strain and it will be interesting to test a causal dependence. In
527 support of causality, we find that the carnitine cluster is absent in *A. calcoaceticus*, the only
528 species of the ACB clade that is nonpathogenic or at least has substantially reduced virulence
529 (cf. S2 Suppl. Text: $ESGC_{ACB}$-0016).

530 Novel carbon sources

531 The functional annotations of the $ESGC_{ACB}$ in Figure 5 indicate that the list of potential
532 carbon sources for *A. baumannii* and other members of the ACB clade is still incomplete. We
533 find degradation pathways for xanthine, 2-aminoethylphosphonate, acyclic terpenes,
534 vanillin/valinate, taurine, and anthranilate (see S2 Suppl. Text: Gene clusters (ESGCs) not
535 discussed in main manuscript). To the best of our knowledge, none of these metabolites
536 have been considered as potential carbon sources for *A. baumannii,* although a putative
537 Xanthine dehydrogenase has been characterized previously via heterologous expression in *E.*
538 *coli* [102]. One cluster is, however, particularly interesting because it intertwines the
539 bacterial carbohydrate metabolism with the human tryptophan catabolism. $ESGC_{ACB}$-0452
540 (Figure 10A) harbors the kynurenine hydrolase KynU, which catalyzes the cleavage of
541 kynurenine to anthranilic acid and alanine (Figure 10B). Within the same cluster, we
542 identified an AsnC-type transcriptional regulator, a putative amino acid permease, and a
543 gene generically annotated as an alpha/beta-hydrolase. Notably, this hydrolase is listed as
544 an ortholog to the human kynurenine formamidase (KynB) in the OMA database [103] with
545 which it shares the same domain architecture (Fig. 10C). Together with its evolutionarily
546 stable localization in the vicinity of KynU, this provides convincing evidence that the *A.*
547 *baumannii* hydrolase resembles a hitherto overlooked KynB. This enzyme transforms formyl-
548 kynurenine into kynurenine and, thus, acts immediately upstream of KynU in the Kynurenine
549 pathway of tryptophan degradation (*cf.* Fig. 10B). A similar gene cluster was recently
550 described in *P. aeruginosa* (Pae) [104, 105], however with two notable exceptions: $KynB_{Aba}$ is
551 substantially more similar both in sequence and domain architecture to the human KynB
552 than the $KynB_{Pae}$ (Fig. 10C), and we found no trace of an enzyme that catalyzes the formation
553 of N-formyl-kynurenine from tryptophan in *A. baumannii*.

554 We next confirmed that the presence of the kynurenine cluster allows *A. baumannii* to grow
555 on kynurenine as a sole carbon- and energy source (Figure 10D). A deletion of the Kyn-
556 cluster abolished growth on kynurenine but not on anthranilate, the product of KynU (Figure
557 10D). In a last step, we investigated the phylogenetic profile of the Kyn-cluster in greater
558 detail (Figure 10E and S18 Figures SF5). Within *Acinetobacter*, the cluster is almost
559 exclusively present in the pathogens of the ACB clade, and it has been lost several times
560 independently within *A. calcoaceticus*. Along the same lines, we find the Kyn-cluster in a
561 proteobacteria-wide screen across more than 1,000 species (see S19 Table SF3 for the list of
562 genomes and identifiers) only in a few taxa, of which many are opportunistic human
563 pathogens (SF5). Taken together, our findings provide strong evidence that members of the
564 ACB clade possess the genetic infrastructure to interfere with the tryptophan metabolism of
565 humans, as it was already shown for *P. aeruginosa* [105]. This opens up a novel and hitherto
566 unexplored route of how these pathogens interacts with its human host.

567 ## Discussion

568 In contrast to more virulent bacteria, the opportunistic nosocomial pathogens from the
569 genus *Acinetobacter* pursue a resist-and-persist strategy [25]. Instead of pinpointing
570 individual key determinants of bacterial virulence, this requires the unraveling of a likely
571 broad and less specific genetic basis conveying adaptation to clinical environments and, at
572 the same time, to the human host. Experimental studies, either *in vitro* bringing the
573 advantage of controlled experimental conditions, or *in vivo* with the advantage of a realistic
574 infection model have provided fundamental insights into the pathobiology of *Acinetobacter*
575 [19, 20, 40]. However, pathogens encounter – and therefore have to adapt – to diverse
576 environments during host infection [106]. The resulting selective landscape is complex, and
577 therefore hard to reproduce in an experimental setup. Virulence determinants that are

578 relevant only under specific conditions or whose functions blend in with the bacterial
579 metabolism are easy to miss. Evolutionary approaches can close this gap. They focus on the
580 signal if a gene or a gene cluster likely contributes to pathogenicity, reflected by their
581 prevalence preferentially in pathogens, independent of the precise conditions when it is
582 active. Here, we have charted the genetic specifics of the pathogenic ACB clade at a
583 resolution ranging from a genus-wide overview down to individual clonal lineages within *A.*
584 *baumannii*. To ease the future integration of evolutionary evidence with functional studies,
585 we have developed the *Acinetobacter* dashboard Aci-Dash. This is the first web application
586 that allows the community to mine the abundance profiles of genes encoded in 232
587 representative genomes together with their functional annotations and their connection to
588 virulence factors.
589 Comparative genomics studies across the genus *Acinetobacter* have been performed before
590 (e.g. [9, 107]). The integration of orthology assignments with shared synteny analyses at a
591 scale that spans several thousand *Acinetobacter* genomes is yet unprecedented. The $ESGC_{ACB}$
592 detected here form relevant starting points for further unravelling the regulatory and
593 functional network in a human pathogen. They result in a rich set of testable hypotheses
594 whose experimental validations will likely deepen the understanding of the genetic basis of
595 *Acinetobacter* pathogenicity. Moreover, the lineage specific absence of ESGC within the
596 pathogenic clade, most prominently demonstrated by the loss of the QS-NRPS cluster
597 together with the Csu cluster in the IC 8, or of several clusters in *A. calcoaceticus*, helps to
598 better predict in which characteristics individual strains, clonal lineages, and species differ
599 from the prototype of an *Acinetobacter* pathogen.
600 The functions conveyed by these clusters are diverse and many can be readily connected to
601 *Acinetobacter* pathogenicity: Quorum sensing and biofilm formation [93], ROS response

602 [108], and micronutrient acquisition [77]. On top of these, the abundance of gene clusters
603 involved the carbohydrate metabolism, a largely uncharted area of *Acinetobacter* virulence
604 factors [29], strongly suggests that members of the ACB clade follow a general evolutionary
605 trend towards greater metabolic flexibility, which is common to many bacterial pathogens
606 [30, 106]. Such generalists have a selective advantage over niche-specialists in environments
607 that are frequently disturbed or altered [109].
608 Metabolic interaction with the host, in particular those involving amino acids, have an
609 interesting further implication, that has thus far not been considered in the context of
610 *Acinetobacter* pathogens. They can modulate regulatory systems involved, for example, in
611 the finetuning of the host immune response [30, 110]. The Kynurenine (Kyn) pathway
612 detected in this study is a likely example of this connection. This cluster is almost entirely
613 confined to the pathogenic members of the ACB-clade. Interestingly, and in contrast to the
614 human pathogen *P. aeruginosa,* which also harbors a Kyn pathway, the key enzyme, IDO
615 (KynA), that allows the bacteria to directly metabolize tryptophan via the kynurenine
616 pathway is missing (cf. Fig. 10B). How then do they fuel this pathway? Interestingly,
617 tryptophan depletion via the kynurenine pathway is an important human immune defense
618 mechanism upon bacterial infection [111]. Here, we provide first time evidence that
619 pathogenic *Acinetobacter* species from the ACB clade can use the intermediate metabolites
620 of the host response as additional carbon- and energy sources, likely further promoting its
621 growth. However, the ability to degrade the intermediates of the human tryptophan
622 catabolism has a further interesting implication for in the host-pathogen interaction. While it
623 was shown that *P. aeruginosa* produces elevated levels of kynurenine to inhibit ROS
624 production and aid bacterial survival [112], *Acinetobacter* species in possession of the Kyn
625 cluster must pursue a different strategy. By scavenging kynurenine from their environment,

626 they can potentially interfere with the homeostasis of the human immune system, in
627 particular with its suppressive effect on T cells and Natural killer cells. This potentially leads
628 to host tissue damage due to the now uncontrolled production of ROS [76, 79]. Though at a
629 high cost, this would allow the bacteria to use the rich nutrient resources enclosed in the
630 host cells.
631 In summary, antimicrobial resistance is one of largest threats to global health. On the
632 example of *Acinetobacter*, we have shown that the incorporation of a broad evolutionary
633 perspective can pinpoint individual genes or entire pathways that result in novel and viable
634 hypotheses of how the bacteria persist, feed off and interact with the host. At an early phase
635 of drug development, these candidates provide promising anchor points from which the
636 development of new therapeutic strategies to either prevent or treat *Acinetobacter*
637 infections can be initiated.
638

639 Methods

640 Data Acquisition

641 The full data set (Set-F) comprises all assemblies in the NCBI RefSeq data base (version 87)
642 stating 'Acinetobacter' in the 'organism' field [S1 SA1]. From Set-F, we selected in total 232
643 representative strains covering all available type, reference and representative genomes, as
644 well as all validly named species (https://apps.szu.cz/anemec/Classification.pdf) for which a
645 genome sequence was available at the study onset are represented. We further picked
646 genomes of several *A. baumannii* strains that are of interest due to e.g., their context of
647 isolation as well as representatives of eight international clone types. Lastly, we included
648 genomes from Set-F into Set-R that allow for an increase of the fraction of total phylogenetic

649 diversity covered without compromising the quality (cf. S2 Suppl. Text: Taxon Set
650 Construction). An overview of Set-R is provided in S3 SA2.
651 To compile the *Proteobacteria* data set (n=1363), we selected all *Proteobacteria* represented
652 in NCBI RefSeq data base (version 204) and selected one representative per species, which
653 was either annotated as "reference" or "representative" strain.

654 International Clone Type (IC) and MLST assignments

655 For all strains in Set-F, we determined the sequence type with MLSTcheck v2.1.17 [113]
656 using two different schemes, Oxford [114] and Pasteur [115], that were obtained from the
657 PubMLST website (http://pubmlst.org/abaumannii/). All members of the *A. baumannii* clade
658 were assigned to an international clone (IC) type whenever we found literature evidence
659 that the predicted sequence types and IC were unambiguously linked using the following
660 publications as a source: [35, 115-124]. The final assignments are provided in S1 SA1 and S3
661 SA2 based on strain typing results provided in S22 Tables SC2.

662 Phylogenetic diversity

663 Phylogenetic diversity scores of SET-F and SET-R were computed with PDA v.1.0.3 [125]
664 using the options *-k=234:3027* and *-if=handpicked.list* based on the ML tree of SET-F. 25 low
665 quality assemblies were pruned prior to this analysis to avoid overestimation because of
666 long branches resulting from sequencing errors. A detailed description of the quality
667 assessment is provided in S2 Suppl. Text: Taxon Set Construction.

668 Average Nucleotide Identity

669 All genome sequences within Set-R were pair-wise aligned with Nucmer v3 [126], and the
670 Average Nucleotide Identities (ANIm) were calculated with the script
671 average_nucleotide_identity.py from the Python package pyani v0.2.7 [127] using the
672 following options*: -i ./genomes -o ./output/ -m ANIm -g --gmethod seaborn –maxmatch*.

673 ## Ortholog Search

674 All against all orthology searches were performed with OMA standalone v.2.2.0 [45] and
675 default parameter settings, except for decreasing the minimum length threshold for
676 sequences considered (MinLen) to 40 residues. Targeted ortholog searches were performed
677 with fDOG [128] using the OMA orthologous groups from SET-R to train the profile hidden
678 Markov models.

679 ## Inference of the pan and core gene sets (SET-R)

680 The pan-genome size was calculated as the sum of the number of OGs and number of strain
681 specific proteins (i.e. proteins without orthologs). For the rarefaction analysis, we identified
682 the number of new orthologs and singletons per added genome in Set-R. The core genome
683 was defined as the subset of OGs where each taxon of Set-R contributed exactly one
684 ortholog. However, the strict definition of the core genome, yielded very small core genome
685 estimates due to qualitative differences and incomplete draft genomes (S2 Suppl. Text:
686 Table 1). We therefore relaxed the core genome definition and allowed a core-gene to be
687 absent in 1% of the genomes (max. 3 out of the 232) in Set-R (see S2 for further details). To
688 obtain these values as a function of the number of genomes considered, we simulated a
689 sequential inclusion of genomes in SET-R. Following the approach from Tettelin et al. [129],
690 Pan- and core genome sizes were extrapolated by fitting the power law function $yP = \kappa Pn$
691 $^{\gamma} + c$ and an exponential decaying function $yc = \kappa c \exp[-n*\tau c] + \Omega$, respectively, with
692 nonlinear least-squares (Levenberg–Marquardt algorithm). Given the large taxon set in our
693 study, we limited the simulation to 100 random permutations of a sequential inclusion.

694 ## Phylogenetic tree reconstruction

695 SET-R: Multiple sequence alignments (MSAs) for each orthologous group were generated
696 with MAFFT-LiNSI [130] (v7.394, default parameters). Next, each protein's CDS was obtained

697 and PAL2NAL v14 [131] with the option *-codontable 11* was employed to infer protein
698 sequence guided nucleotide MSAs. Supermatrices built from concatenated MSAs served as
699 input for the maximum likelihood (ML) tree reconstruction. The best fitting substitution
700 model (GTR + empirical base frequencies + free rate heterogeneity with 10 categories) was
701 determined using IQ-Tree v1.6.8 [132] using the option *-m TEST*, and the following
702 parameters were used for the ML tree reconstruction with IQ-Tree: *-m GTR+F+R10 -nt 6*
703 *AUTO -bb 1000 -alrt 1000*. Additionally, statistical branch supports were assessed with 1000
704 repetitions of UF bootstraps and SH-aLR branch tests. Trees were outgroup-rooted with
705 *Moraxella catarrhalis* (strains BBH18 and FDAARGOS_213) and *Alkanindiges illinoisensis* DSM
706 15370.
707 SET-F: The phylogenetic tree reconstruction of SET-F followed the same general work flow as
708 described for Set-R. However, to decrease the computational burden, trees were computed
709 on the amino acid sequence alignments. MAFFT was run with the '--auto' parameter.
710 Supermatrices of resulting protein MSAs were used as input for ML tree reconstruction with
711 IQ-TREE ('-alrt 1000 -bb 1000 -nt 8 -m LG+I+G+').
712 Majority-rule consensus trees were computed with SplitsTree v4.14.4 [133].

713 Inference of hierarchical orthologous groups and reconstruction of last common ancestor
714 dispensable and core gene sets

715 Hierarchical orthologous groups (HOGs) for the Set-R were inferred from the pairwise OMA
716 orthology relations and the consensus ML species tree using the GETHOG algorithm [134] as
717 implemented in OMA stand-alone v. 2.2.0. The Set-R pan genome was stratified by assigning
718 each HOG to the internal node of the tree that represents the last common ancestor (LCA) of
719 the two most distantly related taxa in the HOG. Clade-specific losses of a gene were inferred
720 when all members of a clade lacked an ortholog that was assigned to an evolutionarily older

721 node. On this basis, we reconstructed the pan-genomes for each internal node of the tree as
722 following: We united all genes assigned to internal nodes on the path from the root to the
723 node under study and removed the union of genes that have been lost on this path.

724 ## GO annotation and GO term enrichment analysis

725 All 502,095 unique protein accessions represented in SET-R were mapped to uniprotKB
726 identifiers (UniProt accessed 9th of Febr. 2018) to obtain the annotated gene ontology (GO)
727 terms [135]. Significantly enriched GO terms were identified using a two-tailed Fischer's
728 exact test at a significance level of 0.05. Multiple test correction was done by computing the
729 false discovery rate for each term and considering only terms with an FDR < 0.05. For GO
730 term enrichment analyses at the individual internal nodes of the tree, we used the LCA pan
731 gene sets as background sets (population) and the set of genes assigned to this node as test
732 (study) set. Both sets were limited to include only genes for which orthologs are represented
733 in at least 50% of the taxa descending from this node (analysis without this cutoff is included
734 in S10 Table SD1.3). Information about the GO terms were pulled from
735 http://purl.obolibrary.org/obo/go/go-basic.obo (accessed 22nd of June 2018). Visualization
736 of tree maps were performed with REVIGO [136].

737 ## Prediction of Secreted Proteins

738 Unless the subcellular localization of a protein was provided by uniprot, we prediceted
739 Its subcellular localization with Psortb v3.06 [137] and ngLOC v1.0 [138]. All proteins
740 classified as 'Extracellular' or 'OuterMembrane' by either tool were combined into a set of
741 secreted and accessible proteins. Conflicting predictions or cases where Psortb labeled the
742 localization of a protein as 'unknown' were resolved in favor of the ngLOC classification as it
743 demonstrated higher precision for these classes when we benchmarked both against a test-
744 set of experimentally verified proteins published by Shen et al. [139].

745 ## Annotation of Protein Function

746 For each protein, we considered, where available, its functional annotation provided in
747 RefSeq, in the uniprot database, and the assigned GO terms. Additionally, we annotated the
748 proteins with KEGG Orthology (KO) identifiers [47] using GhostKoala v2.2 [140]. Eventually,
749 for proteins with reciprocal best blast hit orthologs in *A. baumannii* ATCC 17978, we
750 transferred the functional annotation provided by the COG database [46] (accessed in May
751 21st 2020).

752 ## Virulence Factor Identification

753 HOGs representing known virulence factors were identified via blastp searches (v2.10.1)
754 [141] against a custom database of virulence factors. To compile this database, we united
755 entries of PATRIC [21] and VFDB [48] (both accessed September 23rd 2020). Subsequently,
756 we clustered the proteins at 95% sequence similarity with cd-hit v4.6.4 [142] using the
757 options *-G -al 0.95 -s 0.9 -c 0.95* to reduce redundancy. A HOG represents a virulence factor
758 if any of the subsumed orthologs has a hit with >50% alignment coverage and an e-value
759 <0.01. For all such instance the best hit's annotation was transferred.

760 ## Identification of Evolutionarily Stable Gene Clusters (ESGC)

761 Using the genome of *A. baumannii* ATCC 19606 as a reference, we identified clusters of
762 consecutive genes with highly similar phyletic profiles. For this purpose, each protein-coding
763 gene's corresponding HOG and its profile were analyzed to obtain an 8-dimensional feature
764 vector comprised of the following values: (i-vi) clade-specific fractions of total taxa in *A.*
765 *baumannii* (B), *A. calcoaceticus* (CA), *A. haemolyticus* (HA), *A. baylyi* (BA), A*. lwoffii* (LW), *A.*
766 *brisouii* (BR), and *A. qingfengensis* (QI), (vii) the fraction of the total phylogenetic diversity of
767 the ACB clade covered, and (viii) the label of the inner node the HOG was assigned to (cf. Fig.
768 3). Four genes were excluded from the orthology search due to their short length. For these,

769 we imputed the values using the mean values of the two flanking genes. Based on these
770 vector representations, we computed a pairwise dissimilarity matrix, using the Gower
771 dissimilarity index [143]. We then arranged the genes in a graph, where a vertex between a
772 gene and its downstream neighbor was drawn, if a) their pairwise dissimilarities is smaller
773 than the 5th percentile of the gene's dissimilarity distribution across the full gene set or b) if
774 the condition *a* is met by the two genes flanking the gene. The resulting set of connected
775 components were then extracted as candidate evolutionary units.

776 ### Candidate ESGC Abundance Statistics

777 For each gene in a candidate ESGC, we computed its retention difference (RD) as the
778 difference in the fraction of taxa within the ACB clade subtracted by the fraction of taxa
779 outside the ACB clade harboring an ortholog. The candidate ESGCs were then ranked by the
780 median of the RD across all genes in the cluster. As a further measure, we devised the
781 cluster-conservation score difference (CCD), which is calculated similar to the RD score, but
782 this time assessing presence of the cluster rather than that of an individual gene. A cluster
783 was considered present only if at least 80% of its genes (orthologs) were identified and at
784 least 25% of the gene order was conserved in the genome. Here, we treated the cluster as a
785 set of ordered and oriented (considering direction of transcription) two-element tuples.
786 Clusters with a CCD below 0.25 were not further considered. For each of the resulting top
787 150 ranked clusters, we inspected cluster conservation across the taxa in Set-R and Set-F
788 using Vicinator v0.32 (https://github.com/BIONF/Vicinator). Cluster boundaries of an ESGC
789 were manually curated, when the Vicinator analysis indicated a miss due to an individually
790 bloated abundance profile (false-positive orthologs or paralogs).

791 Kynurenine (Kyn) cluster deletion mutant and growth experiments with *A. baumannii* Ab04

792 Ab04 mutant with deletion of the locus of $ESGC_{ACB}$-0452 (Ab04 Δkyn) were constructed as
793 described previously [144]. Briefly, a FRT site-flanked apramycin resistance cassette was
794 amplified from a variant of pKD4 [145] with primers harboring 18-25 nucleotides matching in
795 sequence the flanking regions of the locus of $ESGC_{ACB}$-0452 (see S20 Table SF8). Also,
796 upstream and downstream regions of $ESGC_{ACB}$-0452 were amplified and the obtained
797 fragments were assembled by overlap extension PCR. The PCR product was electroporated
798 into *A. baumannii* Ab04 electrocompetent cells carrying pAT04, which expresses the RecAB
799 recombinase induced with 2mM IPTG [1]. Mutants were selected with apramycin and
800 integration of the resistance marker was verified by PCR. To remove the resistance cassette,
801 electrocompetent mutants were transformed with pAT03 plasmid (which expresses the FLP
802 recombinase) and apramycin-sensitive clones of unmarked deletion mutants were obtained.
803 Finally, the mutant strains were confirmed by antibiotic resistance profile, PCR and genome
804 sequencing.

805 Ab04 WT and Ab04 Δkyn mutant strains were grown in lysogeny broth (LB) liquid medium
806 under shaking conditions (200 rpm) at 37°C. Overnight cultures were washed three times
807 with PBS and diluted to an OD_{600} of 0.01 in 150 µl of M9 minimal medium supplemented
808 with 0.2% casamino acids (M9CAA), 2.5 mM L-kynurenine (Sigma, A8625) or 2.5 mM
809 anthranilic acid (Sigma, A89855) in 96-well plates, followed by incubation at 37°C under
810 shaking conditions in a BioTek microplate spectrophotometer. The OD_{600} values were
811 measured every 30 min for 16h. Three independent experiments were performed with three
812 wells per assay for each strain and condition.

813 ## Growth Experiments for Carnitine, Malate, and Glucarate

814 *A. baumannii, A. baylyi* and *A. calcoaceticus* strains were grown at 37 °C (*A. baumannii*) or
815 30 °C (*A. baylyi* and *A. calcoaceticus*) in mineral medium (MM) that consists of 50 mM
816 phosphate buffer, pH 6.8, and different salts (1 g NH_4Cl, 580 mg $MgSO_4 \times 7$ H2O, 100 mg
817 KNO_3, 67 mg $CaCl_2 \times 2\ H_2O$, 2 mg $(NH_4)_6Mo_7O_{24} \times 4\ H_2O$, 1 ml SL9 (per liter: 12.8 g Titriplex, 2
818 g $FeSO_4 \times 7\ H_2O$, 190 mg $CoCl_2 \times 6\ H_2O$, 122 mg $MnCl_2 \times 4\ H_2O$, 70 mg $ZnCl_2$, 36 mg $MoNa_2O_4$
819 $\times 2\ H_2O$, 24 mg $NiCl_2 \times 6\ H_2O$, 6 mg H_3BO_3, 2 mg $CuCl_2 \times H_2O$ per l medium; pH 6.5) [146] and
820 20 mM of the given carbon source. Precultures were grown in MM with 20 mM Na-acetate
821 as carbon source. Each value is the mean of +/- S.E.M. of at least three independent
822 measurements. Growth curves were fitted manually.

823

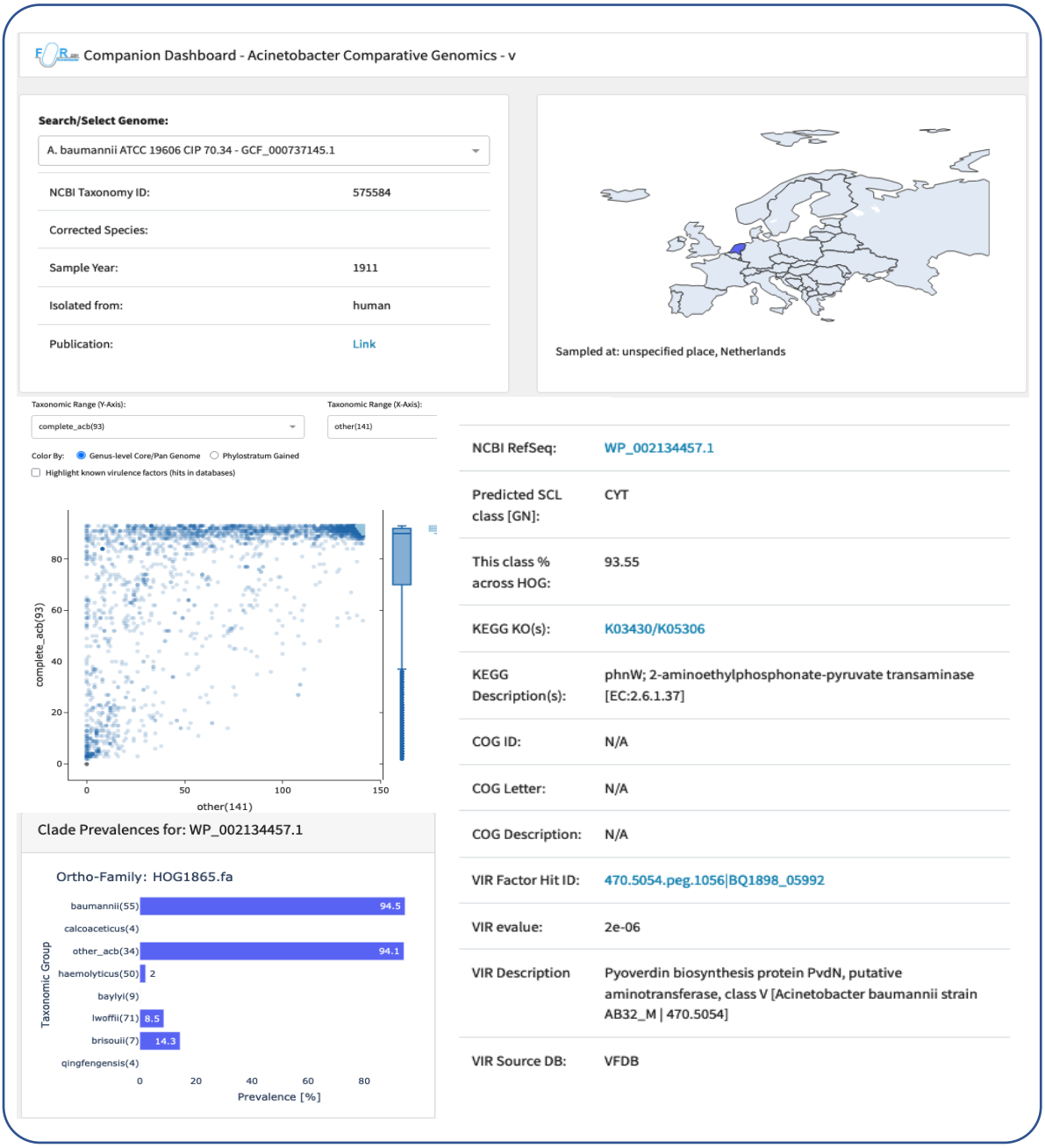

Figure 1: Aci-Dash – An interactive web-application to explore phylogenetic abundance patterns and accessory annotations for the Set-R pan-genome. For each of the 232 strains, Aci-Dash provides further details about year and site of sampling. The interactive scatter plot reveals, for each gene of the selected strain, the abundance of orthologs in a user-defined in- and outgroup. For each gene individually, the ortholog abundance can be resolved on a clade level (cf. Fig. 2), and further information including functional annotation transfer from KEGG and COG as well as known virulence factors is displayed.

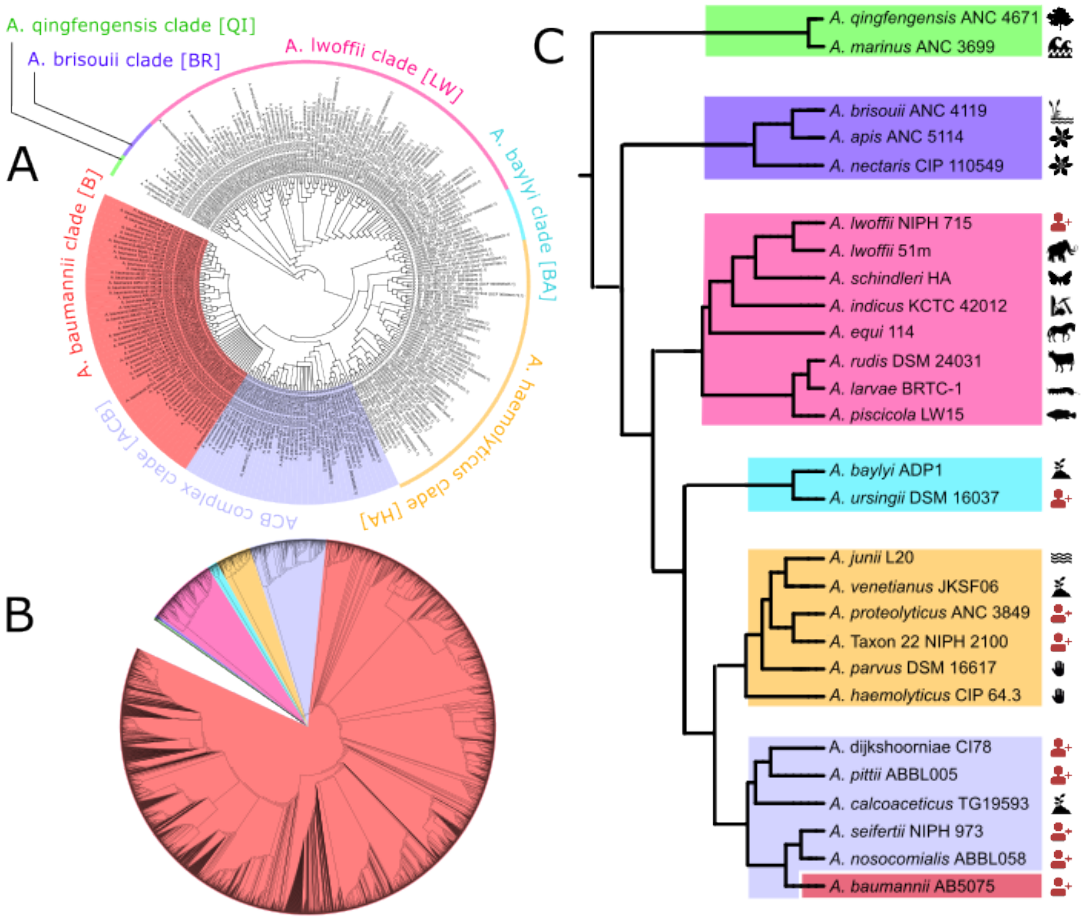

Figure 2: The phylogeny of the genus Acinetobacter. A) *Majority-rule consensus phylogeny of 232 Acinetobacter strains represented in SET-R. Solid branches are supported by all, and hatched branches by two out of three trees.* ***B)*** *The maximum likelihood tree for all 3052 taxa in Set-F. Colored clades represent the same clades as in A). A high-resolution image of this tree is provided in S21 Fig. SB3.* ***C)*** *The evolutionary backbone of the Acinetobacter genus with exemplarily chosen strains as clade representatives. The color scheme resembles that of Fig. 2A. The pictograms next to the leaf labels indicate the sampling source of the particular strain. Red pictograms signal a strain that was isolated from an infected patient.*

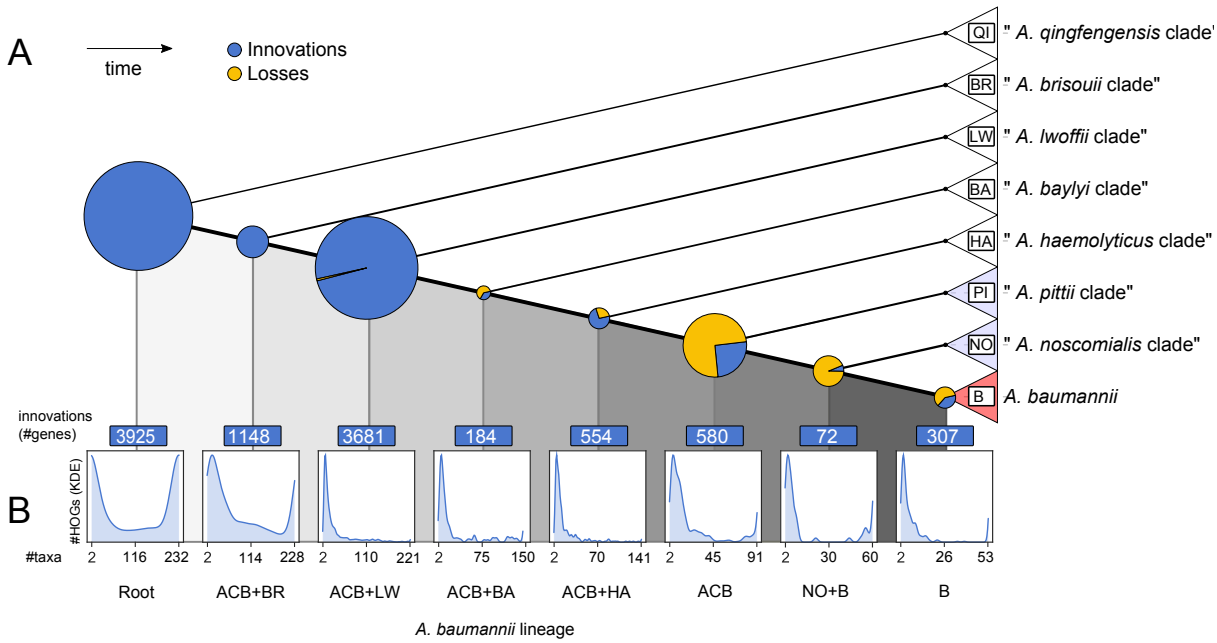

Figure 3: A phylogenetic stratification of the Acinetobacter pan-genome*. (A) Pie charts on the internal nodes indicate numbers of genes added (blue) or lost (yellow) from the respective pan-genome where the diameter is proportional to the sum of both gained and lost genes. Clades resemble those from Fig. 2. (B) For each node, histograms represent the number*

of descending taxa an added gene is represented in. The minimum value is 2, the maximum value is the number of taxa subsumed in the corresponding clade.

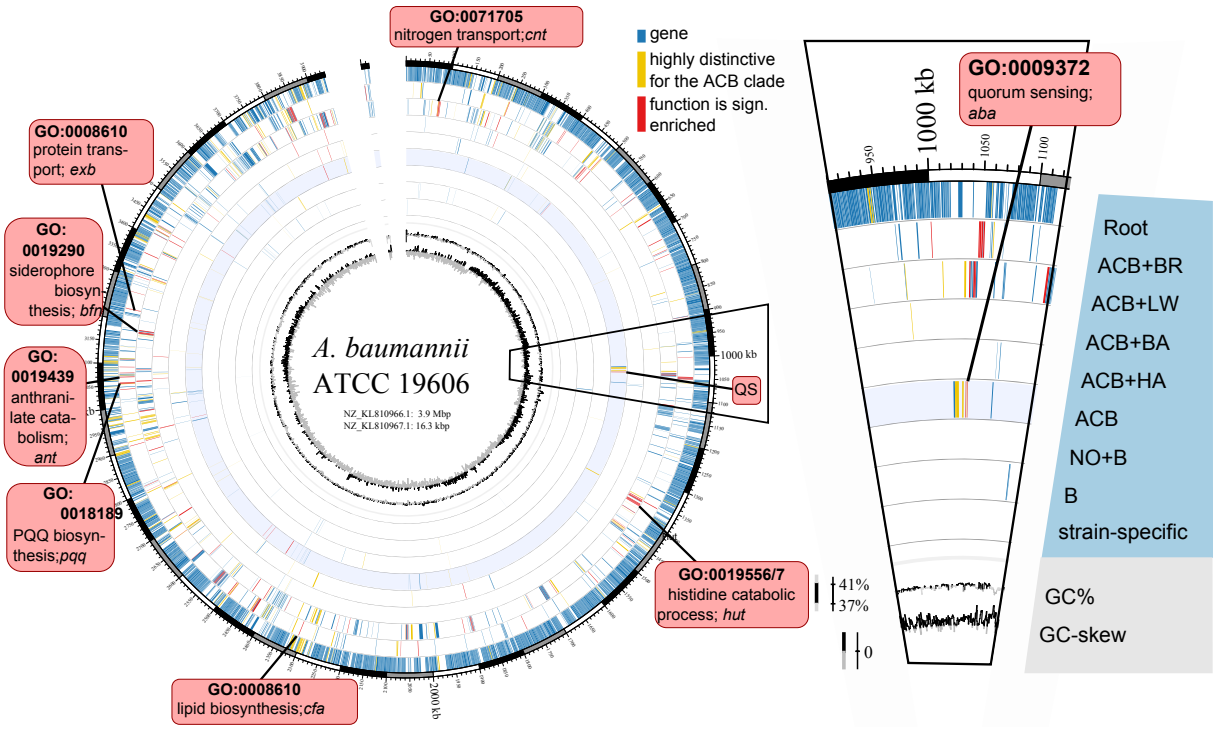

Figure 4: Phylogenetic strata in the protein-coding gene set of Ab. ATCC 19606. *Each protein-coding gene was assigned to one of the nine layers specified in the inlay to the right (cf. Fig. 3). All genes annotated with GO terms that were significantly enriched in the individual layers are colored in red. Genes assigned to orthologous groups which were ranked within the 10 percent groups with highest retention differences (RD >=0.708, n=355) across the ATCC 19606 gene set are colored in yellow. Red boxes highlight selected gene loci where neighboring genes contributed to the enrichment of the same GO term (biological processes).*

Figure 5: Phylogenetic profiles of 44 functionally annotated ESGC$_{ACB}$ across the Set-F. *Shown are the selection of ESGC$_{ACB}$ with the highest abundance difference between the ACB clade and non-ACB taxa (RD). Ids refer to the corresponding connected components provided in S11 Table SE1.3. Gene clusters are ranked by decreasing RD. The CCD (cluster conservation difference, violet) is calculated as the difference between the relative fractions of ACB-genomes minus non-ACB genomes where the cluster is present. The heat map informs about the fraction of taxa per clade harboring the ESGC$_{ACB}$ ranging from 0 (white) to 1 (dark blue). The total number of subsumed taxa per clade are given next to the leaf label in the above tree. IC1-8 represent the cluster abundance in the 8 international clone types of A. baumannii. Clusters associated with metabolic pathways are highlighted in red. "#" marks an ESGC where we curated cluster boundaries based on literature evidence and confirmed cluster conservation using microsynteny (cf. Fig. 4B). '*' marks ESGC$_{ACB}$ that encompass additional genes not covered by the functional annotation. Abbreviations: NRPS = non-ribosomal peptide synthesis; QS = quorum sensing; 2-AEP =2-aminoethylphosphonate; PNAG = polymeric β-1,6-linked N-acetylglucosamine; NAMPT = nicotinamide phosphoribosyl transferase; PRPS = 5-phosphoribosyl pyrophosphate synthetase; GABA = gamma-aminobutyric acid; PQQ = pyrroloquinoline quinone.*

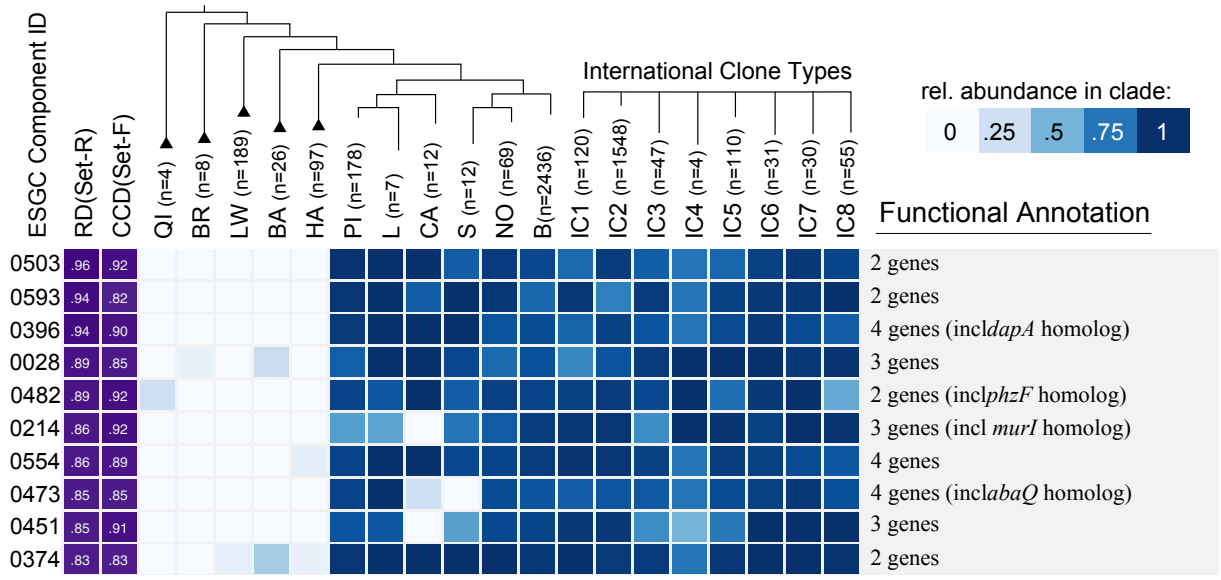

Figure 6: Top 10 ESGC$_{ACB}$ with unknown cluster function. *The genes of these clusters are mostly annotated as 'hypothetical" or "DUF-containing protein", i.e. proteins with annotated with a domain of unknown function. Due to their stable microsynteny and high prevalence across the ACB clade, they are highly interesting candidates for further functional characterization. The figure layout follows Fig. 5.*

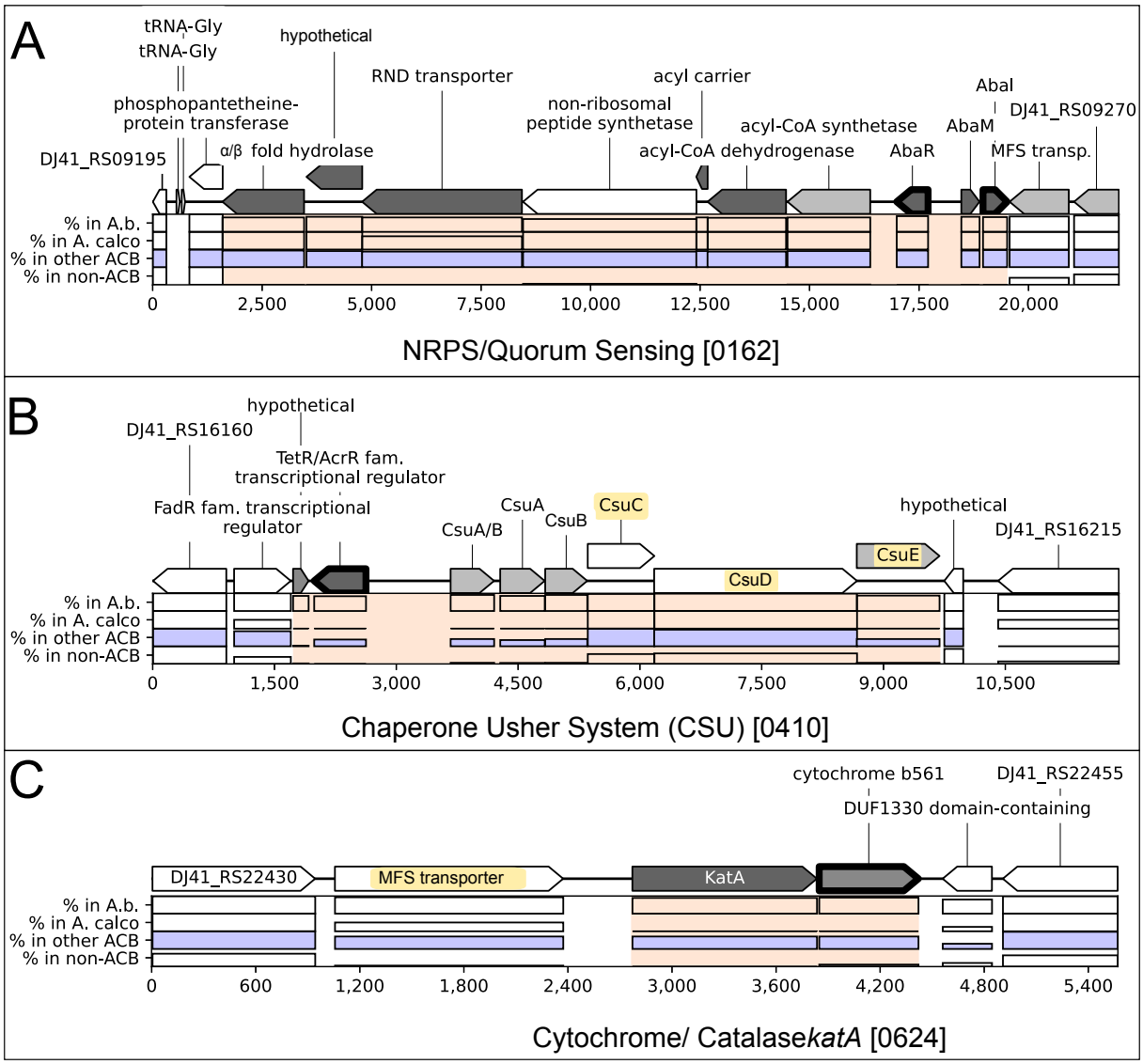

Figure 7: Three examples for ESGC$_{ACB}$ in the genome of Ab ATCC 19606. *Bar plots indicate relative abundance within the selected taxonomic groups (see legend). The ESGC$_{ACB}$ are embedded into two flanking protein-coding genes on each side that are not part of the cluster. Cluster boundaries are indicated by a pink background. Genes indicated in yellow have been either added to or excluded from the automatically generated clusters based on microsynteny analyses across Set-R. A) ESGC$_{ACB}$ – 0162 unites AbaR and AbaI (quorum sensing) with a non-ribosomal peptide synthetase cluster upstream. B) ESGC$_{ACB}$ – 0410 encompasses the cluster necessary for the Csu pilus formation. Note the deviating abundance pattern for CsuC and CsuD, which is due to the presence of prpC and prpD, two paralogous genes from the photoregulated pilus ABCD (prpABCD), in the respective orthologous groups. Microsynteny analyses confirmed that the entire Csu cluster forms one evolutionary unit (S15 SE2.0410). C) ESGC$_{ACB}$ – 0624 harbors a catalase, a cytochrome b561. Although the MFS transporter shares a similar abundance pattern across the taxa of Set-R, this transporter is not evolutionarily stably linked to the other two genes (S15 SE2.0624).*

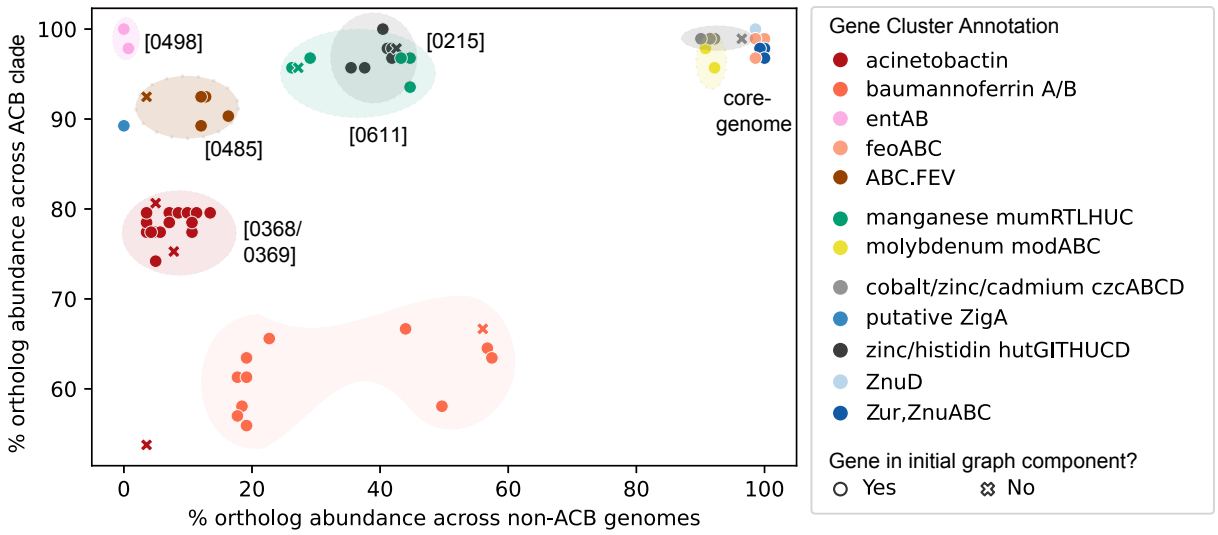

Figure 8: Abundances of micronutrient acquisition genes/clusters of Ab ATCC 19606 within and outside the ACB clade. *Absolute abundances were based on cluster-evaluation using micro-synteny. Genes clusters are annotated with the* $ESGC_{ACB}$ *identifiers in Fig. 5. Genes that are part of a cluster but missed by the initial ESGC compilation share the same color but are marked as x. Gene clusters at the top right, e.g., feoABC, represent micronutrient acquisition clusters belonging to the genus' core genome. Gene clusters at the top left, e.g., entAB, are confined to the ACB clade where they are ubiquitously present.*

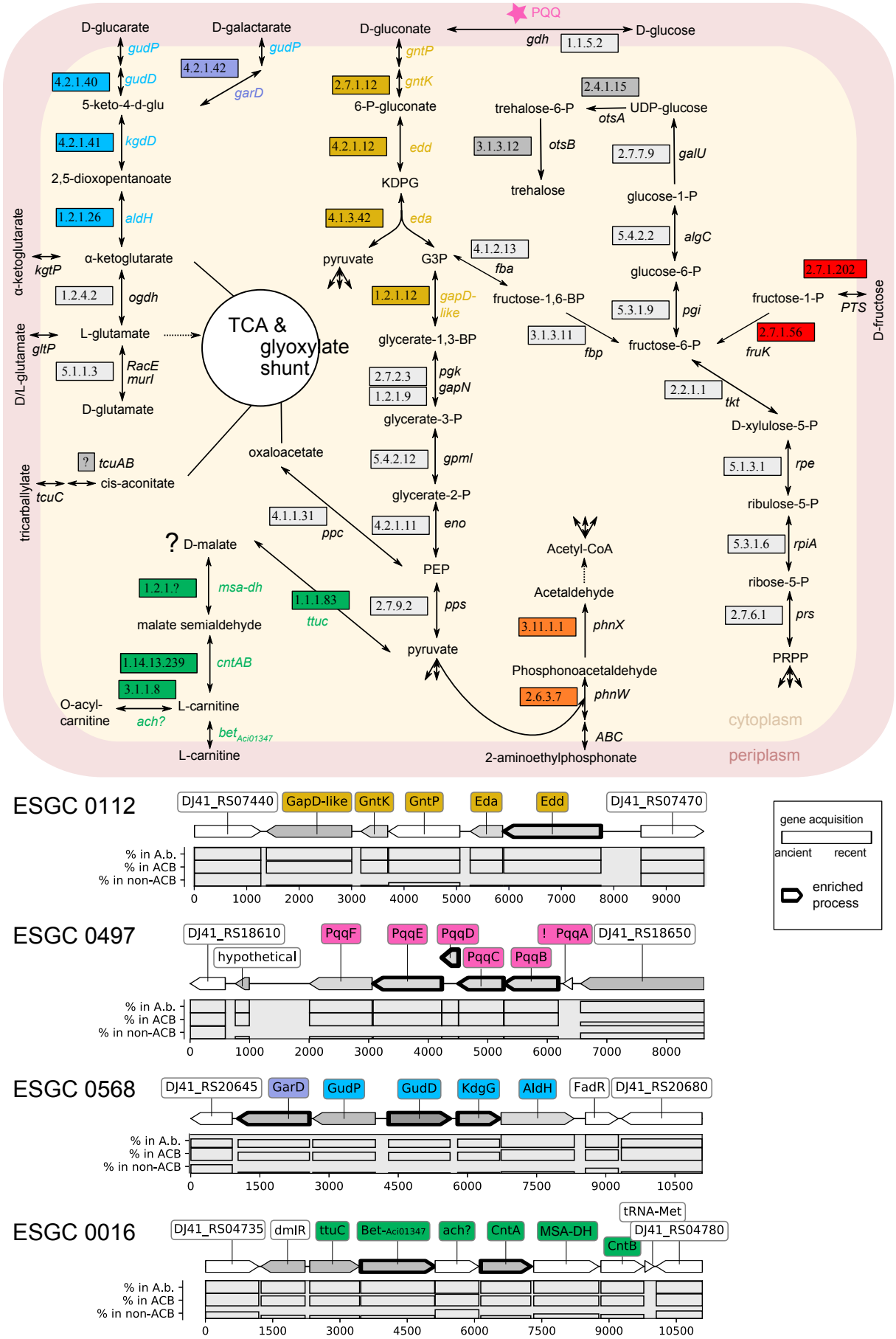

Figure 9: Members of the ACB clade have extended their basal carbohydrate metabolism. *The pathway map shows a model integrating four metabolic pathways represented by the ESGC$_{ACB}$ 0112 (Entner-Doudoroff pathway; yellow), 0497 (biosynthesis of Pyrroloquinoline quinone; magenta), 0568 (glucarate/galactarate catabolism; blue/violet) and 0016*

(carnitine catabolism; green) into the bacterial carbohydrate metabolism (grey boxes). Abbreviations: KDPG - 2-keto-3-deoxy-6-phosphogluconate; G3P – glycerinealdehyde-3-phosphate. The corresponding gene clusters are shown below the pathway map with one protein-coding flanking gene on either side that is not part of the cluster. The layout follows Fig. 7. $ESGC_{ACB}$ 0112: GapD-like – glyceraldehyde-3-phosphate dehydrogenase [1.2.1.12]; GntK - gluconokinase [EC:2.7.1.12]; Edd - phosphogluconate dehydratase [EC:4.2.1.12]); Eda - 2-dehydro-3-deoxyphosphogluconate aldolase / (4S)-4-hydroxy-2-oxoglutarate aldolase [EC:4.1.2.14 4.1.3.42]; GntP - gluconate permease [E2.7.1.12]. Note, GntP shares high sequence similarity with a gluconate transporter (H+ symporter) in Escherichia coli (98% coverage, 45% identity). $ESGC_{ACB}$ 0497: pqqA-F. No abundance profile is shown for pqqA, since its length excluded it from orthology prediction (indicated by an '!'. See main text for details). $ESGC_{ACB}$ 0568: GarD - galactarate dehydratase [EC:4.2.1.42]; gudD - glucarate dehydratase [EC:4.2.1.40]; kdgD - 5-dehydro-4-deoxyglucarate dehydratase [EC:4.2.1.41]; aldH - 2,5-dioxopentanoate dehydrogenase [EC:1.2.1.26]; gudP - MFS transporter, D-glucarate/D-galactarate permease; FadR - Fatty acid metabolism regulator protein. $ESGC_{ACB}$ 0016: ttuc - D-malate dehydrogenase [EC:1.1.1.83]; Bet-Aci01347 - glycine/betaine transporter Aci01347; ach? – putative acylcarnitine hydrolase [EC:3.1.1.8]; CntAB – carnitine monooxygenase reductase subunit A and B [EC:1.14.13.239]; MSA-DH – malic semialdehyde dehydrogenase [EC:1.2.1.?]. Further colored pathways represent the clusters $ESGC_{ACB}$ 0627 (2-aminoethylphosphonate metabolism, orange), $ESGC_{ACB}$ 0453 (fructose transport/metabolism, red), $ESGC_{ACB}$ 0064 (trehalose biosynthesis, dark grey), and $ESGC_{ACB}$ 0078 tricarballylate metabolism, brown). Their corresponding genomic regions are available in S12.

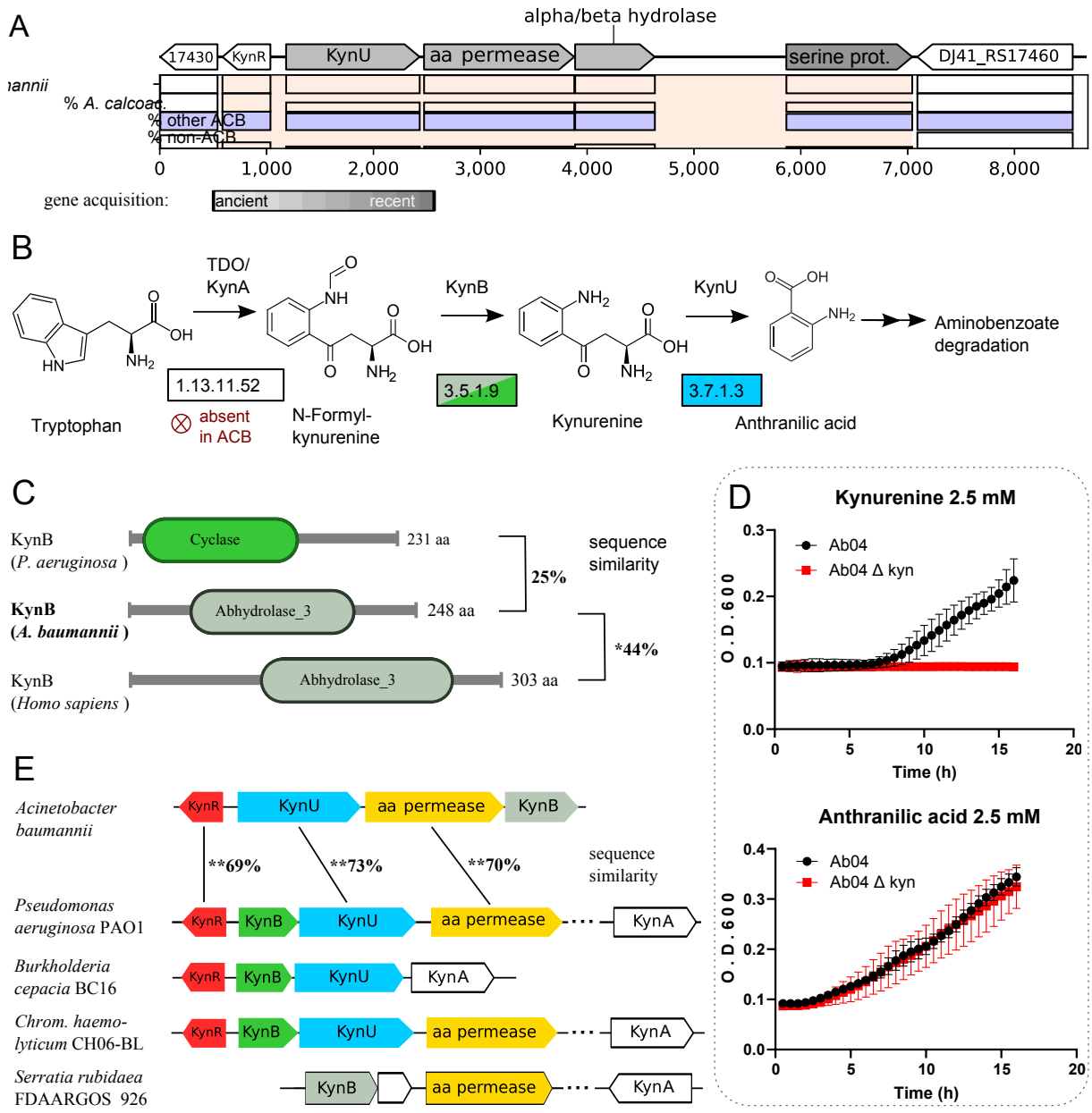

Figure 10: Evolutionary and functional characterization of the A. baumannii kynurenine pathway. *A) The locus of ESGC$_{ACB}$ 0452 in A. baumannii ATCC 19606. KynR - Lrp/AsnC family transcriptional regulator; KynU - kynurenine hydrolase; amino acid (aa) permease (uncharacterized); alpha/beta hydrolase (uncharacterized; putative kynB); serine proteinase. Cluster layout follows that of Fig. 7. B) The Kynurenine pathway of tryptophan degradation. EC numbers of the enzymes catalyzing the individual reactions are given in the boxes. KynB is represented in two versions in bacteria (see C), which are represented by different colors. C) The alpha/beta hydrolase shares a significant sequence similarity and the presence of the Abhydrolase_3 Pfam domain (PF04199) with the human kynurenine formamidase (KynB or KFA) but not with KynB of P. aeruginosa, which instead harbors a Cyclase Pfam domain (PF04199) suggesting an independent evolutionary origin. D) The kynurenine cluster is necessary and sufficient for growth on kynurenine but not on anthranilic acid. Growth of Ab 04 and Ab 04 Δkyn on minimal medium supplemented with kynurenine (top) and anthranilate (bottom). E) Phylogenetic profile of the A. baumannii Kyn cluster. Numbers between the corresponding genes in Ab ATCC 19606 and PA01 represent percent sequence similarity on the amino acid level. KynB of Ab ATCC 19606 and PAO1 are not significantly similar. The Kyn cluster is shared among many proteobacterial (opportunistic) pathogens where the the Pseudomonas-type KynB is prevalent. The human-type KynB has homologs e.g., in Serratia (including S. rubideae). KynA is almost always encoded at a distant locus and entirely absent in Acinetobacter.*

930 ## Declarations

931 **Availability of data and materials**

932 Genomic data analyzed during the current study are publicly available in the NCBI Reference
933 Sequence Database (RefSeq) version 87 and 204. For each selected genome, the assembly
934 accession listed in S1 and S19, respectively. From individual entries, we obtained genome
935 annotation files (*.gff and *_feature_table.txt), protein sequences and coding sequences
936 (*.faa and *cds_from_genomic.fna), and genome sequence (*_genomic.fna) files from the
937 database [ftp://ftp.ncbi.nlm.nih.gov/refseq/release/release-catalog/archive/].
938 In addition, the datasets used and/or analyzed during the current study are available from
939 the corresponding author on reasonable request.
940 All data generated or analyzed during this study and necessary for the interpretation are
941 included in this published article as additional files.
942 Our custom tool Vicinator is linked (https://github.com/BIONF/Vicinator) and publicly
943 available under the GNP license 3.0.
944

945 **Competing interests**

946 The authors declare that they have no competing interests.
947

948 **Funding**

949 This study was supported by a grant by the German Research Foundation (DFG) in the scope
950 of the Research Group FOR2251 “Adaptation and persistence of A. baumannii.” Grant ID EB-
951 285-2/2 to IE, AV 9/7-2 to BA, GO 2491/1-2 to SG, and WI 3272/3-2 to GW. MFF was
952 supported by grants from the National Institute of Allergy and Infectious Diseases (grant

953 R01AI144120). Cloud computational resources through the de.NBI cloud are granted by the
954 German Bundesministerium für Bildung und Forschung grant FKZ 031A533B to AG.
955

956 **Authors' contribution**

957 BD and IE conceived the study. BD performed data collection and curation, tool and app
958 development and performed bioinformatics/statistical analyses. BD and IE together with
959 GDV, MF, GW, BA and SG interpreted the data. SD and GDV performed and interpreted wild
960 type and mutant strain growth experiments on kynurenine and anthranilate. JB performed
961 growth experiments on carnitine, malate and gluconate. MAD developed the CI/CD pipeline
962 for a containerized deployment of Aci-Dash in a cloud-platform under the supervision of AG.
963 BD and IE drafted the manuscript, and all authors contributed to the final manuscript. All
964 authors read and approved the final manuscript.
965

966 **Acknowledgements**

967 The authors wish to thank all researchers for making annotated genome sequences available
968 to the public domain, Prof. Alexandr Nemec for providing on his website an accessible and
969 up-to-date resource of the current species nomenclature of *Acinetobacter*, Vinh Tran for
970 support with fDOG, and Ruben Iruegas for helpful discussion.
971

972 ## References

973 1. Garnacho-Montero J, Amaya-Villar R. Multiresistant Acinetobacter baumannii
974 infections: epidemiology and management. Curr Opin Infect Dis. 2010;23(4):332-9. Epub
975 2010/06/29. doi: 10.1097/QCO.0b013e32833ae38b. PubMed PMID: 20581674.
976 2. Peleg AY, Seifert H, Paterson DL. Acinetobacter baumannii: emergence of a successful
977 pathogen. Clin Microbiol Rev. 2008;21(3):538-82. Epub 2008/07/16. doi:
978 10.1128/CMR.00058-07. PubMed PMID: 18625687; PubMed Central PMCID:
979 PMCPMC2493088.
980 3. Gupta N, Gandham N, Jadhav S, Mishra RN. Isolation and identification of
981 Acinetobacter species with special reference to antibiotic resistance. J Nat Sci Biol Med.

982 2015;6(1):159-62. Epub 2015/03/27. doi: 10.4103/0976-9668.149116. PubMed PMID:
983 25810655; PubMed Central PMCID: PMCPMC4367029.
984 4. Sahl JW, Gillece JD, Schupp JM, Waddell VG, Driebe EM, Engelthaler DM, et al.
985 Evolution of a pathogen: a comparative genomics analysis identifies a genetic pathway to
986 pathogenesis in Acinetobacter. PLoS ONE. 2013;8(1):e54287. Epub 2013/02/01. doi:
987 10.1371/journal.pone.0054287. PubMed PMID: 23365658; PubMed Central PMCID:
988 PMC3554770.
989 5. Visca P, Seifert H, Towner KJ. Acinetobacter infection--an emerging threat to human
990 health. Iubmb Life. 2011;63(12):1048-54. Epub 2011/10/19. doi: 10.1002/iub.534. PubMed
991 PMID: 22006724.
992 6. Wong D, Nielsen TB, Bonomo RA, Pantapalangkoor P, Luna B, Spellberg B. Clinical and
993 Pathophysiological Overview of Acinetobacter Infections: a Century of Challenges. Clin
994 Microbiol Rev. 2017;30(1):409-47. Epub 2016/12/16. doi: 10.1128/CMR.00058-16. PubMed
995 PMID: 27974412; PubMed Central PMCID: PMCPMC5217799.
996 7. Weber BS, Harding CM, Feldman MF. Pathogenic Acinetobacter: from the Cell
997 Surface to Infinity and Beyond. J Bacteriol. 2015;198(6):880-7. Epub 2015/12/30. doi:
998 10.1128/JB.00906-15. PubMed PMID: 26712938; PubMed Central PMCID:
999 PMCPMC4772598.
1000 8. Lob SH, Hoban DJ, Sahm DF, Badal RE. Regional differences and trends in
1001 antimicrobial susceptibility of Acinetobacter baumannii. Int J Antimicrob Agents.
1002 2016;47(4):317-23. Epub 2016/03/30. doi: 10.1016/j.ijantimicag.2016.01.015. PubMed
1003 PMID: 27020541.
1004 9. Touchon M, Cury J, Yoon EJ, Krizova L, Cerqueira GC, Murphy C, et al. The genomic
1005 diversification of the whole Acinetobacter genus: origins, mechanisms, and consequences.
1006 Genome Biol Evol. 2014;6(10):2866-82. Epub 2014/10/15. doi: 10.1093/gbe/evu225.
1007 PubMed PMID: 25313016; PubMed Central PMCID: PMCPMC4224351.
1008 10. Giammanco A, Cala C, Fasciana T, Dowzicky MJ. Global Assessment of the Activity of
1009 Tigecycline against Multidrug-Resistant Gram-Negative Pathogens between 2004 and 2014
1010 as Part of the Tigecycline Evaluation and Surveillance Trial. mSphere. 2017;2(1). Epub
1011 2017/01/27. doi: 10.1128/mSphere.00310-16. PubMed PMID: 28124025; PubMed Central
1012 PMCID: PMCPMC5244261.
1013 11. Wilharm G, Piesker J, Laue M, Skiebe E. DNA uptake by the nosocomial pathogen
1014 Acinetobacter baumannii occurs during movement along wet surfaces. J Bacteriol.
1015 2013;195(18):4146-53. Epub 2013/07/16. doi: 10.1128/JB.00754-13. PubMed PMID:
1016 23852865; PubMed Central PMCID: PMCPMC3754747.
1017 12. Gallagher LA, Ramage E, Weiss EJ, Radey M, Hayden HS, Held KG, et al. Resources for
1018 Genetic and Genomic Analysis of Emerging Pathogen Acinetobacter baumannii. J Bacteriol.
1019 2015;197(12):2027-35. Epub 2015/04/08. doi: 10.1128/JB.00131-15. PubMed PMID:
1020 25845845; PubMed Central PMCID: PMCPMC4438207.
1021 13. Weidensdorfer M, Ishikawa M, Hori K, Linke D, Djahanschiri B, Iruegas R, et al. The
1022 Acinetobacter trimeric autotransporter adhesin Ata controls key virulence traits of
1023 Acinetobacter baumannii. Virulence. 2019;10(1):68-81. Epub 2019/12/25. doi:
1024 10.1080/21505594.2018.1558693. PubMed PMID: 31874074; PubMed Central PMCID:
1025 PMCPMC6363060.
1026 14. Wieland K, Chhatwal P, Vonberg RP. Nosocomial outbreaks caused by Acinetobacter
1027 baumannii and Pseudomonas aeruginosa: Results of a systematic review. Am J Infect
1028 Control. 2018;46(6):643-8. Epub 2018/02/06. doi: 10.1016/j.ajic.2017.12.014. PubMed
1029 PMID: 29398072.

1030 15. Lowman W, Kalk T, Menezes CN, John MA, Grobusch MP. A case of community-
1031 acquired Acinetobacter baumannii meningitis - has the threat moved beyond the hospital? J
1032 Med Microbiol. 2008;57(Pt 5):676-8. Epub 2008/04/26. doi: 10.1099/jmm.0.47781-0.
1033 PubMed PMID: 18436607.
1034 16. Banin E, Hughes D, Kuipers OP. Editorial: Bacterial pathogens, antibiotics and
1035 antibiotic resistance. FEMS Microbiol Rev. 2017;41(3):450-2. Epub 2017/05/10. doi:
1036 10.1093/femsre/fux016. PubMed PMID: 28486583.
1037 17. Tacconelli E, Carrara E, Savoldi A, Harbarth S, Mendelson M, Monnet DL, et al.
1038 Discovery, research, and development of new antibiotics: the WHO priority list of antibiotic-
1039 resistant bacteria and tuberculosis. Lancet Infect Dis. 2018;18(3):318-27. Epub 2017/12/26.
1040 doi: 10.1016/S1473-3099(17)30753-3. PubMed PMID: 29276051.
1041 18. Garcia-Quintanilla M, Pulido MR, Lopez-Rojas R, Pachon J, McConnell MJ. Emerging
1042 therapies for multidrug resistant Acinetobacter baumannii. Trends Microbiol.
1043 2013;21(3):157-63. doi: 10.1016/j.tim.2012.12.002. PubMed PMID: 23317680.
1044 19. Morris FC, Dexter C, Kostoulias X, Uddin MI, Peleg AY. The Mechanisms of Disease
1045 Caused by Acinetobacter baumannii. Frontiers in microbiology. 2019;10:1601. Epub
1046 2019/08/06. doi: 10.3389/fmicb.2019.01601. PubMed PMID: 31379771; PubMed Central
1047 PMCID: PMCPMC6650576.
1048 20. Sarshar M, Behzadi P, Scribano D, Palamara AT, Ambrosi C. Acinetobacter baumannii:
1049 An Ancient Commensal with Weapons of a Pathogen. Pathogens. 2021;10(4). Epub
1050 2021/04/04. doi: 10.3390/pathogens10040387. PubMed PMID: 33804894; PubMed Central
1051 PMCID: PMCPMC8063835.
1052 21. Davis JJ, Wattam AR, Aziz RK, Brettin T, Butler R, Butler RM, et al. The PATRIC
1053 Bioinformatics Resource Center: expanding data and analysis capabilities. Nucleic Acids Res.
1054 2020;48(D1):D606-D12. Epub 2019/11/02. doi: 10.1093/nar/gkz943. PubMed PMID:
1055 31667520; PubMed Central PMCID: PMCPMC7145515.
1056 22. Liu B, Zheng D, Jin Q, Chen L, Yang J. VFDB 2019: a comparative pathogenomic
1057 platform with an interactive web interface. Nucleic Acids Res. 2019;47(D1):D687-D92. Epub
1058 2018/11/06. doi: 10.1093/nar/gky1080. PubMed PMID: 30395255; PubMed Central PMCID:
1059 PMCPMC6324032.
1060 23. Juttukonda LJ, Green ER, Lonergan ZR, Heffern MC, Chang CJ, Skaar EP. Acinetobacter
1061 baumannii OxyR Regulates the Transcriptional Response to Hydrogen Peroxide. Infect
1062 Immun. 2019;87(1). Epub 2018/10/10. doi: 10.1128/IAI.00413-18. PubMed PMID: 30297527;
1063 PubMed Central PMCID: PMCPMC6300632.
1064 24. McConnell MJ, Actis L, Pachon J. Acinetobacter baumannii: human infections, factors
1065 contributing to pathogenesis and animal models. FEMS Microbiol Rev. 2013;37(2):130-55.
1066 Epub 2012/05/10. doi: 10.1111/j.1574-6976.2012.00344.x. PubMed PMID: 22568581.
1067 25. Harding CM, Hennon SW, Feldman MF. Uncovering the mechanisms of Acinetobacter
1068 baumannii virulence. Nat Rev Microbiol. 2018;16(2):91-102. Epub 2017/12/19. doi:
1069 10.1038/nrmicro.2017.148. PubMed PMID: 29249812; PubMed Central PMCID:
1070 PMCPMC6571207.
1071 26. Giles SK, Stroeher UH, Eijkelkamp BA, Brown MH. Identification of genes essential for
1072 pellicle formation in Acinetobacter baumannii. BMC Microbiol. 2015;15:116. Epub
1073 2015/06/07. doi: 10.1186/s12866-015-0440-6. PubMed PMID: 26047954; PubMed Central
1074 PMCID: PMCPMC4457973.
1075 27. Green ER, Juttukonda LJ, Skaar EP. The Manganese-Responsive Transcriptional
1076 Regulator MumR Protects Acinetobacter baumannii from Oxidative Stress. Infect Immun.

1077 2020;88(3). Epub 2019/12/04. doi: 10.1128/IAI.00762-19. PubMed PMID: 31792075;
1078 PubMed Central PMCID: PMCPMC7035938.
1079 28. Ramirez MS, Penwell WF, Traglia GM, Zimbler DL, Gaddy JA, Nikolaidis N, et al.
1080 Identification of Potential Virulence Factors in the Model Strain Acinetobacter baumannii
1081 A118. Frontiers in microbiology. 2019;10:1599. Epub 2019/08/10. doi:
1082 10.3389/fmicb.2019.01599. PubMed PMID: 31396168; PubMed Central PMCID:
1083 PMCPMC6663985.
1084 29. Eisenreich W, Dandekar T, Heesemann J, Goebel W. Carbon metabolism of
1085 intracellular bacterial pathogens and possible links to virulence. Nat Rev Microbiol.
1086 2010;8(6):401-12. Epub 2010/05/11. doi: 10.1038/nrmicro2351. PubMed PMID: 20453875.
1087 30. Passalacqua KD, Charbonneau ME, O'Riordan MXD. Bacterial Metabolism Shapes the
1088 Host-Pathogen Interface. Microbiol Spectr. 2016;4(3). Epub 2016/06/24. doi:
1089 10.1128/microbiolspec.VMBF-0027-2015. PubMed PMID: 27337445; PubMed Central
1090 PMCID: PMCPMC4922512.
1091 31. Nemec A. Classification and nomenclature of species in the genus Acinetobacter
1092 2020. Available from: https://apps.szu.cz/anemec/Classification.pdf.
1093 32. Al Atrouni A, Joly-Guillou ML, Hamze M, Kempf M. Reservoirs of Non-baumannii
1094 Acinetobacter Species. Front Microbiol. 2016;7:49. Epub 2016/02/13. doi:
1095 10.3389/fmicb.2016.00049. PubMed PMID: 26870013; PubMed Central PMCID:
1096 PMCPMC4740782.
1097 33. Wallace L, Daugherty SC, Nagaraj S, Johnson JK, Harris AD, Rasko DA. Use of
1098 Comparative Genomics To Characterize the Diversity of Acinetobacter baumannii
1099 Surveillance Isolates in a Health Care Institution. Antimicrob Agents Chemother.
1100 2016;60(10):5933-41. Epub 2016/07/28. doi: 10.1128/AAC.00477-16. PubMed PMID:
1101 27458211; PubMed Central PMCID: PMCPMC5038335.
1102 34. Holt K, Kenyon JJ, Hamidian M, Schultz MB, Pickard DJ, Dougan G, et al. Five decades
1103 of genome evolution in the globally distributed, extensively antibiotic-resistant
1104 Acinetobacter baumannii global clone 1. Microb Genom. 2016;2(2):e000052. Epub
1105 2017/03/30. doi: 10.1099/mgen.0.000052. PubMed PMID: 28348844; PubMed Central
1106 PMCID: PMCPMC5320584.
1107 35. Chan AP, Sutton G, DePew J, Krishnakumar R, Choi Y, Huang XZ, et al. A novel method
1108 of consensus pan-chromosome assembly and large-scale comparative analysis reveal the
1109 highly flexible pan-genome of Acinetobacter baumannii. Genome Biol. 2015;16:143. Epub
1110 2015/07/22. doi: 10.1186/s13059-015-0701-6. PubMed PMID: 26195261; PubMed Central
1111 PMCID: PMCPMC4507327.
1112 36. Imperi F, Antunes LCS, Blom J, Villa L, Iacono M, Visca P, et al. The Genomics of
1113 Acinetobacter baumannii: Insights into Genome Plasticity, Antimicrobial Resistance and
1114 Pathogenicity. Iubmb Life. 2011;63(12):1068-74. doi: Doi 10.1002/Iub.531. PubMed PMID:
1115 ISI:000297947900005.
1116 37. Abbott I, Cerqueira GM, Bhuiyan S, Peleg AY. Carbapenem resistance in
1117 Acinetobacter baumannii: laboratory challenges, mechanistic insights and therapeutic
1118 strategies. Expert Rev Anti Infect Ther. 2013;11(4):395-409. Epub 2013/04/10. doi:
1119 10.1586/eri.13.21. PubMed PMID: 23566149.
1120 38. Eijkelkamp BA, Stroeher UH, Hassan KA, Paulsen IT, Brown MH. Comparative analysis
1121 of surface-exposed virulence factors of Acinetobacter baumannii. BMC Genomics.
1122 2014;15:1020. Epub 2014/11/26. doi: 10.1186/1471-2164-15-1020. PubMed PMID:
1123 25422040; PubMed Central PMCID: PMCPMC4256060.

1124 39. Antunes LC, Visca P, Towner KJ. Acinetobacter baumannii: evolution of a global
1125 pathogen. Pathog Dis. 2014;71(3):292-301. Epub 2014/01/01. doi: 10.1111/2049-
1126 632X.12125. PubMed PMID: 24376225.
1127 40. Peleg AY, de Breij A, Adams MD, Cerqueira GM, Mocali S, Galardini M, et al. The
1128 success of acinetobacter species; genetic, metabolic and virulence attributes. PLoS ONE.
1129 2012;7(10):e46984. Epub 2012/11/13. doi: 10.1371/journal.pone.0046984. PubMed PMID:
1130 23144699; PubMed Central PMCID: PMC3483291.
1131 41. Meumann EM, Anstey NM, Currie BJ, Piera KA, Kenyon JJ, Hall RM, et al. Genomic
1132 epidemiology of severe community-onset Acinetobacter baumannii infection. Microb
1133 Genom. 2019;5(3). Epub 2019/02/27. doi: 10.1099/mgen.0.000258. PubMed PMID:
1134 30806611; PubMed Central PMCID: PMCPMC6487312.
1135 42. O'Leary NA, Wright MW, Brister JR, Ciufo S, Haddad D, McVeigh R, et al. Reference
1136 sequence (RefSeq) database at NCBI: current status, taxonomic expansion, and functional
1137 annotation. Nucleic Acids Res. 2016;44(D1):D733-45. Epub 2015/11/11. doi:
1138 10.1093/nar/gkv1189. PubMed PMID: 26553804; PubMed Central PMCID:
1139 PMCPMC4702849.
1140 43. Comai S, Bertazzo A, Brughera M, Crotti S. Chapter Five - Tryptophan in health and
1141 disease. In: Makowski GS, editor. Advances in Clinical Chemistry. 95: Elsevier; 2020. p. 165-
1142 218.
1143 44. Costantini C, Bellet MM, Renga G, Stincardini C, Borghi M, Pariano M, et al.
1144 Tryptophan Co-Metabolism at the Host-Pathogen Interface. Front Immunol. 2020;11:67.
1145 Epub 2020/02/23. doi: 10.3389/fimmu.2020.00067. PubMed PMID: 32082324; PubMed
1146 Central PMCID: PMCPMC7001157.
1147 45. Altenhoff AM, Levy J, Zarowiecki M, Tomiczek B, Warwick Vesztrocy A, Dalquen DA,
1148 et al. OMA standalone: orthology inference among public and custom genomes and
1149 transcriptomes. Genome Res. 2019;29(7):1152-63. Epub 2019/06/27. doi:
1150 10.1101/gr.243212.118. PubMed PMID: 31235654; PubMed Central PMCID:
1151 PMCPMC6633268.
1152 46. Galperin MY, Kristensen DM, Makarova KS, Wolf YI, Koonin EV. Microbial genome
1153 analysis: the COG approach. Brief Bioinform. 2019;20(4):1063-70. Epub 2017/10/03. doi:
1154 10.1093/bib/bbx117. PubMed PMID: 28968633; PubMed Central PMCID: PMCPMC6781585.
1155 47. Kanehisa M, Sato Y, Kawashima M, Furumichi M, Tanabe M. KEGG as a reference
1156 resource for gene and protein annotation. Nucleic Acids Res. 2016;44(D1):D457-62. doi:
1157 10.1093/nar/gkv1070. PubMed PMID: 26476454; PubMed Central PMCID:
1158 PMCPMC4702792.
1159 48. Chen L, Yang J, Yu J, Yao Z, Sun L, Shen Y, et al. VFDB: a reference database for
1160 bacterial virulence factors. Nucleic Acids Res. 2005;33(Database issue):D325-8. Epub
1161 2004/12/21. doi: 10.1093/nar/gki008. PubMed PMID: 15608208; PubMed Central PMCID:
1162 PMCPMC539962.
1163 49. Snitkin ES, Zelazny AM, Montero CI, Stock F, Mijares L, Murray PR, et al. Genome-
1164 wide recombination drives diversification of epidemic strains of Acinetobacter baumannii.
1165 Proc Natl Acad Sci U S A. 2011;108(33):13758-63. doi: 10.1073/pnas.1104404108.
1166 50. Mirarab S, Warnow T. ASTRAL-II: coalescent-based species tree estimation with many
1167 hundreds of taxa and thousands of genes. Bioinformatics. 2015;31(12):i44-52. Epub
1168 2015/06/15. doi: 10.1093/bioinformatics/btv234. PubMed PMID: 26072508; PubMed
1169 Central PMCID: PMCPMC4765870.
1170 51. Mateo-Estrada V, Grana-Miraglia L, Lopez-Leal G, Castillo-Ramirez S. Phylogenomics
1171 Reveals Clear Cases of Misclassification and Genus-Wide Phylogenetic Markers for

1172 Acinetobacter. Genome Biol Evol. 2019;11(9):2531-41. Epub 2019/08/14. doi:
1173 10.1093/gbe/evz178. PubMed PMID: 31406982; PubMed Central PMCID: PMCPMC6740150.
1174 52. Qin J, Feng Y, Lu X, Zong Z. Precise Species Identification for Acinetobacter: a
1175 Genome-Based Study with Description of Two Novel Acinetobacter Species. mSystems.
1176 2021;6(3):e0023721. Epub 2021/06/02. doi: 10.1128/mSystems.00237-21. PubMed PMID:
1177 34061620; PubMed Central PMCID: PMCPMC8269215.
1178 53. Kim PS, Shin NR, Kim JY, Yun JH, Hyun DW, Bae JW. Acinetobacter apis sp. nov.,
1179 isolated from the intestinal tract of a honey bee, Apis mellifera. J Microbiol. 2014;52(8):639-
1180 45. Epub 2014/08/08. doi: 10.1007/s12275-014-4078-0. PubMed PMID: 25098562.
1181 54. Ellegaard KM, Engel P. Genomic diversity landscape of the honey bee gut microbiota.
1182 Nature communications. 2019;10(1):446. Epub 2019/01/27. doi: 10.1038/s41467-019-
1183 08303-0. PubMed PMID: 30683856; PubMed Central PMCID: PMCPMC6347622.
1184 55. McFrederick QS, Rehan SM. Characterization of pollen and bacterial community
1185 composition in brood provisions of a small carpenter bee. Molecular ecology.
1186 2016;25(10):2302-11. Epub 2016/03/08. doi: 10.1111/mec.13608. PubMed PMID: 26945527.
1187 56. Karah N, Haldorsen B, Hegstad K, Simonsen GS, Sundsfjord A, Samuelsen O, et al.
1188 Species identification and molecular characterization of Acinetobacter spp. blood culture
1189 isolates from Norway. The Journal of antimicrobial chemotherapy. 2011;66(4):738-44. Epub
1190 2011/03/12. doi: 10.1093/jac/dkq521. PubMed PMID: 21393175.
1191 57. Turton JF, Shah J, Ozongwu C, Pike R. Incidence of Acinetobacter species other than
1192 A. baumannii among clinical isolates of Acinetobacter: evidence for emerging species. J Clin
1193 Microbiol. 2010;48(4):1445-9. Epub 2010/02/26. doi: 10.1128/JCM.02467-09. PubMed
1194 PMID: 20181894; PubMed Central PMCID: PMCPMC2849580.
1195 58. Niu C, Clemmer KM, Bonomo RA, Rather PN. Isolation and characterization of an
1196 autoinducer synthase from Acinetobacter baumannii. J Bacteriol. 2008;190(9):3386-92. Epub
1197 2008/02/19. doi: 10.1128/JB.01929-07. PubMed PMID: 18281398; PubMed Central PMCID:
1198 PMCPMC2347373.
1199 59. Bhargava N, Sharma P, Capalash N. Quorum sensing in Acinetobacter: an emerging
1200 pathogen. Crit Rev Microbiol. 2010;36(4):349-60. Epub 2010/09/18. doi:
1201 10.3109/1040841X.2010.512269. PubMed PMID: 20846031.
1202 60. Clemmer KM, Bonomo RA, Rather PN. Genetic analysis of surface motility in
1203 Acinetobacter baumannii. Microbiology. 2011;157(Pt 9):2534-44. Epub 2011/06/28. doi:
1204 10.1099/mic.0.049791-0. PubMed PMID: 21700662; PubMed Central PMCID:
1205 PMCPMC3352170.
1206 61. Choudhary KS, Hudaiberdiev S, Gelencser Z, Goncalves Coutinho B, Venturi V, Pongor
1207 S. The organization of the quorum sensing luxI/R family genes in Burkholderia. Int J Mol Sci.
1208 2013;14(7):13727-47. Epub 2013/07/04. doi: 10.3390/ijms140713727. PubMed PMID:
1209 23820583; PubMed Central PMCID: PMCPMC3742214.
1210 62. Le Guillouzer S, Groleau MC, Deziel E. Two rsaM Homologues Encode Central
1211 Regulatory Elements Modulating Quorum Sensing in Burkholderia thailandensis. J Bacteriol.
1212 2018;200(14). Epub 2018/03/07. doi: 10.1128/JB.00727-17. PubMed PMID: 29507087;
1213 PubMed Central PMCID: PMCPMC6018367.
1214 63. Lopez-Martin M, Dubern JF, Alexander MR, Williams P. AbaM Regulates Quorum
1215 Sensing, Biofilm Formation, and Virulence in Acinetobacter baumannii. J Bacteriol.
1216 2021;203(8). Epub 2021/01/27. doi: 10.1128/JB.00635-20. PubMed PMID: 33495249;
1217 PubMed Central PMCID: PMCPMC8088503.
1218 64. Rumbo-Feal S, Gomez MJ, Gayoso C, Alvarez-Fraga L, Cabral MP, Aransay AM, et al.
1219 Whole transcriptome analysis of Acinetobacter baumannii assessed by RNA-sequencing

1220 reveals different mRNA expression profiles in biofilm compared to planktonic cells. PLoS
1221 One. 2013;8(8):e72968. Epub 2013/09/12. doi: 10.1371/journal.pone.0072968. PubMed
1222 PMID: 24023660; PubMed Central PMCID: PMCPMC3758355.
1223 65. Rumbo-Feal S, Perez A, Ramelot TA, Alvarez-Fraga L, Vallejo JA, Beceiro A, et al.
1224 Contribution of the A. baumannii A1S_0114 Gene to the Interaction with Eukaryotic Cells
1225 and Virulence. Front Cell Infect Microbiol. 2017;7:108. Epub 2017/04/20. doi:
1226 10.3389/fcimb.2017.00108. PubMed PMID: 28421168; PubMed Central PMCID:
1227 PMCPMC5376624.
1228 66. Puri AW, Schaefer AL, Fu Y, Beck DAC, Greenberg EP, Lidstrom ME. Quorum Sensing
1229 in a Methane-Oxidizing Bacterium. J Bacteriol. 2017;199(5). Epub 2016/12/21. doi:
1230 10.1128/JB.00773-16. PubMed PMID: 27994019; PubMed Central PMCID:
1231 PMCPMC5309911.
1232 67. Gonzalez O, Ortiz-Castro R, Diaz-Perez C, Diaz-Perez AL, Magana-Duenas V, Lopez-
1233 Bucio J, et al. Non-ribosomal Peptide Synthases from Pseudomonas aeruginosa Play a Role in
1234 Cyclodipeptide Biosynthesis, Quorum-Sensing Regulation, and Root Development in a Plant
1235 Host. Microb Ecol. 2017;73(3):616-29. Epub 2016/12/03. doi: 10.1007/s00248-016-0896-4.
1236 PubMed PMID: 27900439.
1237 68. Tomaras AP, Dorsey CW, Edelmann RE, Actis LA. Attachment to and biofilm
1238 formation on abiotic surfaces by Acinetobacter baumannii: involvement of a novel
1239 chaperone-usher pili assembly system. Microbiology. 2003;149(Pt 12):3473-84. Epub
1240 2003/12/10. doi: 10.1099/mic.0.26541-0. PubMed PMID: 14663080.
1241 69. Pakharukova N, Tuittila M, Paavilainen S, Malmi H, Parilova O, Teneberg S, et al.
1242 Structural basis for Acinetobacter baumannii biofilm formation. Proc Natl Acad Sci U S A.
1243 2018;115(21):5558-63. Epub 2018/05/08. doi: 10.1073/pnas.1800961115. PubMed PMID:
1244 29735695; PubMed Central PMCID: PMCPMC6003481.
1245 70. Colclough AL, Scadden J, Blair JMA. TetR-family transcription factors in Gram-
1246 negative bacteria: conservation, variation and implications for efflux-mediated antimicrobial
1247 resistance. BMC Genomics. 2019;20(1):731. Epub 2019/10/14. doi: 10.1186/s12864-019-
1248 6075-5. PubMed PMID: 31606035; PubMed Central PMCID: PMCPMC6790063.
1249 71. Cuthbertson L, Nodwell JR. The TetR family of regulators. Microbiol Mol Biol Rev.
1250 2013;77(3):440-75. Epub 2013/09/06. doi: 10.1128/MMBR.00018-13. PubMed PMID:
1251 24006471; PubMed Central PMCID: PMCPMC3811609.
1252 72. Tomaras AP, Flagler MJ, Dorsey CW, Gaddy JA, Actis LA. Characterization of a two-
1253 component regulatory system from Acinetobacter baumannii that controls biofilm formation
1254 and cellular morphology. Microbiology. 2008;154(Pt 11):3398-409. Epub 2008/10/30. doi:
1255 10.1099/mic.0.2008/019471-0. PubMed PMID: 18957593.
1256 73. Cerqueira GM, Kostoulias X, Khoo C, Aibinu I, Qu Y, Traven A, et al. A global virulence
1257 regulator in Acinetobacter baumannii and its control of the phenylacetic acid catabolic
1258 pathway. J Infect Dis. 2014;210(1):46-55. Epub 2014/01/17. doi: 10.1093/infdis/jiu024.
1259 PubMed PMID: 24431277.
1260 74. Sun D, Crowell SA, Harding CM, De Silva PM, Harrison A, Fernando DM, et al. KatG
1261 and KatE confer Acinetobacter resistance to hydrogen peroxide but sensitize bacteria to
1262 killing by phagocytic respiratory burst. Life Sci. 2016;148:31-40. Epub 2016/02/11. doi:
1263 10.1016/j.lfs.2016.02.015. PubMed PMID: 26860891; PubMed Central PMCID:
1264 PMCPMC4792659.
1265 75. Slauch JM. How does the oxidative burst of macrophages kill bacteria? Still an open
1266 question. Mol Microbiol. 2011;80(3):580-3. Epub 2011/03/08. doi: 10.1111/j.1365-
1267 2958.2011.07612.x. PubMed PMID: 21375590; PubMed Central PMCID: PMCPMC3109634.

1268 76. Nguyen GT, Green ER, Mecsas J. Neutrophils to the ROScue: Mechanisms of NADPH
1269 Oxidase Activation and Bacterial Resistance. Front Cell Infect Microbiol. 2017;7:373. Epub
1270 2017/09/12. doi: 10.3389/fcimb.2017.00373. PubMed PMID: 28890882; PubMed Central
1271 PMCID: PMCPMC5574878.
1272 77. Mortensen BL, Skaar EP. The contribution of nutrient metal acquisition and
1273 metabolism to Acinetobacter baumannii survival within the host. Front Cell Infect Microbiol.
1274 2013;3:95. Epub 2014/01/01. doi: 10.3389/fcimb.2013.00095. PubMed PMID: 24377089;
1275 PubMed Central PMCID: PMCPMC3859900.
1276 78. Eijkelkamp BA, Hassan KA, Paulsen IT, Brown MH. Investigation of the human
1277 pathogen Acinetobacter baumannii under iron limiting conditions. BMC Genomics.
1278 2011;12:126. Epub 2011/02/24. doi: 10.1186/1471-2164-12-126. PubMed PMID: 21342532;
1279 PubMed Central PMCID: PMCPMC3055841.
1280 79. El-Zaatari M, Chang YM, Zhang M, Franz M, Shreiner A, McDermott AJ, et al.
1281 Tryptophan catabolism restricts IFN-gamma-expressing neutrophils and Clostridium difficile
1282 immunopathology. J Immunol. 2014;193(2):807-16. Epub 2014/06/18. doi:
1283 10.4049/jimmunol.1302913. PubMed PMID: 24935925; PubMed Central PMCID:
1284 PMCPMC4091639.
1285 80. Sheldon JR, Skaar EP. Acinetobacter baumannii can use multiple siderophores for iron
1286 acquisition, but only acinetobactin is required for virulence. PLoS Pathog.
1287 2020;16(10):e1008995. Epub 2020/10/20. doi: 10.1371/journal.ppat.1008995. PubMed
1288 PMID: 33075115; PubMed Central PMCID: PMCPMC7595644 following competing interests:
1289 Dr. Eric Skaar served as a consultant to Shionogi Inc.
1290 81. Nairn BL, Lonergan ZR, Wang J, Braymer JJ, Zhang Y, Calcutt MW, et al. The Response
1291 of Acinetobacter baumannii to Zinc Starvation. Cell Host Microbe. 2016;19(6):826-36. Epub
1292 2016/06/10. doi: 10.1016/j.chom.2016.05.007. PubMed PMID: 27281572; PubMed Central
1293 PMCID: PMCPMC4901392.
1294 82. Jakubovics NS, Jenkinson HF. Out of the iron age: new insights into the critical role of
1295 manganese homeostasis in bacteria. Microbiology (Reading). 2001;147(Pt 7):1709-18. Epub
1296 2001/06/29. doi: 10.1099/00221287-147-7-1709. PubMed PMID: 11429449.
1297 83. Anjem A, Varghese S, Imlay JA. Manganese import is a key element of the OxyR
1298 response to hydrogen peroxide in Escherichia coli. Mol Microbiol. 2009;72(4):844-58. Epub
1299 2009/04/30. doi: 10.1111/j.1365-2958.2009.06699.x. PubMed PMID: 19400769; PubMed
1300 Central PMCID: PMCPMC2776087.
1301 84. Juttukonda LJ, Chazin WJ, Skaar EP. Acinetobacter baumannii Coordinates Urea
1302 Metabolism with Metal Import To Resist Host-Mediated Metal Limitation. mBio. 2016;7(5).
1303 Epub 2016/09/30. doi: 10.1128/mBio.01475-16. PubMed PMID: 27677795; PubMed Central
1304 PMCID: PMCPMC5050338.
1305 85. Krizova L, Maixnerova M, Sedo O, Nemec A. Acinetobacter albensis sp. nov., isolated
1306 from natural soil and water ecosystems. Int J Syst Evol Microbiol. 2015;65(11):3905-12. Epub
1307 2015/08/08. doi: 10.1099/ijsem.0.000511. PubMed PMID: 26245775.
1308 86. Zhao J, Zhu Y, Han J, Lin YW, Aichem M, Wang J, et al. Genome-Scale Metabolic
1309 Modeling Reveals Metabolic Alterations of Multidrug-Resistant Acinetobacter baumannii in a
1310 Murine Bloodstream Infection Model. Microorganisms. 2020;8(11). Epub 2020/11/20. doi:
1311 10.3390/microorganisms8111793. PubMed PMID: 33207684; PubMed Central PMCID:
1312 PMCPMC7696501.
1313 87. Zhu Y, Zhao J, Maifiah MHM, Velkov T, Schreiber F, Li J. Metabolic Responses to
1314 Polymyxin Treatment in Acinetobacter baumannii ATCC 19606: Integrating Transcriptomics
1315 and Metabolomics with Genome-Scale Metabolic Modeling. mSystems. 2019;4(1). Epub

1316 2019/02/13. doi: 10.1128/mSystems.00157-18. PubMed PMID: 30746493; PubMed Central
1317 PMCID: PMCPMC6365644.
1318 88. Farrugia DN, Elbourne LD, Hassan KA, Eijkelkamp BA, Tetu SG, Brown MH, et al. The
1319 complete genome and phenome of a community-acquired Acinetobacter baumannii. PLoS
1320 One. 2013;8(3):e58628. Epub 2013/03/26. doi: 10.1371/journal.pone.0058628. PubMed
1321 PMID: 23527001; PubMed Central PMCID: PMCPMC3602452.
1322 89. Durot M, Le Fevre F, de Berardinis V, Kreimeyer A, Vallenet D, Combe C, et al.
1323 Iterative reconstruction of a global metabolic model of Acinetobacter baylyi ADP1 using
1324 high-throughput growth phenotype and gene essentiality data. BMC Syst Biol. 2008;2:85.
1325 Epub 2008/10/09. doi: 10.1186/1752-0509-2-85. PubMed PMID: 18840283; PubMed Central
1326 PMCID: PMCPMC2606687.
1327 90. Nemec A. Metabolic and physiological characteristics of Acinetobacter species 2021.
1328 Available from: https://apps.szu.cz/anemec/Phenotype.pdf.
1329 91. Matsushita K, Toyama H, Ameyama M, Adachi O, Dewanti A, Duine JA. Soluble and
1330 Membrane-bound Quinoprotein D-Glucose Dehydrogenases of the Acinetobacter
1331 calcoaceticus: The Binding Process of PQQ to the Apoenzymes. Bioscience, Biotechnology,
1332 and Biochemistry. 1995;59(8):1548-55. doi: 10.1271/bbb.59.1548.
1333 92. Shen YQ, Bonnot F, Imsand EM, RoseFigura JM, Sjolander K, Klinman JP. Distribution
1334 and properties of the genes encoding the biosynthesis of the bacterial cofactor,
1335 pyrroloquinoline quinone. Biochemistry. 2012;51(11):2265-75. Epub 2012/02/14. doi:
1336 10.1021/bi201763d. PubMed PMID: 22324760; PubMed Central PMCID: PMCPMC3334298.
1337 93. Riquelme SA, Ahn D, Prince A. Pseudomonas aeruginosa and Klebsiella pneumoniae
1338 Adaptation to Innate Immune Clearance Mechanisms in the Lung. J Innate Immun.
1339 2018;10(5-6):442-54. Epub 2018/04/05. doi: 10.1159/000487515. PubMed PMID: 29617698;
1340 PubMed Central PMCID: PMCPMC6785651.
1341 94. Nemec A. 2021.
1342 95. Blumenthal HJ, Lucuta VL, Blumenthal DC. Specific enzymatic assay for D-glucarate in
1343 human serum. Anal Biochem. 1990;185(2):286-93. Epub 1990/03/01. doi: 10.1016/0003-
1344 2697(90)90294-j. PubMed PMID: 2187374.
1345 96. Lamichhane-Khadka R, Benoit SL, Maier SE, Maier RJ. A link between gut community
1346 metabolism and pathogenesis: molecular hydrogen-stimulated glucarate catabolism aids
1347 Salmonella virulence. Open Biol. 2013;3(12):130146. Epub 2013/12/07. doi:
1348 10.1098/rsob.130146. PubMed PMID: 24307595; PubMed Central PMCID:
1349 PMCPMC3877842.
1350 97. Rosas-Lemus M, Minasov G, Shuvalova L, Wawrzak Z, Kiryukhina O, Mih N, et al.
1351 Structure of galactarate dehydratase, a new fold in an enolase involved in bacterial fitness
1352 after antibiotic treatment. Protein Sci. 2020;29(3):711-22. Epub 2019/12/08. doi:
1353 10.1002/pro.3796. PubMed PMID: 31811683; PubMed Central PMCID: PMCPMC7021002.
1354 98. Reuter SE, Evans AM. Carnitine and acylcarnitines: pharmacokinetic, pharmacological
1355 and clinical aspects. Clin Pharmacokinet. 2012;51(9):553-72. Epub 2012/07/19. doi:
1356 10.2165/11633940-000000000-00000
1357 10.1007/BF03261931. PubMed PMID: 22804748.
1358 99. Zhu Y, Jameson E, Crosatti M, Schafer H, Rajakumar K, Bugg TD, et al. Carnitine
1359 metabolism to trimethylamine by an unusual Rieske-type oxygenase from human
1360 microbiota. Proc Natl Acad Sci U S A. 2014;111(11):4268-73. Epub 2014/03/05. doi:
1361 10.1073/pnas.1316569111. PubMed PMID: 24591617; PubMed Central PMCID:
1362 PMCPMC3964110.

1363 100. Bouvet PJM, Grimont PAD. Taxonomy of the Genus Acinetobacter with the
1364 Recognition of Acinetobacter baumannii sp. nov., Acinetobacter haemolyticus sp. nov.,
1365 Acinetobacter johnsonii sp. nov., and Acinetobacter junii sp. nov. and Emended Descriptions
1366 of Acinetobacter calcoaceticus and Acinetobacter lwoffii. International Journal of Systematic
1367 and Evolutionary Microbiology. 1986;36(2):228-40. doi: https://doi.org/10.1099/00207713-
1368 36-2-228.
1369 101. Breisch J, Waclawska I, Averhoff B. Identification and characterization of a carnitine
1370 transporter in Acinetobacter baumannii. Microbiologyopen. 2019;8(6):e00752. Epub
1371 2018/10/16. doi: 10.1002/mbo3.752. PubMed PMID: 30318737; PubMed Central PMCID:
1372 PMCPMC6562126.
1373 102. Wang CH, Zhao TX, Li M, Zhang C, Xing XH. Characterization of a novel Acinetobacter
1374 baumannii xanthine dehydrogenase expressed in Escherichia coli. Biotechnol Lett.
1375 2016;38(2):337-44. Epub 2015/11/07. doi: 10.1007/s10529-015-1986-y. PubMed PMID:
1376 26543035.
1377 103. Altenhoff AM, Glover NM, Train CM, Kaleb K, Warwick Vesztrocy A, Dylus D, et al. The
1378 OMA orthology database in 2018: retrieving evolutionary relationships among all domains of
1379 life through richer web and programmatic interfaces. Nucleic Acids Res. 2018;46(D1):D477-
1380 D85. Epub 2017/11/07. doi: 10.1093/nar/gkx1019. PubMed PMID: 29106550; PubMed
1381 Central PMCID: PMCPMC5753216.
1382 104. Knoten CA, Hudson LL, Coleman JP, Farrow JM, 3rd, Pesci EC. KynR, a Lrp/AsnC-type
1383 transcriptional regulator, directly controls the kynurenine pathway in Pseudomonas
1384 aeruginosa. J Bacteriol. 2011;193(23):6567-75. Epub 2011/10/04. doi: 10.1128/JB.05803-11.
1385 PubMed PMID: 21965577; PubMed Central PMCID: PMCPMC3232868.
1386 105. Bortolotti P, Hennart B, Thieffry C, Jausions G, Faure E, Grandjean T, et al. Tryptophan
1387 catabolism in Pseudomonas aeruginosa and potential for inter-kingdom relationship. BMC
1388 Microbiol. 2016;16(1):137. Epub 2016/07/09. doi: 10.1186/s12866-016-0756-x. PubMed
1389 PMID: 27392067; PubMed Central PMCID: PMCPMC4938989.
1390 106. Rohmer L, Hocquet D, Miller SI. Are pathogenic bacteria just looking for food?
1391 Metabolism and microbial pathogenesis. Trends Microbiol. 2011;19(7):341-8. Epub
1392 2011/05/24. doi: 10.1016/j.tim.2011.04.003. PubMed PMID: 21600774; PubMed Central
1393 PMCID: PMCPMC3130110.
1394 107. Fournier P-E, Vallenet D, Barbe V, Audic S, Ogata H, Poirel L, et al. Comparative
1395 Genomics of Multidrug Resistance in Acinetobacter baumannii. PLoS Genet. 2006;2(1):e7.
1396 doi: 10.1371/journal.pgen.0020007.
1397 108. Sato Y, Unno Y, Miyazaki C, Ubagai T, Ono Y. Multidrug-resistant Acinetobacter
1398 baumannii resists reactive oxygen species and survives in macrophages. Sci Rep.
1399 2019;9(1):17462. Epub 2019/11/27. doi: 10.1038/s41598-019-53846-3. PubMed PMID:
1400 31767923; PubMed Central PMCID: PMCPMC6877552.
1401 109. Chen YJ, Leung PM, Wood JL, Bay SK, Hugenholtz P, Kessler AJ, et al. Metabolic
1402 flexibility allows bacterial habitat generalists to become dominant in a frequently disturbed
1403 ecosystem. ISME J. 2021. Epub 2021/05/05. doi: 10.1038/s41396-021-00988-w. PubMed
1404 PMID: 33941890.
1405 110. Ren W, Rajendran R, Zhao Y, Tan B, Wu G, Bazer FW, et al. Amino Acids As Mediators
1406 of Metabolic Cross Talk between Host and Pathogen. Front Immunol. 2018;9:319. Epub
1407 2018/03/15. doi: 10.3389/fimmu.2018.00319. PubMed PMID: 29535717; PubMed Central
1408 PMCID: PMCPMC5835074.

1409 111. Chen Y, Guillemin GJ. Kynurenine pathway metabolites in humans: disease and
1410 healthy States. Int J Tryptophan Res. 2009;2:1-19. Epub 2009/01/01. doi: 10.4137/ijtr.s2097.
1411 PubMed PMID: 22084578; PubMed Central PMCID: PMCPMC3195227.
1412 112. Genestet C, Le Gouellec A, Chaker H, Polack B, Guery B, Toussaint B, et al. Scavenging
1413 of reactive oxygen species by tryptophan metabolites helps Pseudomonas aeruginosa
1414 escape neutrophil killing. Free Radic Biol Med. 2014;73:400-10. Epub 2014/06/15. doi:
1415 10.1016/j.freeradbiomed.2014.06.003. PubMed PMID: 24929180.
1416 113. Page AJ, Taylor B, Keane JA. Multilocus sequence typing by blast from de novo
1417 assemblies against PubMLST. Journal of Open Source Software. 2016;1(8):118. doi:
1418 10.21105/joss.00118.
1419 114. Bartual SG, Seifert H, Hippler C, Luzon MA, Wisplinghoff H, Rodriguez-Valera F.
1420 Development of a multilocus sequence typing scheme for characterization of clinical isolates
1421 of Acinetobacter baumannii. J Clin Microbiol. 2005;43(9):4382-90. Epub 2005/09/08. doi:
1422 10.1128/JCM.43.9.4382-4390.2005. PubMed PMID: 16145081; PubMed Central PMCID:
1423 PMCPMC1234098.
1424 115. Diancourt L, Passet V, Nemec A, Dijkshoorn L, Brisse S. The population structure of
1425 Acinetobacter baumannii: expanding multiresistant clones from an ancestral susceptible
1426 genetic pool. PLoS One. 2010;5(4):e10034. Epub 2010/04/13. doi:
1427 10.1371/journal.pone.0010034. PubMed PMID: 20383326; PubMed Central PMCID:
1428 PMCPMC2850921.
1429 116. Wang X, Qiao F, Yu R, Gao Y, Zong Z. Clonal diversity of Acinetobacter baumannii
1430 clinical isolates revealed by a snapshot study. BMC Microbiol. 2013;13:234. Epub
1431 2013/10/23. doi: 10.1186/1471-2180-13-234. PubMed PMID: 24144168; PubMed Central
1432 PMCID: PMCPMC3815251.
1433 117. Wilharm G, Skiebe E, Higgins PG, Poppel MT, Blaschke U, Leser S, et al. Relatedness of
1434 wildlife and livestock avian isolates of the nosocomial pathogen Acinetobacter baumannii to
1435 lineages spread in hospitals worldwide. Environ Microbiol. 2017;19(10):4349-64. Epub
1436 2017/09/20. doi: 10.1111/1462-2920.13931. PubMed PMID: 28925528.
1437 118. Cerezales M, Xanthopoulou K, Wille J, Bustamante Z, Seifert H, Gallego L, et al.
1438 Acinetobacter baumannii analysis by core genome multi-locus sequence typing in two
1439 hospitals in Bolivia: endemicity of international clone 7 isolates (CC25). Int J Antimicrob
1440 Agents. 2019;53(6):844-9. Epub 2019/04/01. doi: 10.1016/j.ijantimicag.2019.03.019.
1441 PubMed PMID: 30928684.
1442 119. Kumar S, Patil PP, Singhal L, Ray P, Patil PB, Gautam V. Molecular epidemiology of
1443 carbapenem-resistant Acinetobacter baumannii isolates reveals the emergence of blaOXA-
1444 23 and blaNDM-1 encoding international clones in India. Infect Genet Evol. 2019;75:103986.
1445 Epub 2019/07/31. doi: 10.1016/j.meegid.2019.103986. PubMed PMID: 31362071.
1446 120. Higgins PG, Hrenovic J, Seifert H, Dekic S. Characterization of Acinetobacter
1447 baumannii from water and sludge line of secondary wastewater treatment plant. Water Res.
1448 2018;140:261-7. Epub 2018/05/04. doi: 10.1016/j.watres.2018.04.057. PubMed PMID:
1449 29723815.
1450 121. Levy-Blitchtein S, Roca I, Plasencia-Rebata S, Vicente-Taboada W, Velasquez-Pomar J,
1451 Munoz L, et al. Emergence and spread of carbapenem-resistant Acinetobacter baumannii
1452 international clones II and III in Lima, Peru. Emerg Microbes Infect. 2018;7(1):119. Epub
1453 2018/07/05. doi: 10.1038/s41426-018-0127-9. PubMed PMID: 29970918; PubMed Central
1454 PMCID: PMCPMC6030224.
1455 122. Tomaschek F, Higgins PG, Stefanik D, Wisplinghoff H, Seifert H. Head-to-Head
1456 Comparison of Two Multi-Locus Sequence Typing (MLST) Schemes for Characterization of

1457 Acinetobacter baumannii Outbreak and Sporadic Isolates. PLoS One. 2016;11(4):e0153014.
1458 Epub 2016/04/14. doi: 10.1371/journal.pone.0153014. PubMed PMID: 27071077; PubMed
1459 Central PMCID: PMCPMC4829225.
1460 123. Higgins PG, Prior K, Harmsen D, Seifert H. Development and evaluation of a core
1461 genome multilocus typing scheme for whole-genome sequence-based typing of
1462 Acinetobacter baumannii. PLoS One. 2017;12(6):e0179228. Epub 2017/06/09. doi:
1463 10.1371/journal.pone.0179228. PubMed PMID: 28594944; PubMed Central PMCID:
1464 PMCPMC5464626.
1465 124. Gaiarsa S, Batisti Biffignandi G, Esposito EP, Castelli M, Jolley KA, Brisse S, et al.
1466 Comparative Analysis of the Two Acinetobacter baumannii Multilocus Sequence Typing
1467 (MLST) Schemes. Frontiers in microbiology. 2019;10:930. Epub 2019/05/28. doi:
1468 10.3389/fmicb.2019.00930. PubMed PMID: 31130931; PubMed Central PMCID:
1469 PMCPMC6510311.
1470 125. Chernomor O, Minh BQ, Forest F, Klaere S, Ingram T, Henzinger M, et al. Split
1471 diversity in constrained conservation prioritization using integer linear programming.
1472 Methods Ecol Evol. 2015;6(1):83-91. Epub 2015/04/22. doi: 10.1111/2041-210X.12299.
1473 PubMed PMID: 25893087; PubMed Central PMCID: PMCPMC4392707.
1474 126. Kurtz S, Phillippy A, Delcher AL, Smoot M, Shumway M, Antonescu C, et al. Versatile
1475 and open software for comparing large genomes. Genome Biol. 2004;5(2):R12. Epub
1476 2004/02/05. doi: 10.1186/gb-2004-5-2-r12. PubMed PMID: 14759262; PubMed Central
1477 PMCID: PMCPMC395750.
1478 127. Pritchard L, Glover RH, Humphris S, Elphinstone JG, Toth IK. Genomics and taxonomy
1479 in diagnostics for food security: soft-rotting enterobacterial plant pathogens. Analytical
1480 Methods. 2016;8(1):12-24. doi: 10.1039/C5AY02550H.
1481 128. Birikmen M, Bohnsack KE, Tran V, Somayaji S, Bohnsack MT, Ebersberger I. Tracing
1482 Eukaryotic Ribosome Biogenesis Factors Into the Archaeal Domain Sheds Light on the
1483 Evolution of Functional Complexity. Frontiers in microbiology. 2021;12:2598.
1484 129. Tettelin H, Masignani V, Cieslewicz MJ, Donati C, Medini D, Ward NL, et al. Genome
1485 analysis of multiple pathogenic isolates of Streptococcus agalactiae: implications for the
1486 microbial "pan-genome". Proc Natl Acad Sci U S A. 2005;102(39):13950-5. Epub 2005/09/21.
1487 doi: 10.1073/pnas.0506758102. PubMed PMID: 16172379; PubMed Central PMCID:
1488 PMCPMC1216834.
1489 130. Katoh K, Toh H. Recent Developments in the MAFFT Multiple Sequence Alignment
1490 Program. Brief Bioinform. 2008;9(4):286-98.
1491 131. Suyama M, Torrents D, Bork P. PAL2NAL: robust conversion of protein sequence
1492 alignments into the corresponding codon alignments. Nucleic Acids Res. 2006;34(Web
1493 Server issue):W609-12. Epub 2006/07/18. doi: 10.1093/nar/gkl315. PubMed PMID:
1494 16845082; PubMed Central PMCID: PMCPMC1538804.
1495 132. Nguyen LT, Schmidt HA, von Haeseler A, Minh BQ. IQ-TREE: a fast and effective
1496 stochastic algorithm for estimating maximum-likelihood phylogenies. Mol Biol Evol.
1497 2015;32(1):268-74. doi: 10.1093/molbev/msu300. PubMed PMID: 25371430; PubMed
1498 Central PMCID: PMCPMC4271533.
1499 133. Huson DH. SplitsTree: analyzing and visualizing evolutionary data. Bioinformatics.
1500 1998;14(1):68-73. PubMed PMID: 9520503.
1501 134. Altenhoff AM, Gil M, Gonnet GH, Dessimoz C. Inferring hierarchical orthologous
1502 groups from orthologous gene pairs. PLoS One. 2013;8(1):e53786. Epub 2013/01/24. doi:
1503 10.1371/journal.pone.0053786. PubMed PMID: 23342000; PubMed Central PMCID:
1504 PMCPMC3544860.

135. The Gene Ontology C. The Gene Ontology Resource: 20 years and still GOing strong. Nucleic Acids Res. 2019;47(D1):D330-D8. Epub 2018/11/06. doi: 10.1093/nar/gky1055. PubMed PMID: 30395331; PubMed Central PMCID: PMCPMC6323945.
136. Supek F, Bošnjak M, Škunca N, Šmuc T. REVIGO Summarizes and Visualizes Long Lists of Gene Ontology Terms. PLOS ONE. 2011;6(7):e21800. doi: 10.1371/journal.pone.0021800.
137. Yu NY, Wagner JR, Laird MR, Melli G, Rey S, Lo R, et al. PSORTb 3.0: improved protein subcellular localization prediction with refined localization subcategories and predictive capabilities for all prokaryotes. Bioinformatics. 2010;26(13):1608-15. Epub 2010/05/18. doi: 10.1093/bioinformatics/btq249. PubMed PMID: 20472543; PubMed Central PMCID: PMCPMC2887053.
138. King BR, Vural S, Pandey S, Barteau A, Guda C. ngLOC: software and web server for predicting protein subcellular localization in prokaryotes and eukaryotes. BMC research notes. 2012;5:351. Epub 2012/07/12. doi: 10.1186/1756-0500-5-351. PubMed PMID: 22780965; PubMed Central PMCID: PMCPMC3532370.
139. Shen HB, Chou KC. Gneg-mPLoc: a top-down strategy to enhance the quality of predicting subcellular localization of Gram-negative bacterial proteins. J Theor Biol. 2010;264(2):326-33. Epub 2010/01/23. doi: 10.1016/j.jtbi.2010.01.018. PubMed PMID: 20093124.
140. Kanehisa M, Sato Y, Morishima K. BlastKOALA and GhostKOALA: KEGG Tools for Functional Characterization of Genome and Metagenome Sequences. J Mol Biol. 2016;428(4):726-31. doi: 10.1016/j.jmb.2015.11.006. PubMed PMID: 26585406.
141. Altschul SF, Madden TL, Schäffer AA, Zhang J, Zhang Z, Miller W, et al. Gapped BLAST and PSI-BLAST: a new generation of protein database search programs. Nucleic Acids Res. 1997;25(17):3389-402.
142. Fu L, Niu B, Zhu Z, Wu S, Li W. CD-HIT: accelerated for clustering the next-generation sequencing data. Bioinformatics. 2012;28(23):3150-2. Epub 2012/10/13. doi: 10.1093/bioinformatics/bts565. PubMed PMID: 23060610; PubMed Central PMCID: PMCPMC3516142.
143. Gower JC, Warrens MJ. Similarity, Dissimilarity, and Distance, Measures of. Wiley StatsRef: Statistics Reference Online. Hoboken, New Jersey, US: John Wiley & Sons, Ltd.; 2014.
144. Tucker AT, Nowicki EM, Boll JM, Knauf GA, Burdis NC, Trent MS, et al. Defining gene-phenotype relationships in Acinetobacter baumannii through one-step chromosomal gene inactivation. mBio. 2014;5(4):e01313-14. Epub 2014/08/07. doi: 10.1128/mBio.01313-14. PubMed PMID: 25096877; PubMed Central PMCID: PMCPMC4128354.
145. Datsenko KA, Wanner BL. One-step inactivation of chromosomal genes in Escherichia coli K-12 using PCR products. Proc Natl Acad Sci U S A. 2000;97(12):6640-5. Epub 2000/06/01. doi: 10.1073/pnas.120163297. PubMed PMID: 10829079; PubMed Central PMCID: PMCPMC18686.
146. Tschech A, Pfennig N. Growth yield increase linked to caffeate reduction in Acetobacterium woodii. Archives of Microbiology. 1984;137(2):163-7. doi: 10.1007/BF00414460.

1549 **Supplementary Information**

1550

1551 **S1 Table SA1: Full list of genomes used in this study.**

1552 The set of assemblies represented in Set-F is provided in tabular format as extracted from

1553 NCBI RefSeq. Among other, the table lists RefSeq assembly and sample accessions,

1554 taxonomy ids (on strain and species level if available), species labels, and strain labels,

1555 assembly status, submission date, submission institute, and ftp link to resource.

1556 (.xlsx)

1557 **S2: Supplementary Text**

1558 Contains supplemental sections covering additional information on the taxon set

1559 compilation, a statistical exploration of all protein-coding genes, genomes and orthologs in

1560 Set-R, details on the method and workflow of the ESGC prediction, and provides additional

1561 results and discussions for the predicted $ESGCs_{ACB}$ including several clusters not discussed in

1562 the main manuscript.

1563 (.docx)

1564 **S3 Table SA2: Representative genomes selected with corrections and descriptive statistics.**

1565 The subset of assemblies in Set-R is provided in tabular format. The table lists RefSeq

1566 assembly and sample accessions, taxonomy ids, species labels, and corrected labels (see

1567 main text), strain names, clone type assignments (via MLST and literature) sampling site, and

1568 sampling year (where available) of the strains. The table further features the results of our

1569 genome sequence-specific quantitative and qualitative analyses. The descriptive statistics

1570 are described in the documents' sheet 'ColumnLegends'.

1571 (.xlsx)

1572 **S4 Fig. SA3: In Set-R there is a significant difference in the number of coding sequences**
1573 **between the ACB clade members and non-members.**
1574 (A) Comparison of the number of coding sequences (CDS) per genome between members
1575 and non-members of ACB clade across *Acinetobacter*. It reveals a significant difference. ACB
1576 clade members, on average, contain 14% more protein coding genes. (B) Correlation matrix
1577 for a range of summary statistics on genome level across SET-R. Colored cells indicate value
1578 of spearman correlation coefficient [-1,1]. The descriptive statistics analyzed are explained in
1579 S3 Table SA2. (C) Phylogenetic diversity of the orthologous groups (OGs) calculated from the
1580 sum of branch lengths of the subtree spanned by the taxa represented in an OG**.** This
1581 distribution contrasts the taxa belonging to the ACB clade vs. the total phylogenetic
1582 diversity. Data points are colored black if the corresponding OG belongs to the set of genus-
1583 wide core genes that were also used for phylogeny reconstruction. OGs represented closer
1584 to the upper left corner are especially interesting as they are approaching ubiquitous
1585 presence within the ACB clade but are rare in the rest of the genus (colored orange for
1586 illustrative purposes).
1587 (.pdf)
1588 **S5 Tables SB1: Orthology matrix as calculated from the all vs. all orthology search across**
1589 **Set-R (OMA orthologous groups)**
1590 The column header contains the labels of the NCBI RefSeq assembly accession of each
1591 genome. Row indices refer to the orthologous group identifier. The matrix fields contain the
1592 NCBI RefSeq protein sequence accession if an ortholog was identified and left empty
1593 otherwise. Table SB1.2 lists the identifiers of those orthologous groups constituting the core
1594 genome by our definition. These were used for the tree reconstruction (.xlsx).

1595 **S6 Fig. SC5: Majority-rule consensus phylogeny of 232 Acinetobacter strains represented in**
1596 **SET-R.**
1597 A high resolution image of the majority-rule consensus dendrogram of the Set-R taxa as
1598 shown in Figure 2A. Branches supported by only two out of three partition trees are
1599 indicated with dashed lines, branches supported by only one partition are not resolved. Leaf
1600 labels colored in green indicate changed species assignments. Such changes can either (i)
1601 correct (i.e. the original species assignment was at odds with the species assignment based
1602 on phylogenetic and ANI evidences), (ii) newly specify (i.e. the original species assignment
1603 was set to "unknown" (sp.)) or (iii) de-specify (the original species assignment could not be
1604 confirmed by phylogenetic evidences, and no alternative assignment was possible. The
1605 species label was set to "sp.") the species assignments as retrieved from NCBI RefSeq at the
1606 time of download.
1607 (.pdf)

1608 **S7 Fig. SC6: Maximum likelihood (ML) tree for Set-F based on partition 1 of the core gene**
1609 **set (296 proteins).**
1610 Branch labels denote percent bootstrap support. The newick strings for the ML trees from all
1611 three partitions are given in S23. A high-resolution figure of the consensus tree is provided in
1612 S24 Fig. SC8.
1613 (.pdf)

1614 **S8 Tables SC1: Phylogeny-based taxonomic classifications of the genomes in Set-F into the**
1615 **defined clades**
1616 Consists of 15 sheets in total. Each sheet lists the NCBI RefSeq assembly accession and taxon
1617 label (species and strain label) of the genomes that were phylogenetically classified to
1618 belong to the following clades: B clade (*A. baumannii*), S clade (*A. seifertii*), NO clade (*A.*

1619 *nosocomialis*), BNS clade (three aforementioned), L clade (*A. lactucae*), PI clade (*A. pittii*), CA
1620 clade (*A. calcoaceticus*), CPL clade (three aforementioned), ACB clade, HA clade, BA clade,
1621 LW clade, BR clade, QI clade, and the outgroup. Genome assignments to *A. baumannii* which
1622 were at odds with its phylogenetic placement in our study are indicated by a blue line. In the
1623 same way, we highlighted assignments to *A. pittii* in light orange and *A. calcoaceticus* in dark
1624 orange.
1625 (.xlsx)

1626 **S9 Fig. SC3: Hierarchically clustered ANIm heatmap across Set-R combined with**
1627 **phylogenetic information reveals unknown species diversity within the ACB clade.**
1628 The figure shows the color-graded average nucleotide identity (ANIm, all vs all) of the
1629 genomes across SET-R (both axes). Strains with high genomic identity generate clusters of
1630 high sequence identity (>95%: increasingly saturated red; 95%: white, <95%: saturating blue)
1631 along the diagonal. These clusters and cutoffs are typically used for bacterial species
1632 delineation. In the ACB clade, we observe a large and distinct cluster with 98-100% sequence
1633 identity (rounded) for the *A. baumannii* species (top left). Following the diagonal to the
1634 bottom right corner, the strains of *A. seifertii* (2, n=2) and *A. nosocomialis* (3, n=5) are
1635 clustered similarly. The percent identities decrease, for the following two clusters of
1636 genomes with mainly *A. calcoaceticus* species assignments (4 and 5). Specifically, only three
1637 pairs in cluster 4 and one pair in cluster 5 reach the species threshold ANI. Next to putatively
1638 misidentified *A. calcoaceticus*, cluster 5 features a strain of the tentative species *A.*
1639 *oleivorans* (strain CIP 110421) as well as the unassigned *A.* sp. WC-141 and *A.* sp. NIPH 817
1640 suggesting the existence of undescribed species in the ACB clade. Two further genomes,
1641 here located between cluster 5 and cluster 6 are putatively mislabeled strains *A. baumannii*
1642 strain 573719 and *A. pittii* ANC 4050. These strains again potentially represent undescribed

1643 species in the ACB clade. Clusters 6 and 7 comprise the strains from *A. lactucae* and from *A.*
1644 *pittii*, respectively. S25 Table SC4 contains the full matrix of pairwise ANIm in a tabulated
1645 format.
1646 (.png)

1647 **S10 Tables SD1: Results of consecutive GO term enrichment analysis**

1648 Table SD1.1 shows the significantly enriched GO terms ($p_{adjusted} < 0.001$) for proteins in those
1649 HOGs at a node where an ortholog was detected in at least 50% of the subsumed taxa. If
1650 genes of the same HOG are the source for multiple enriched terms, only the most specific
1651 term (highest depth) was kept for the final results. The raw results of the GO term
1652 enrichment analysis are presented in Table SD1.2. The results of the GO term enrichment
1653 analyses considering all HOGs at a node are provided in Table SD1.3. Detailed explanations
1654 of the column headers are placed in the sheet 'ColumnLegends'. The test results from SD1.3
1655 were extracted to generate input tables for REVIGO (sheets SD1.4-8). The resulting treemaps
1656 are shown in S26 Figures SD2.1-5.
1657 (.xlsx)

1658 **S11 Tables SE1: ESGC identification and underlying data.**

1659 This file gives detailed information about the ESGC identification and provides the underlying
1660 data. Table SE1.1 gives for each gene along the genome of *A. baumannii* ATCC 19606 the
1661 number of taxa per clade (and per international clone type) that harbor an ortholog. Table
1662 SE1.2 gives, for each gene, the input vector used for the dissimilarity calculations, the
1663 individual thresholds (5th percentile) and, as an example, the calculated dissimilarity
1664 between each gene and the gene immediately upstream. The full matrix containing all
1665 pairwise dissimilarity calculations for the prediction of clusters is deposited on figshare
1666 [10.6084/m9.figshare.16910974, https://figshare.com/s/caa9a6680bc90e004365 (temporary

1667 private link)]. Table SE1.3 lists the identified graph components along with abundance
1668 statistics (median of the proteins in a component) across the clades (both absolute and
1669 relative), retention difference between ACB vs. non-ACB (RD), and CCD scores. Table SE1.4
1670 lists detailed contextual information for the components including all functional annotations
1671 from various sources. Detailed explanations of the column headers for all tables are placed
1672 in the sheet 'ColumnLegends'.
1673 (.xlsx)

1674 **S12 Figures SE3: Genomic regions of all ESGC along the genome of ATCC 19606.**

1675 Graphical representations of the genomic regions for each ESGC with RD > 0 (see Methods)
1676 along the genome of ATCC 19606 with abbreviated abundance profiles and functional
1677 annotations.
1678 (.pdf)

1679 **S13 Fig. SF6: Growth of *A. baumannii* ATCC 19606, *A. calcoaceticus* DSM 30006 and *A.***
1680 ***baylyi* on different carbon source.**
1681 *A. baumannii* ATCC 19606 (△), *A. calcoaceticus* (□) and *A. baylyi* ADP1 (○) were grown in
1682 mineral medium with 20 mM carnitine (A), gluconate (B) or D-malate (C) as carbon source.
1683 Each value is the mean of +/- S. E.M. of at least three independent measurements.
1684 (.pdf)

1685 **S14 Table SF2: Summary statistics of collected experimental evidence found in the**
1686 **literature for the assimilation of >100 potential carbon sources for *A. baumannii*.**
1687 (.xlsx)

1688 **S15 Files SE2: Phylogenetic profiles and micro-synteny plots in html format for the curated**
1689 **top 150 ESGCs$_{ACB}$ across Set-F as provided by the Vicinator analysis.**

1690 Files can also be downloaded in zip-format via figshare:

1691 https://figshare.com/s/caa9a6680bc90e004365 (temporary private link).

1692 (.zip)

1693 **S16 Fig. SF3: Ortholog abundance profiles and functional characterizations of *gdhA* and**

1694 ***gdhB*.**

1695 (.pdf)

1696 **S17 Table SF7: List of all non-ACB genomes across Set-R that harbor $ESGC_{ACB}$ 0016 including**

1697 **meta information regarding sampling and isolation.**

1698 (.pdf)

1699 **S18 Files SF5: Phylogenetic profiles and micro-synteny plots in html format for $ESGC_{ACB}$-**

1700 **0452 and the kynurenine pathway cluster in *P. aeruginosa* across a sample of all**

1701 ***Proteobacteria*.**

1702 Files can also be downloaded in zip-format via figshare:

1703 https://figshare.com/s/caa9a6680bc90e004365 (temporary private link).

1704 (.zip)

1705 **S19 Table SF4: Assembly accession and species/strain labels for the Proteobacteria sample**

1706 **(n=1363).**

1707 (.xlsx)

1708 **S20 Table SF8: List of primers used for Ab04 mutant deletions Δkyn mutant strains.**

1709 (.xlsx)

1710 **S21 Fig. SB3: Numbers of HOG innovations and losses at each node of the majority-rule**

1711 **consensus tree of Set-R.**

1712 A consensus tree representation of Set-R with each inner node of the tree annotated with

1713 the number of HOGs associated to it as well as the number of lost HOGs in the subsumed
1714 clade according to the rules of Dollo (+) Parsimony (see Methods). All HOGs are provided in
1715 S28 Table SB2. The nodes are labeled with an incremental id. On the lineage of *A. baumannii*
1716 we used the following replacements in the manuscript: NODE_1 = "ACB+BR", NODE_8 =
1717 "ACB+LW", NODE_9 = "ACB+BA", NODE_10 = "ACB+HA", NODE_11 = "ACB", NODE_12 =
1718 "BNS", NODE_13 = "B". Tip labels are represented as NCBI RefSeq Identifiers. Tip labels also
1719 show unique assembly accession and, if applicable either clone type assignment or
1720 (corrected) species assignment in form of the first four letters of the species names.
1721 (.pdf)

1722 **S22 Tables SC2: In silico MLST classifications of the genomes in Set-F**.
1723 Results are shown in Tables SC2.1 (Oxford-scheme) and SC2.2 (Pasteur-scheme). Tables
1724 SC2.3 – SC2.10 list NCBI RefSeq assembly accession and strain labels for all genomes in the *A.*
1725 *baumannii* clade where the MLST classification allowed a mapping to one of the 8
1726 international clone types.
1727 (.xlsx)

1728 **S23 Files SC7: ML trees for all three partitions in newick format including support values.**
1729 Files can also be downloaded in zip-format via figshare:
1730 https://figshare.com/s/caa9a6680bc90e004365 (temporary private link).
1731 (.zip)

1732 **S24 Fig. SC8: Majority-rule consensus tree (dendrogram) for Set-F summarizing the**
1733 **information in the maximum likelihood trees based on the three partitions of the core**
1734 **gene set**.
1735 (.pdf)

1736 **S25 Table SC4: Raw values of the paiwrise ANIm comparisons shown in S9.**

1737 (.xlsx)

1738 **S26: Figures SD2: Treemaps (SD2.1-5) of enrichment biological processes as generated by**

1739 **REVIGO (*cf.* S10).**

1740 (.pdf)

1741 **S27 Table SF1: Results of BLAST search for homologues of the QS cluster against non-**

1742 ***Acinetobacter* genomes.**

1743 (.xlsx).

1744 **S28 Table SB2: Hierarchical orthology matrix as calculated from the all vs. all orthology**

1745 **search across Set-R along the phylogenetic tree (OMA hierarchical orthologous groups,**

1746 **HOGs).**

1747 The column header contains the labels of the NCBI RefSeq assembly accession of each

1748 genome. The second column (LCA) indicates the associated inner node of the HOG in the

1749 reconstructed phylogenetic tree. The values either refer to the node label on the lineage of

1750 *A. baumannii* or, if the node is not on lineage, an incremental node id. The corresponding

1751 nodes together with summary statistics are provided in S31. Row indices refer to the

1752 hierarchical orthologous group ID. The matrix fields contain the NCBI RefSeq protein

1753 sequence accession if an ortholog was identified otherwise they are left empty. Table SB1.2

1754 lists the identifiers of HOGs with prevalence in at least 231 genomes. These were used for

1755 the definition of core components during cluster identification

1756 (.xlsx)

1757

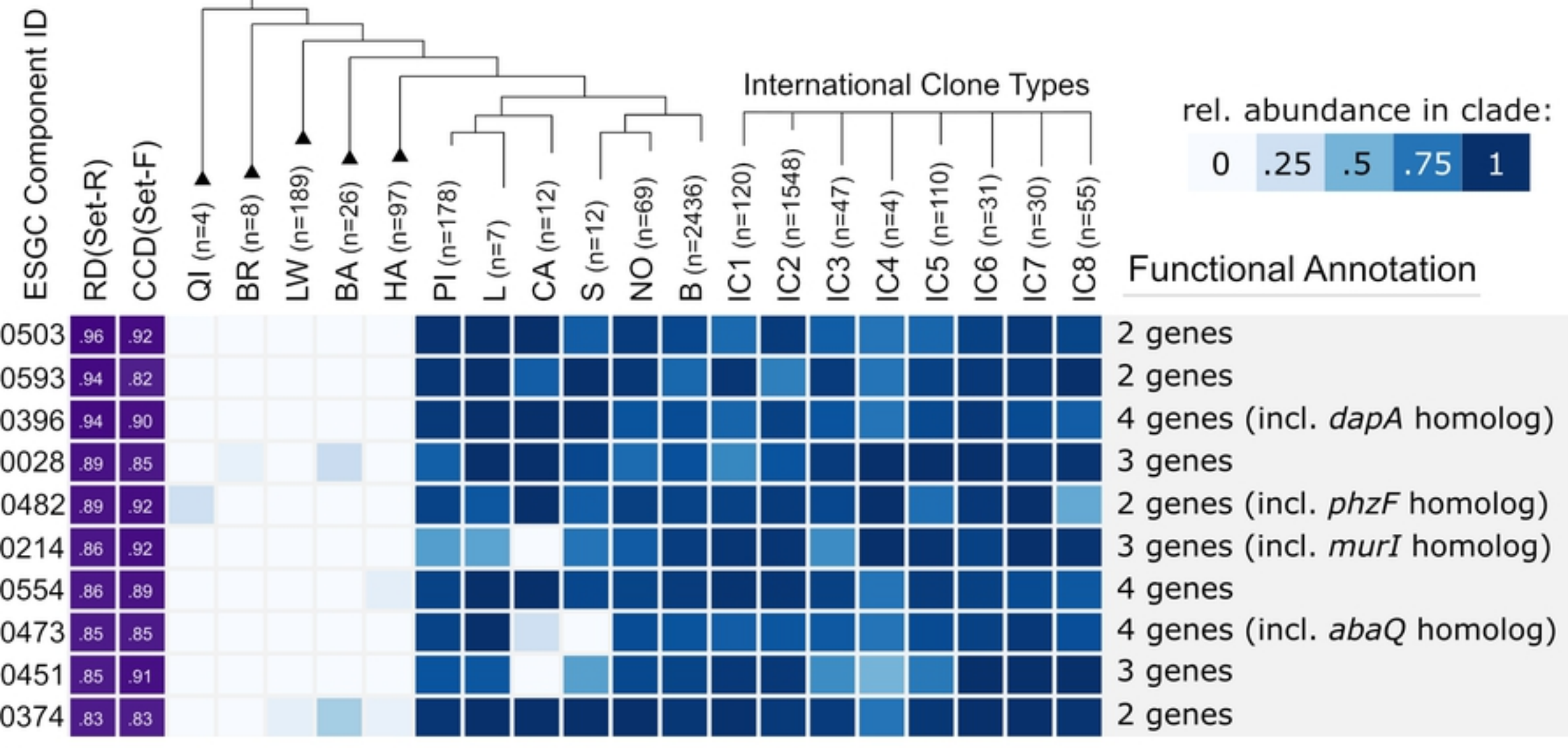
ESGC Component ID
RD(Set-R)
CCD(Set-F)
QI (n=4)
BR (n=8)
LW (n=189)
BA (n=26)
HA (n=97)
PI (n=178)
L (n=7)
CA (n=12)
S (n=12)
NO (n=69)
B (n=2436)
International Clone Types
IC1 (n=120)
IC2 (n=1548)
IC3 (n=47)
IC4 (n=4)
IC5 (n=110)
IC6 (n=31)
IC7 (n=30)
IC8 (n=55)
rel. abundance in clade:
0
.25
.5
.75
1
Functional Annotation
0503 .96 .92 2 genes
0593 .94 .82 2 genes
0396 .94 .90 4 genes (incl. dapA homolog)
0028 .89 .85 3 genes
0482 .89 .92 2 genes (incl. phzF homolog)
0214 .86 .92 3 genes (incl. murI homolog)
0554 .86 .89 4 genes
0473 .85 .85 4 genes (incl. abaQ homolog)
0451 .85 .91 3 genes
0374 .83 .83 2 genes

Figure 6

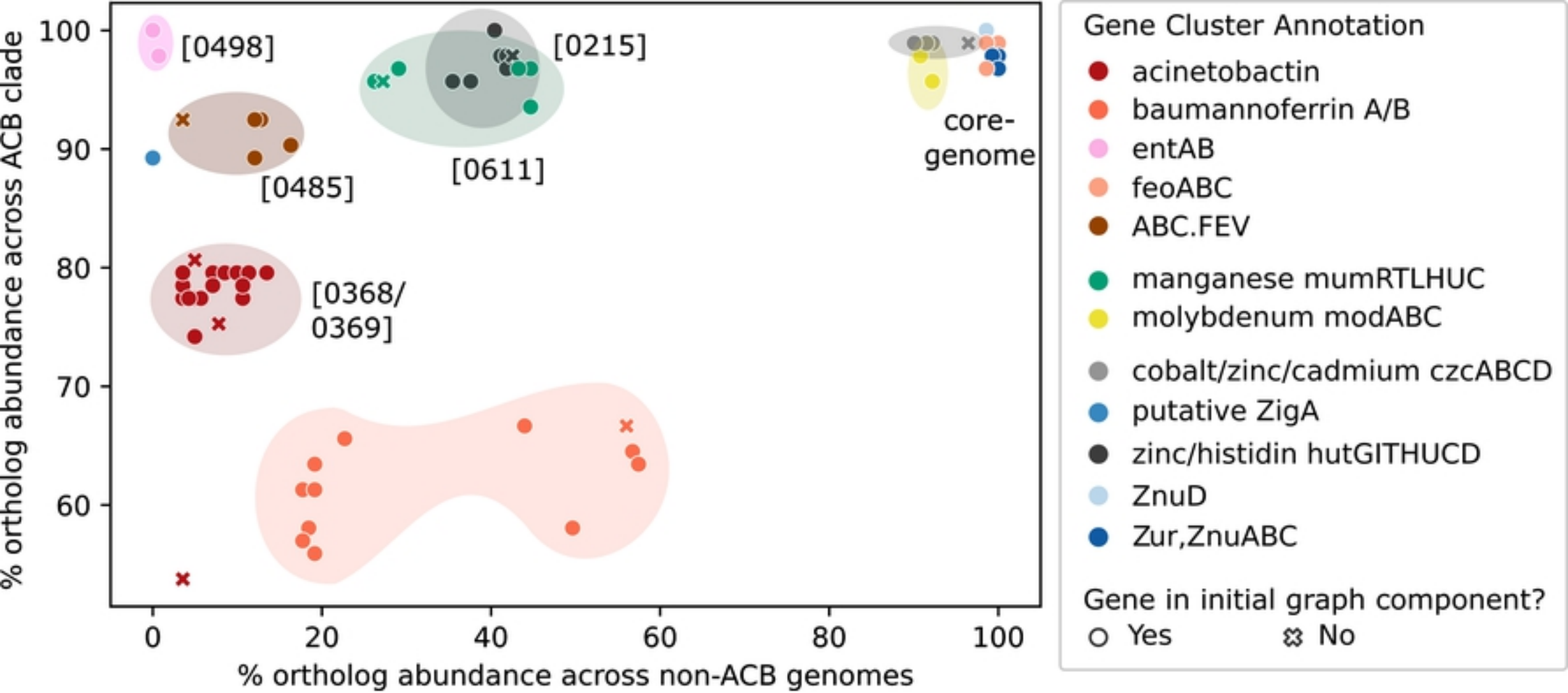
% ortholog abundance across ACB clade
% ortholog abundance across non-ACB genomes
100
90
80
70
60
0
20
40
60
80
100
[0498]
[0215]
[0611]
[0485]
[0368/
0369]
core-
genome
Gene Cluster Annotation
acinetobactin
baumannoferrin A/B
entAB
feoABC
ABC.FEV
manganese mumRTLHUC
molybdenum modABC
cobalt/zinc/cadmium czcABCD
putative ZigA
zinc/histidin hutGITHUCD
ZnuD
Zur,ZnuABC
Gene in initial graph component?
Yes
No

Figure 8

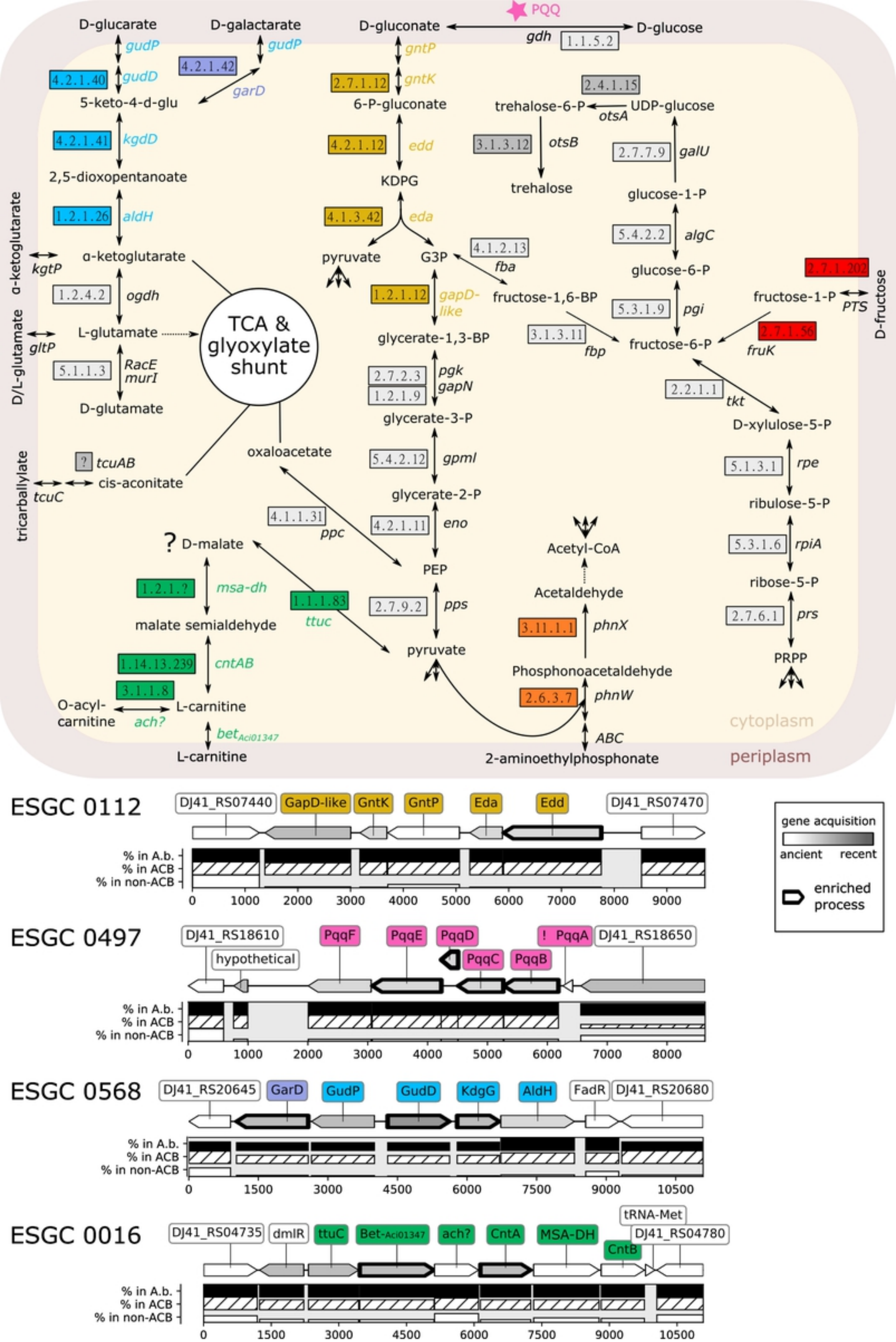
PQQ
D-glucarate
D-galactarate
D-gluconate
D-glucose
gdh
1.1.5.2
gudP
gudD
4.2.1.40
4.2.1.42
garD
5-keto-4-d-glu
gntP
gntK
2.7.1.12
6-P-gluconate
2.4.1.15
trehalose-6-P
UDP-glucose
otsA
4.2.1.41
kgdD
4.2.1.12
edd
3.1.3.12
otsB
2.7.7.9
galU
2,5-dioxopentanoate
KDPG
trehalose
glucose-1-P
1.2.1.26
aldH
4.1.3.42
eda
5.4.2.2
algC
α-ketoglutarate
kgtP
pyruvate
G3P
4.1.2.13
fba
glucose-6-P
2.7.1.202
1.2.4.2
ogdh
1.2.1.12
gapD-like
fructose-1,6-BP
5.3.1.9
pgi
fructose-1-P
PTS
D-fructose
L-glutamate
gltP
TCA & glyoxylate shunt
glycerate-1,3-BP
3.1.3.11
fbp
fructose-6-P
2.7.1.56
fruK
5.1.1.3
RacE murI
2.7.2.3
1.2.1.9
pgk gapN
2.2.1.1
tkt
D-glutamate
glycerate-3-P
D-xylulose-5-P
α-ketoglutarate
D/L-glutamate
tricarballylate
? tcuAB
tcuC
cis-aconitate
oxaloacetate
5.4.2.12
gpml
5.1.3.1
rpe
glycerate-2-P
ribulose-5-P
4.1.1.31
ppc
4.2.1.11
eno
? D-malate
Acetyl-CoA
5.3.1.6
rpiA
PEP
ribose-5-P
1.2.1.?
msa-dh
1.1.1.83
ttuc
2.7.9.2
pps
Acetaldehyde
2.7.6.1
prs
malate semialdehyde
3.11.1.1
phnX
pyruvate
PRPP
1.14.13.239
cntAB
Phosphonoacetaldehyde
3.1.1.8
2.6.3.7
phnW
O-acyl-carnitine
ach?
L-carnitine
cytoplasm
bet Aci01347
ABC
L-carnitine
2-aminoethylphosphonate
periplasm
ESGC 0112
DJ41_RS07440
GapD-like
GntK
GntP
Eda
Edd
DJ41_RS07470
% in A.b.
% in ACB
% in non-ACB
0 1000 2000 3000 4000 5000 6000 7000 8000 9000
gene acquisition
ancient recent
enriched process
ESGC 0497
DJ41_RS18610
hypothetical
PqqF
PqqE
PqqD
PqqC
PqqB
! PqqA
DJ41_RS18650
% in A.b.
% in ACB
% in non-ACB
0 1000 2000 3000 4000 5000 6000 7000 8000
ESGC 0568
DJ41_RS20645
GarD
GudP
GudD
KdgG
AldH
FadR
DJ41_RS20680
% in A.b.
% in ACB
% in non-ACB
0 1500 3000 4500 6000 7500 9000 10500
ESGC 0016
tRNA-Met
DJ41_RS04735
dmlR
ttuC
Bet-Aci01347
ach?
CntA
MSA-DH
CntB
DJ41_RS04780
% in A.b.
% in ACB
% in non-ACB
0 1500 3000 4500 6000 7500 9000 10500

Figure 9

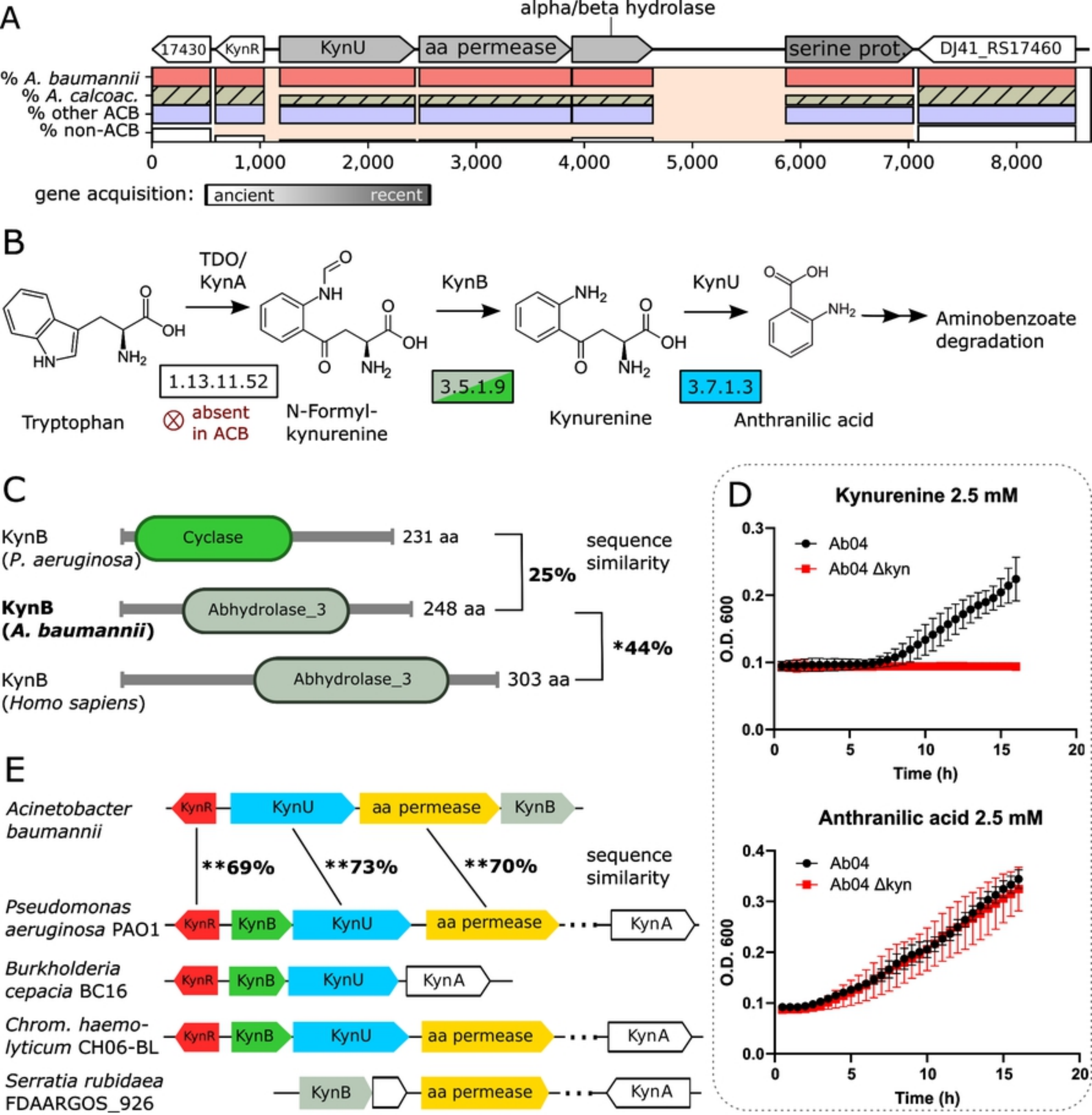
A
alpha/beta hydrolase
17430
KynR
KynU
aa permease
serine prot.
DJ41_RS17460
% A. baumannii
% A. calcoac.
% other ACB
% non-ACB
0
1,000
2,000
3,000
4,000
5,000
6,000
7,000
8,000
gene acquisition:
ancient
recent
B
TDO/
KynA
KynB
KynU
Aminobenzoate
degradation
1.13.11.52
3.5.1.9
3.7.1.3
Tryptophan
absent
in ACB
N-Formyl-
kynurenine
Kynurenine
Anthranilic acid
C
KynB
(P. aeruginosa)
Cyclase
231 aa
KynB
(A. baumannii)
Abhydrolase_3
248 aa
25%
sequence
similarity
*44%
KynB
(Homo sapiens)
Abhydrolase_3
303 aa
D
Kynurenine 2.5 mM
Ab04
Ab04 Δkyn
O.D. 600
Time (h)
Anthranilic acid 2.5 mM
Ab04
Ab04 Δkyn
O.D. 600
Time (h)
E
Acinetobacter
baumannii
KynR
KynU
aa permease
KynB
**69%
**73%
**70%
sequence
similarity
Pseudomonas
aeruginosa PAO1
KynR
KynB
KynU
aa permease
KynA
Burkholderia
cepacia BC16
KynR
KynB
KynU
KynA
Chrom. haemo-
lyticum CH06-BL
KynR
KynB
KynU
aa permease
KynA
Serratia rubidaea
FDAARGOS_926
KynB
aa permease
KynA

Figure 10

Companion Dashboard - Acinetobacter Comparative Genomics - v

Search/Select Genome:

A. baumannii ATCC 19606 CIP 70.34 - GCF_000737145.1

NCBI Taxonomy ID:	575584
Corrected Species:	
Sample Year:	1911
Isolated from:	human
Publication:	Link

Sampled at: unspecified place, Netherlands

Taxonomic Range (Y-Axis): complete_acb(93)

Taxonomic Range (X-Axis): other(141)

Color By: Genus-level Core/Pan Genome Phylostratum Gained

Highlight known virulence factors (hits in databases)

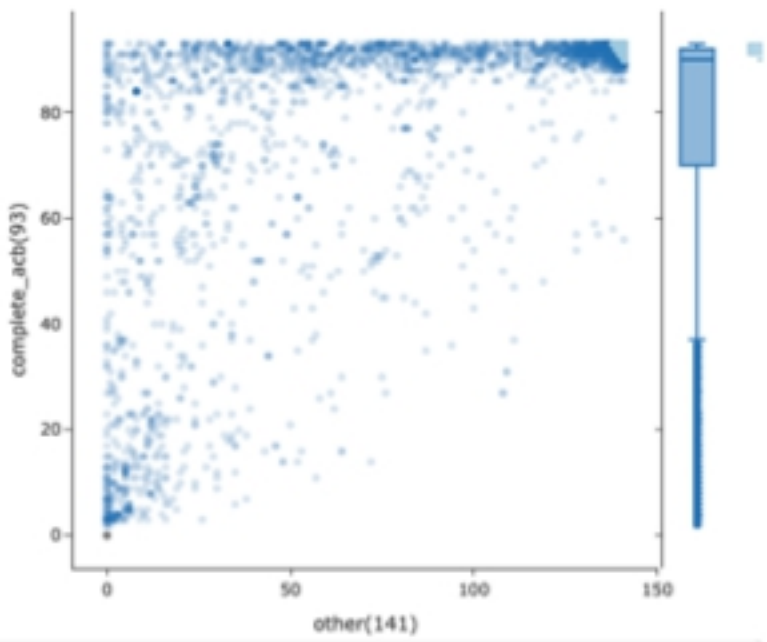

Clade Prevalences for: WP_002134457.1

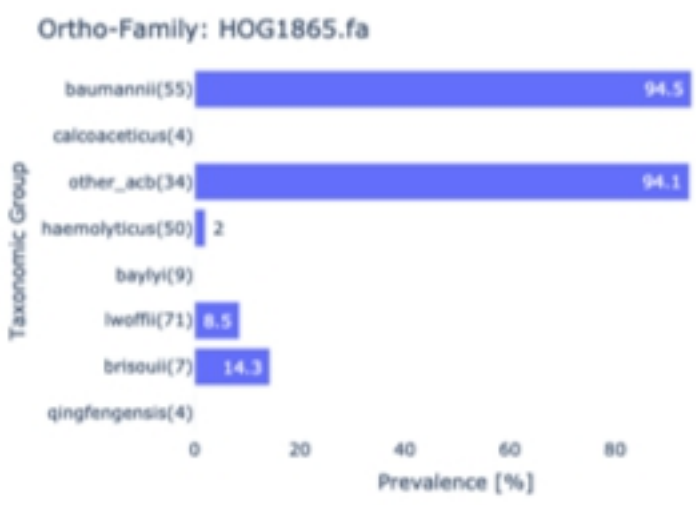

NCBI RefSeq:	WP_002134457.1
Predicted SCL class [GN]:	CYT
This class % across HOG:	93.55
KEGG KO(s):	K03430/K05306
KEGG Description(s):	phnW; 2-aminoethylphosphonate-pyruvate transaminase [EC:2.6.1.37]
COG ID:	N/A
COG Letter:	N/A
COG Description:	N/A
VIR Factor Hit ID:	470.5054.peg.1056|BQ1898_05992
VIR evalue:	2e-06
VIR Description	Pyoverdin biosynthesis protein PvdN, putative aminotransferase, class V [Acinetobacter baumannii strain AB32_M | 470.5054]
VIR Source DB:	VFDB

Figure 1 (lowqual)

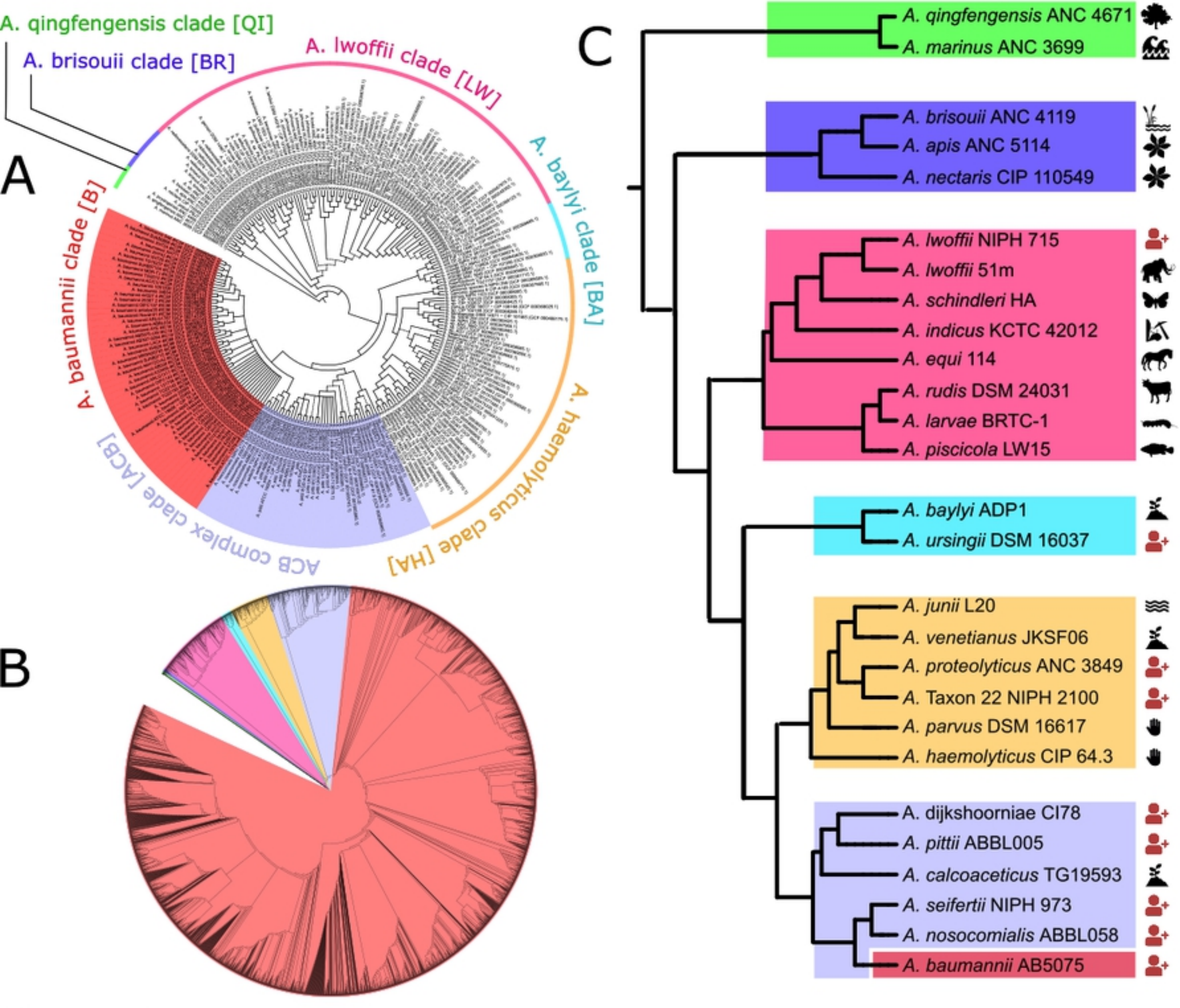
A
A. qingfengensis clade [QI]
A. brisouii clade [BR]
A. lwoffii clade [LW]
A. baylyi clade [BA]
A. haemolyticus clade [HA]
ACB complex clade [ACB]
A. baumannii clade [B]
B
C
A. qingfengensis ANC 4671
A. marinus ANC 3699
A. brisouii ANC 4119
A. apis ANC 5114
A. nectaris CIP 110549
A. lwoffii NIPH 715
A. lwoffii 51m
A. schindleri HA
A. indicus KCTC 42012
A. equi 114
A. rudis DSM 24031
A. larvae BRTC-1
A. piscicola LW15
A. baylyi ADP1
A. ursingii DSM 16037
A. junii L20
A. venetianus JKSF06
A. proteolyticus ANC 3849
A. Taxon 22 NIPH 2100
A. parvus DSM 16617
A. haemolyticus CIP 64.3
A. dijkshoorniae CI78
A. pittii ABBL005
A. calcoaceticus TG19593
A. seifertii NIPH 973
A. nosocomialis ABBL058
A. baumannii AB5075

Figure 2

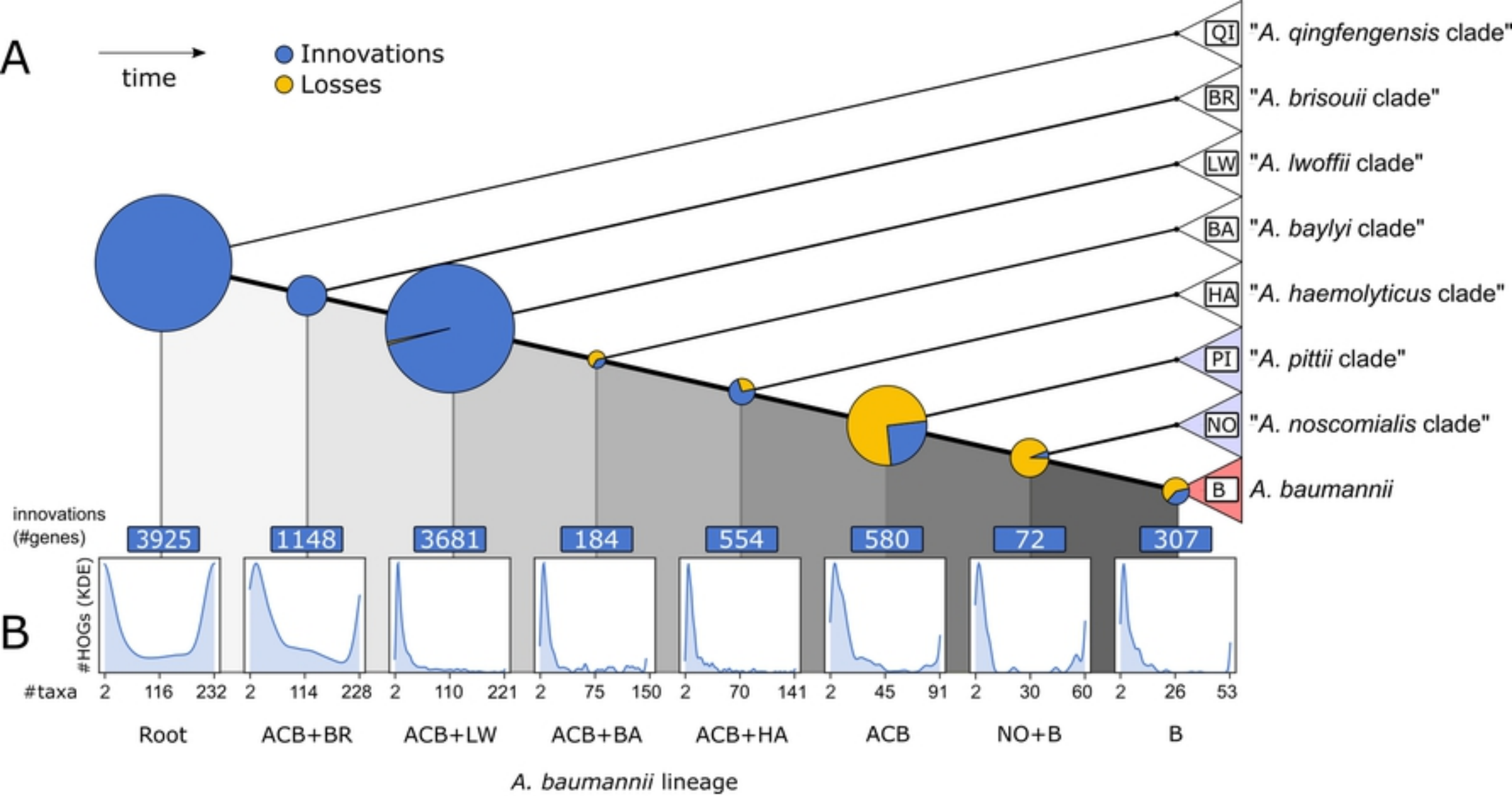
A
time
Innovations
Losses
QI
"A. qingfengensis clade"
BR
"A. brisouii clade"
LW
"A. lwoffii clade"
BA
"A. baylyi clade"
HA
"A. haemolyticus clade"
PI
"A. pittii clade"
NO
"A. noscomialis clade"
B
A. baumannii
innovations
(#genes)
3925
1148
3681
184
554
580
72
307
B
#HOGs (KDE)
#taxa
2 116 232
2 114 228
2 110 221
2 75 150
2 70 141
2 45 91
2 30 60
2 26 53
Root
ACB+BR
ACB+LW
ACB+BA
ACB+HA
ACB
NO+B
B
A. baumannii lineage

Figure 3

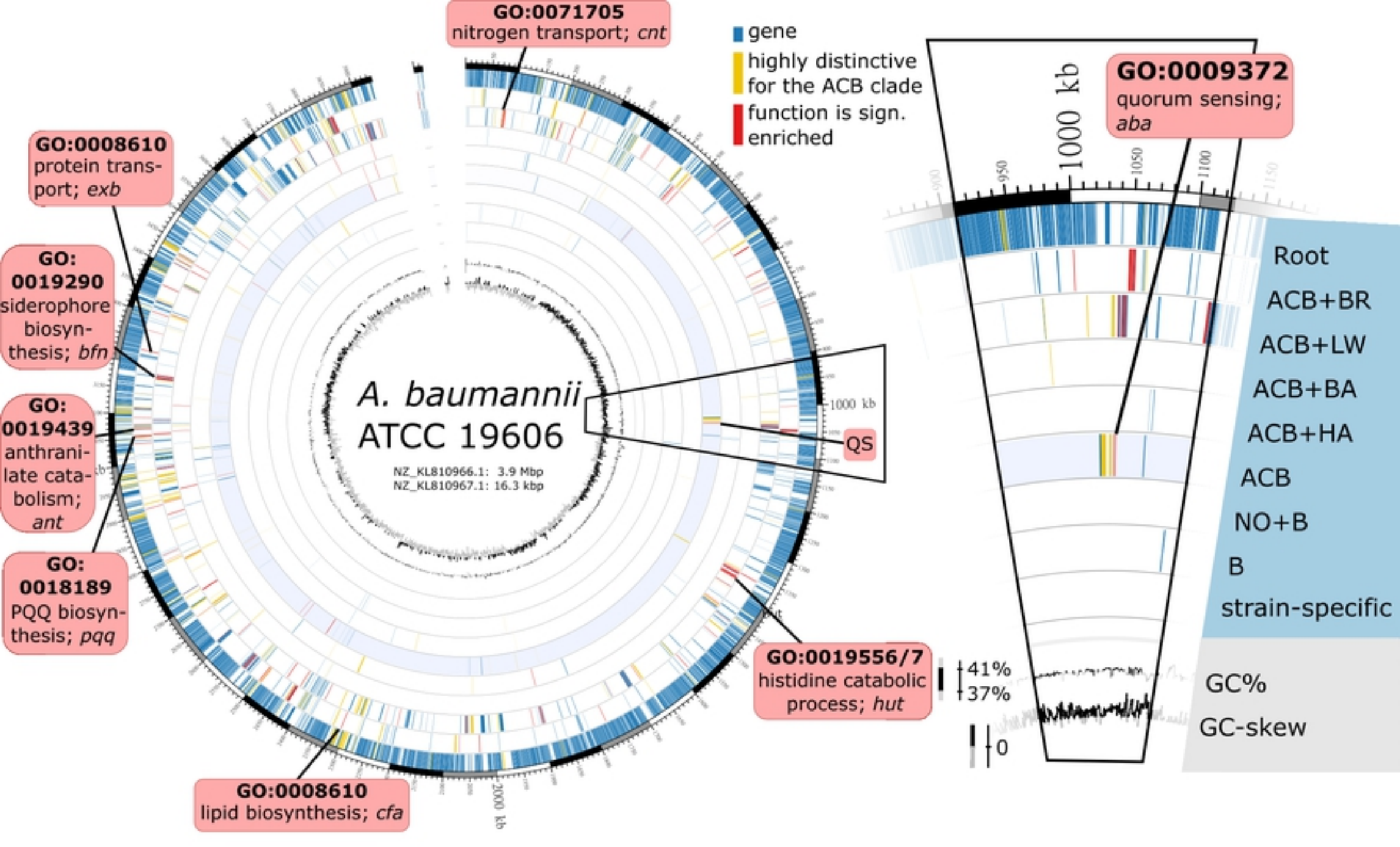
GO:0071705
nitrogen transport; cnt
gene
highly distinctive for the ACB clade
function is sign. enriched
GO:0009372
quorum sensing; aba
1000 kb
GO:0008610
protein transport; exb
GO: 0019290
siderophore biosynthesis; bfn
GO: 0019439
anthranilate catabolism; ant
GO: 0018189
PQQ biosynthesis; pqq
A. baumannii
ATCC 19606
NZ_KL810966.1: 3.9 Mbp
NZ_KL810967.1: 16.3 kbp
QS
GO:0019556/7
histidine catabolic process; hut
GO:0008610
lipid biosynthesis; cfa
2000 kb
Root
ACB+BR
ACB+LW
ACB+BA
ACB+HA
ACB
NO+B
B
strain-specific
41%
37%
0
GC%
GC-skew

Figure 4

ESGC Component ID
RD(Set-R)
CCD(Set-F)
QI (n=4)
BR (n=8)
LW (n=189)
BA (n=26)
HA (n=97)
PI (n=178)
L (n=7)
CA (n=12)
S (n=12)
NO (n=69)
B (n=2436)
IC1 (n=120)
IC2 (n=1548)
IC3 (n=47)
IC4 (n=4)
IC5 (n=110)
IC6 (n=31)
IC7 (n=30)
IC8 (n=55)
International Clone Types
rel. abundance in clade:
0
.25
.5
.75
1
Functional Annotation
0112 .92 .92 - gluconate metabolism [gapD-like,gntKP,edAD]
0162 .87 .90 - NRPS/QS [abaMIR]
0372 .86 .89 - xanthine metabolism [xdhABC]
0452 .83 .90 - kynurenine metabolism [kynRUB]# *
0078 .83 .85 - tricarballylate metabolism [tcuRABC]#
0627 .82 .91 - ABC transp./ 2-AEP metabolism [phnXW]
0497 .82 .78 - PQQ biosynthesis [pqqA-F]
0500 .78 .86 - anthranilate metabolism [antABC]# *
0624 .77 .84 - cytochrome b561/catalase [katA]#
0485 .76 .83 - ABC-type iron uptake system [ABC.FEV]
0394 .74 .92 - AdeGFLH/ histidin uptake [hisQMP]
0498 .74 .96 - iron uptake system [entAB]
0561 .73 .85 - polar amino acid transp. system [ABC.PA]
0368 .71 .89 - acinetobactin biosynthesis [bauA-F]#
0369 .70 .90 - acinetobactin biosynthesis [barAB/basHIJ]
0507 .67 .93 - butanediol [BDH] /acetoine [acoA-D] metab.#
0453 .65 .69 - fructose metabolism [PTS-Fru]
0486 .64 .70 - PRPS/NAMPT *
0016 .64 .75 - carnitine metabolism [cntAB,Aci01347]
0559 .64 .92 - glutathione synth./degrad. [yghU,GST,fabG] *
0320 .64 .70 - capsule formation [capA,ywtB] *
0556 .63 .69 - malonate metabolsim [mdcRAGEDC,madML]
0608 .63 .81 - Kdo2-lipid A [lpxL] *
0410 .62 .71 - chaperone usher system [csuA/B,A-E]# *
0418 .61 .63 - PNAG biosynthesis [pgaA-D]
0560 .61 .62 - cysteine desulfurization [cysE/sufS] *
0566 .61 .53 - putrescine metabolism [puuBP] *
0044 .60 .52 - urea metabolism [ureA-J] *
0621 .60 .84 - drug transp./D-hydroxyproline metab. [lhpA-D] *
0569 .59 .26 - vanillin metabolism [vdH/vanRAB] *
0490 .58 .70 - drug resistence [emrAB,tolC]# *
0505 .56 .85 - ABC-type nitrate uptake system *
0215 .56 .62 - histidine metabolism [hutIGITHDUC]#
0555 .55 .97 - taurine metabolism [tauA-D] *
0568 .54 .36 - glucarate metabolism [garD,gudPD,kdgG,aldH]
0493 .54 .62 - drug efflux [adeTSRAB] *
0274 .54 .61 - acyclic terpenes metabolism [atuB-F] *
0611 .54 .71 - manganese uptake [mumRTLUHC]
0064 .52 .48 - trehalose synthesis [otsAB]
0429 .47 .53 - ethanolamine metabolism [eutCB,eaf]#
0467 .46 .51 - β-ketoadipate [pcaIJBDCHG]/quinone [quiABC]
0622 .46 .61 - phenylacetate metabolism [paaZA-HJKXYI]
0471 .44 .65 - muconate metabolism [catABC]#
0229 .41 .48 - GABA metabolism [puuE,gabDPR]

Figure 5

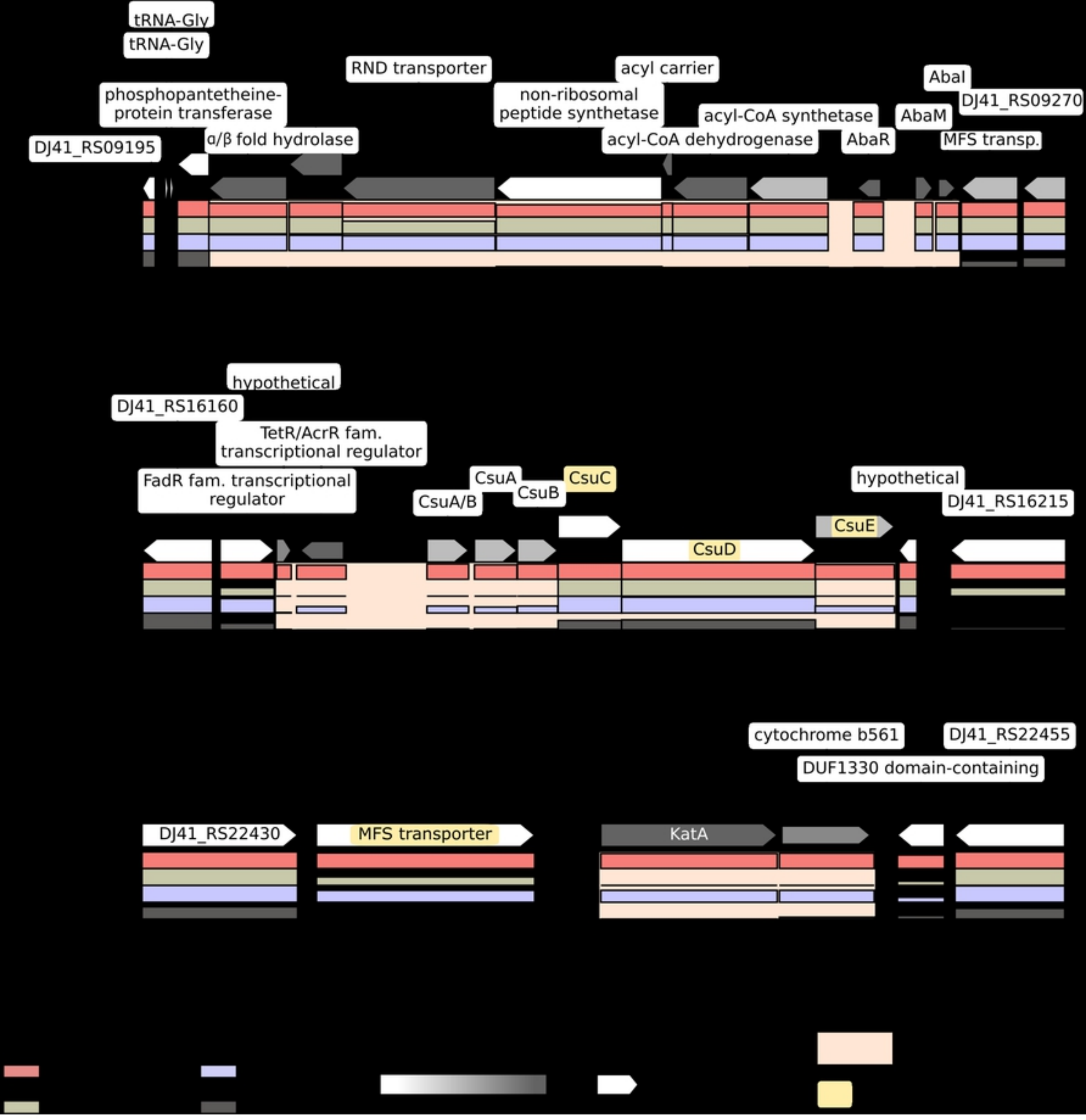
tRNA-Gly
tRNA-Gly
RND transporter
acyl carrier
AbaI
phosphopantetheine-protein transferase
non-ribosomal peptide synthetase
DJ41_RS09270
acyl-CoA synthetase
AbaM
DJ41_RS09195
α/β fold hydrolase
acyl-CoA dehydrogenase
AbaR
MFS transp.
hypothetical
DJ41_RS16160
TetR/AcrR fam. transcriptional regulator
FadR fam. transcriptional regulator
CsuA
CsuC
CsuA/B
CsuB
hypothetical
DJ41_RS16215
CsuE
CsuD
cytochrome b561
DJ41_RS22455
DUF1330 domain-containing
DJ41_RS22430
MFS transporter
KatA

Figure 7